Investigation of signal networks that control dynamic cell shape changes

PhD Dissertation

Department of Systemic Cell Biology,
Max Planck Institute for Molecular Physiology, Dortmund

Faculty of chemistry and chemical biology,
Technical University, Dortmund

International Max-Planck Research School for Living Matter, Dortmund

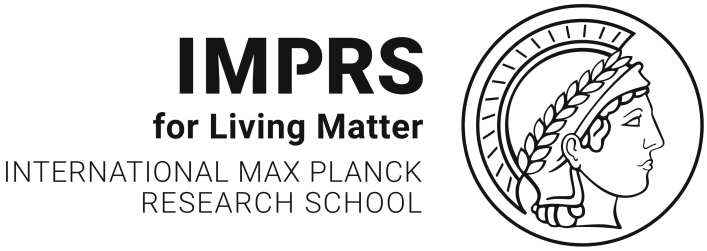

Suchet Nanda

June 2023

Table of contents

Tag der Abgabe der Dissertation: 1 June 2023

Von Suchet Nanda

Erstgutachter: Priv.-Doz. Dr. Leif Dehmelt

Zweitgutachter Prof. Dr. med. Jan G. Hengstler

The work presented in this thesis was performed in the group of Dr. Leif Dehmelt in the Department of Systemic Cell Biology at the Max Planck Institute of Molecular Physiology, Dortmund, Germany, and Department of Chemistry and Chemical Biology, TU Dortmund, Germany.

Eidesstattliche Versicherung (Affidavit)

Nanda, Suchet
Name, Vorname
(Surname, first name)

209186
Matrikel-Nr.
(Enrolment number)

Belehrung:

Wer vorsätzlich gegen eine die Täuschung über Prüfungsleistungen betreffende Regelung einer Hochschulprüfungsordnung verstößt, handelt ordnungswidrig. Die Ordnungswidrigkeit kann mit einer Geldbuße von bis zu 50.000,00 € geahndet werden. Zuständige Verwaltungsbehörde für die Verfolgung und Ahndung von Ordnungswidrigkeiten ist der Kanzler/die Kanzlerin der Technischen Universität Dortmund. Im Falle eines mehrfachen oder sonstigen schwerwiegenden Täuschungsversuches kann der Prüfling zudem exmatrikuliert werden, § 63 Abs. 5 Hochschulgesetz NRW.

Die Abgabe einer falschen Versicherung an Eides statt ist strafbar.

Wer vorsätzlich eine falsche Versicherung an Eides statt abgibt, kann mit einer Freiheitsstrafe bis zu drei Jahren oder mit Geldstrafe bestraft werden, § 156 StGB. Die fahrlässige Abgabe einer falschen Versicherung an Eides statt kann mit einer Freiheitsstrafe bis zu einem Jahr oder Geldstrafe bestraft werden, § 161 StGB.

Die oben stehende Belehrung habe ich zur Kenntnis genommen:

Official notification:

Any person who intentionally breaches any regulation of university examination regulations relating to deception in examination performance is acting improperly. This offence can be punished with a fine of up to EUR 50,000.00. The competent administrative authority for the pursuit and prosecution of offences of this type is the chancellor of the TU Dortmund University. In the case of multiple or other serious attempts at deception, the candidate can also be unenrolled, Section 63, paragraph 5 of the Universities Act of North Rhine-Westphalia.

The submission of a false affidavit is punishable.

Any person who intentionally submits a false affidavit can be punished with a prison sentence of up to three years or a fine, Section 156 of the Criminal Code. The negligent submission of a false affidavit can be punished with a prison sentence of up to one year or a fine, Section 161 of the Criminal Code.

I have taken note of the above official notification.

Dortmund,
Ort, Datum
(Place, date)

Unterschrift
(Signature)

Titel der Dissertation:
(Title of the thesis):

Investigation of signal networks that control dynamic cell shape changes

Ich versichere hiermit an Eides statt, dass ich die vorliegende Dissertation mit dem Titel selbstständig und ohne unzulässige fremde Hilfe angefertigt habe. Ich habe keine anderen als die angegebenen Quellen und Hilfsmittel benutzt sowie wörtliche und sinngemäße Zitate kenntlich gemacht.
Die Arbeit hat in gegenwärtiger oder in einer anderen Fassung weder der TU Dortmund noch einer anderen Hochschule im Zusammenhang mit einer staatlichen oder akademischen Prüfung vorgelegen.

I hereby swear that I have completed the present dissertation independently and without inadmissible external support. I have not used any sources or tools other than those indicated and have identified literal and analogous quotations.

The thesis in its current version or another version has not been presented to the TU Dortmund University or another university in connection with a state or academic examination.*

*Please be aware that solely the German version of the affidavit ("Eidesstattliche Versicherung") for the PhD thesis is the official and legally binding version.

Dortmund,
Ort, Datum
(Place, date)

Unterschrift
(Signature)

Abbreviations used in the thesis

°C	degree Celsius	GEF	Guanine neucleotide exchange factor
ADF	actin depolymerizing factor	GPCR	G-protein coupled receptors
ADP	Adenosine diphosphate	GTP	Guanosine triphosphate
AKAP13	A-kinase anchoring protein 13	HGF	Hepatocyte growth factor
AMP	adenosine monophosphate	IBMX	3-isobutyl-1-methylxanthine
ARHGEF	Rho guanine nucleotide exchange factor	LB	Luria bertani
Arp2/3	Actin related protein 2/3	LOV domain	Light-oxygen-voltage-sensing domain
ATP	Adenosine triphosphate	MCP	MS2-coat protein
BFP	Blue fluorescent proteins	MDCK	Madin-Darby canine kidney
bp	basepairs	PA-Rac1	photoactivable Rac1
cAMP	cyclic adenosine monophosphate	PARC	Presenting artificial receptor construct
Cat-α	Catalytic subunit of PKA	PBS	phosphate buffer saline
CCL	coiled-coiled linker	PCP	PP7-coat protein
Cdc42	Cell division cycle 42	PH Domain	Pleckstrin homology domain
CID	Chemically induced dimerization	PKA	Protein kinase A
CMV	Cytomegalovirus	PUM	pumilio
DDI	DNA directed immobilization	Rac1	ras related C3 botulinum toxin substrate 1
delCMV	truncated CMV promoter	RBD	Ras binding domain
DH Domain	Dbl-homology domain	RH Domain	RGS-homology domain
DMEM	Dulbecco's modifies Eagle's medium	RhoA	ras homolog family member A
dNTPs	deoxyribineucleoside triphoasphate	RIα	PKA regulatory subunit Iα
E.coli	Escherechia coli	RIIβ	PKA regulatory subunit IIβ

ECM	extra cellular matrix	RNA	riboneuclic acid
eDHFR	E.coli dihydrofolate reductase	RNAi	RNA interference
EGF	epithelial growth factor	SEM	standard error of mean
EGFP	Enhanced greef fluorescent protein	siRNA	small interfering RNA
EGFR	EGF receptor	Sos	son of sevenless
et al,	and other	SV40	Simian virus 40
FBS	Fetal bovine serum	TFP	Teal fluorescent protein
FRAP	Fluorescence recovery after photobleaching	TIRF-M	Total internal fluorescnece microscopy
FRET	Fluorescence resonance energy transfer	VASP	vasodialator stimulated phosphoprtein
FSK	Forskolin	WASP	Wiskott:Aldrich Syndrome Protein
GAP	GTPase activating protein	WRC	WAVE regulatory complex
GBD	GTPase binding domain	YFP	Yellow fluorescent protein
GDI	Guanine dissociation inhibitor	μm	microns

Abstract

Cells process information via complex signal networks that include multiple components. Knowledge, about the spatio-temporal organization of these components and their activity state is critical to understand how these signal networks process information. Signal networks involving Rho GTPases play a key role in the spatio-temporal coordination of cytoskeletal dynamics during cell migration. Previous studies that directly investigated the crosstalk between the major Rho GTPases Rho, Rac and Cdc42 revealed a strong increase in Rho activity after Rac1 activation. This Rac1-Rho crosstalk might play a role in mediating the tight spatio-temporal coupling between cell protrusions and retractions that are typically observed during mesenchymal cell migration. To address this question, improved sensors were developed in this thesis to measure the activity state of endogenous small GTPases of the Ras, Rap, Rac, and Rho families in living cells. Using these sensors, Rac activation was observed to be tightly and precisely coupled to local cell protrusions, followed by Rho activation during retraction. In a screen for potential crosstalk mediators, a subset of the Rho activating Lbc-type GEFs, Arhgef11 and Arhgef12, were found to be enriched at the cell periphery during protrusions-retractions cycles. Furthermore, via an optogenetic approach, these Lbc GEFs were observed to recruit to the plasma membrane by active Rac1, suggesting that they indeed might link the cell protrusion signal Rac and the cell retraction signal Rho. Furthermore, depletion of these GEFs via RNA interference impaired cell protrusion-retraction dynamics, which was accompanied with a decrease in migration distance and an increase in migration directionality. These results show that Arhgef11 and Arhgef12 facilitate effective exploratory cell migration by coordinating the cell morphogenic processes of cell protrusion and retraction by coupling the activity of the associated small GTPases Rac and Rho.

Typical activity sensor designs including the improved small GTPase activity sensors described above are limited in the number of readouts that can be combined simultaneously inside a single cell. To extend this number, a new programmable single stranded mRNA-based sensor design was developed. These sensors enable parallel measurements of multiple protein-protein interactions that are dependent on signal

network activity states inside a single living cell. As a proof-of-concept, protein kinase A activity sensors were developed, which allowed to distinguish activity dynamics of their different regulatory subunits in parallel inside living cells. Furthermore, RNA scaffold-based activity sensors for small GTPases were developed which enabled monitoring of the activity kinetics of Ras and Rap during pharmacological perturbations. RNA scaffolds, which were functionalized with dominant positive Rac or Rho GTPases enabled a method to evaluate the specificity of effector molecules in parallel inside living cells. These results show that the application of programmable RNA scaffolds can provide critical information about signal network components inside individual, living cells, which cannot be obtained via available standard methods. Such information can be critical to decipher the spatio-temporal organization of complex signal networks inside cells.

Zusammenfassung

Zellen verarbeiten Informationen über komplexe Signalnetzwerke, die mehrere Komponenten umfassen. Kenntnisse über die räumlich-zeitliche Organisation dieser Komponenten und ihrer Aktivitätszustände sind entscheidend, um zu verstehen, wie diese Signalnetzwerke Informationen verarbeiten. Signalnetzwerke, an denen Rho-GTPasen beteiligt sind, spielen eine Schlüsselrolle bei der räumlich-zeitlichen Koordination der Dynamik des Zytoskeletts während der Zellmigration. Frühere Studien, welche den Crosstalk zwischen den wichtigsten Rho-GTPasen Rho, Rac und Cdc42 direkt untersuchten, zeigten einen starken Anstieg der Rho-Aktivität nach Rac1-Aktivierung. Dieser Rac1/Rho Crosstalk könnte eine Rolle bei der Vermittlung der räumlich-zeitlichen Kopplung von Zellbewegungen in transienten Zellauswüchsen spielen, die typischerweise während der mesenchymalen Zellmigration beobachtet werden. Um diese Frage zu beantworten, wurden in dieser Arbeit verbesserte Sensoren entwickelt, welche den Aktivitätszustand endogener kleiner GTPasen der Ras-, Rap-, Rac- und Rho-Familien in lebenden Zellen messen können. Mithilfe dieser Sensoren wurde beobachtet, dass die Rac-Aktivierung eng und präzise an lokale Zellauswüchse gekoppelt war, gefolgt von der Rho-Aktivierung während des Zurückziehens dieser Auswüchse. In einem Screen zur Identifizierung potenzieller Crosstalk-Vermittler wurde herausgefunden, dass die Rho-aktivierenden Lbc-Typ-GEFs Arhgef11 und Arhgef12 in transienten Zellauswüchsen nahe der Zellperipherie angereichert sind. Außerdem wurde mithilfe eines optogenetischen Ansatzes beobachtet, dass diese Lbc-Typ-GEFs durch aktives Rac1 zur Plasmamembran rekrutiert werden. Dies deutet darauf hin, dass sie tatsächlich die Signalproteine Rac und Rho, welche Zellauswüchse und das darauffolgende Zurückziehen der Zelle verknüpfen könnten. Darüber hinaus beeinträchtigte die Depletion dieser GEFs durch RNA-Interferenz die Dynamik transienter Zellauswüchse, was mit einer Verringerung der Migrationsdistanz und einer Zunahme der Migrationsrichtung einherging. Diese Ergebnisse zeigen, dass Arhgef11 und Arhgef12 die effektive explorative Zellmigration ermöglichen, indem sie Zellauswüchse und das Zurückziehen der Zelle koordinieren, indem sie die Aktivität der assoziierten kleinen GTPasen Rac und Rho koppeln.

Typische Designs von Aktivitätssensoren, einschließlich der oben beschriebenen Aktivitätssensoren für kleine GTPasen, erlauben in einzelnen Zellen nur die parallele Messung einer eingeschränkten Anzahl verschiedener Aktivitäten. Um diese Anzahl zu erhöhen, wurde ein neues Sensordesign entwickelt, welches auf programmierbaren einzelsträngigen mRNA-Gerüstmolekülen basiert. Diese Sensoren ermöglichen parallele Messungen mehrerer Protein-Protein-Wechselwirkungen, welche von Aktivitätszuständen des Signalnetzwerks innerhalb einer einzelnen lebenden Zelle abhängen. Als Machbarkeitsbeweis wurden Proteinkinase-A-Aktivitätssensoren entwickelt, welche es ermöglichten, die Aktivitätsdynamik von Varianten mit verschiedenen regulatorischen Untereinheiten parallel in einzelnen lebenden Zellen zu messen. Darüber hinaus wurden RNA-Gerüstmolekül basierte Aktivitätssensoren für kleine GTPasen entwickelt, welche die Messung der Aktivitätskinetik von Ras und Rap während pharmakologischen Störungen ermöglichten. Gerüstmoleküle, welche mit konstitutiv aktiven Rac- oder Rho-GTPasen funktionalisiert wurden ermöglichten eine Methode zur parallelen Bewertung der Spezifität von Effektormolekülen in lebenden Zellen. Diese Ergebnisse zeigen, dass der Einsatz programmierbarer RNA-Gerüste wichtige Informationen über Signalnetzwerkkomponenten innerhalb einzelner, lebender Zellen liefern kann, welche mit verfügbaren Standardmethoden nicht gewonnen werden können. Solche Informationen können entscheidend sein, um die räumlich-zeitliche Organisation komplexer Signalnetzwerke innerhalb von Zellen zu entschlüsseln.

1. Regulation of protrusion-retraction cycles in exploratory cell migration.

1.1 Introduction

Cell migration is a fundamental process underlying various biological processes. In multicellular organisms, many physiological processes such as tissue formation during embryogenesis, rely on highly regulated migration of cells (Merino-Casallo et al, 2022). In particular, the developmental processes often involve either collective or single cell migration. The development of gametes is a typical and well-studied example for the role of single cell migration during embryogenesis. This process occurs during specification of the primordial germ cells from the epithelial primordia, which then migrate in a signal directed fashion towards the developing gonads in zebrafish (Blaser et al, 2005). In contrast, a collective migration of a larger group of cells occurs during development of mechanosensory organs in zebrafish. During this process, a collective migration of the posterior lateral line placode occurs under a cytokine gradient from the anterior to the posterior axis of the animal. The mass of migrating cells on the way to the tail end periodically deposits cells through the body of the animal, which later form sensory organs (Aman and Piotrowski, 2010). In addition to such central roles during embryogenesis, cell migration also plays a role in pathophysiological conditions, such a cancer cell metastasis or in the immune response (George et al, 2023).

A large body of knowledge about cell migration was derived from studies based on two-dimensional *in vitro* culture systems, first established by Ross Harrison (Harrison, 1906). Many cell types, such as transformed cancer cells, readily attach to permissible surfaces and spontaneously start to migrate. Such cells often have a highly polarized shape with a protrusive front and retracting back region (Sarkar et al, 2020).

1.1.1 Cues directing cell migration.

In the absence of external cues, cells can migrate on a 2D surface by spontaneously generating non-directional protrusions. Various environmental cues, including chemical

and mechanical signals can influence this process and guide the direction of cell migration (Reig et al, 2014). Guidance by soluble and diffusible chemical cues, which is called chemotaxis, has been studied most extensively. Typical chemotactic cues include N-formyl peptides and growth factors. Guidance by surface bound chemical cues, such as components of extracellular matrix (ECM), is called haptotaxis. Many cell types secrete ECM proteins such as fibronectin and collagens. These proteins form insoluble fibers that build up a semi-solid substrate that can function as a migration cue (McCarthy et al, 1983).

In addition to chemical cues, cells can also process mechanical cues. The ability to resist deformation, i.e., the stiffness of a substrate, can be sensed by cells. Guidance of cell migration towards an increasing stiffness gradient is called durotaxis (Lo et al, 2000). Galvanotaxis is another mode of migration in which cell migration is guided by electric fields (Cortese et al, 2014).

1.1.2 Modes of cell migration

Depending on the specific cell type, different modes of migration are observed on two-dimensional surfaces, that are characterized by distinct spatio-temporal dynamics of cell shape changes (Figure 1). Cells such as fibroblasts, stem cells and cancer cells typically display mesenchymal cell migration. They are elongated and generate dynamic protrusions at a well-defined leading edge of the cell. These protrusions are supported via newly formed, integrin-mediated focal adhesions, which link the cell protrusions to the extracellular matrix. Focal adhesions are dissolved in the rear end of these cells, resulting in a retractive force associated net froward push, causing the cell to pull itself forward. Cellular slime molds, such as *Dictyostelium discoideum* and immune cells display an amoeboid cell migration. Cells that migrate in this mode are generally round in shape and generate highly dynamic, transient, randomly directed protrusions. In response to external signals, these protrusions can transform to support a directional net migration. Certain cell types, such as keratocytes, display a particularly highly polarized mode of migration, in which net migration is supported by a persistent protrusion at the cell front and a net retraction at the rear of the cells. (Friedl and Wolf, 2010; Nalbant and Dehmelt, 2018)

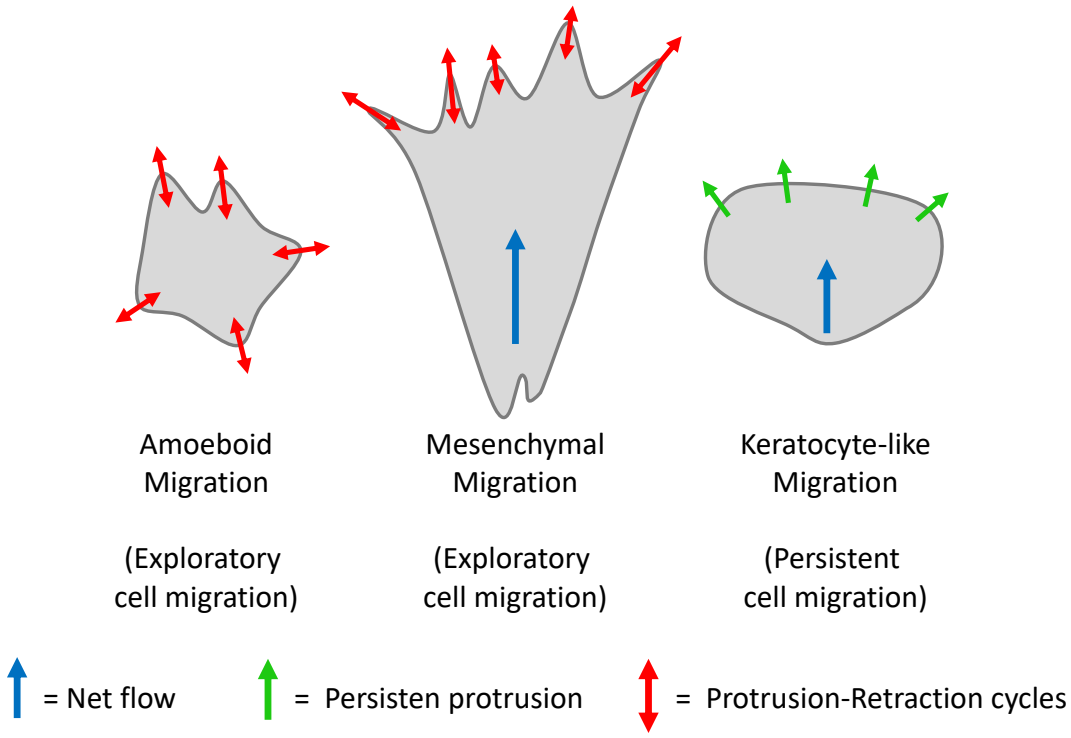

Figure 1. **Modes of cell migration on a two-dimensional substrate.** Dynamic protrusion-retraction cycles are commonly found in amoeboid migration and mesenchymal migration. Nalbant and Dehmelt, 2018.

1.1.3 Cellular processes underlying migration

One of the well-accepted and well-defined models of directional cell migration on 2D surface was developed by Michael Abercrombie and colleagues in the late 1970s. Based on observations with phase contrast and interference reflection microscopy, the process of cell migration was described as a sequence of a few steps. Using modern microscopy techniques and our current understanding of the underlying cellular processes, a more refined model suggests five steps in this sequence (Sheetz et al,1999). (1) The cell establishes a front-rear polarity in the direction of migration. (2) The leading edge then extends and forms sheet-like protrusions, called lamellipodia and/or finger-like protrusions called filopodia. (3) This is followed by formation of new cell adhesions at the cell front, that link the leading edge to the extracellular matrix on the cell substrate. (4) Next, the cell generates contractile forces in specialized intracellular structures called stress fibres. These stress fibres produce contractile forces by anti-parallel sliding of filaments of actin and of the molecular motor protein myosin. (5) The contractile forces then lead to a net retraction at the rear end of the cell along with the dissolution of old

adhesions from the substrate, which leads to a net forward motion. While the stepwise sequence in such models can help to understand cause-and-effect relationships, it should be noted that these steps are highly interlinked and often occur simultaneously. A systems-wide understanding of the spatio-temporal coordination of these processes is still lacking (Seetharaman and Etienne-Manneville, 2020).

The first step that initiates cell migration is the establishment of a front-back polarization of the cell. Conceptually, this event constitutes a break in the initial symmetry of the unpolarized cell (Figure 2). Many cellular components are thought to play a role in this symmetry break, including the three major cytoskeletal networks, which consist of actin filaments, microtubules, and intermediate filaments, and associated regulatory signal networks (Reviewed in Goehring and Grill, 2013). In simple models, force generating protrusive and contractile cytoskeletal structures can by themselves break symmetry, in particular if a small stochastic asymmetry can be reinforced by a mechanical positive feedback loop. In more complex models, reaction-diffusion systems based on signal networks that implement positive and negative feedback spontaneously break symmetry based on small spatial heterogeneities and influence cell shape indirectly by controlling cytoskeletal dynamics (Turing, 1952; Huang, 2016). Early models of chemotaxis include such reaction-diffusion systems that can display symmetry breaking even in shallow gradients (Levchenko and Iglesias, 2002). More recent models propose excitable system dynamics that enable burst-like activation by very small inputs or stochastic processes (Iglesias and Devreotes, 2012). Such excitable systems are known to control both protrusive (Weiner et al, 2007), and contractile structures in cells (Graessl et al, 2017), and they are proposed to originate from various signal systems (Huang et al, 2013).

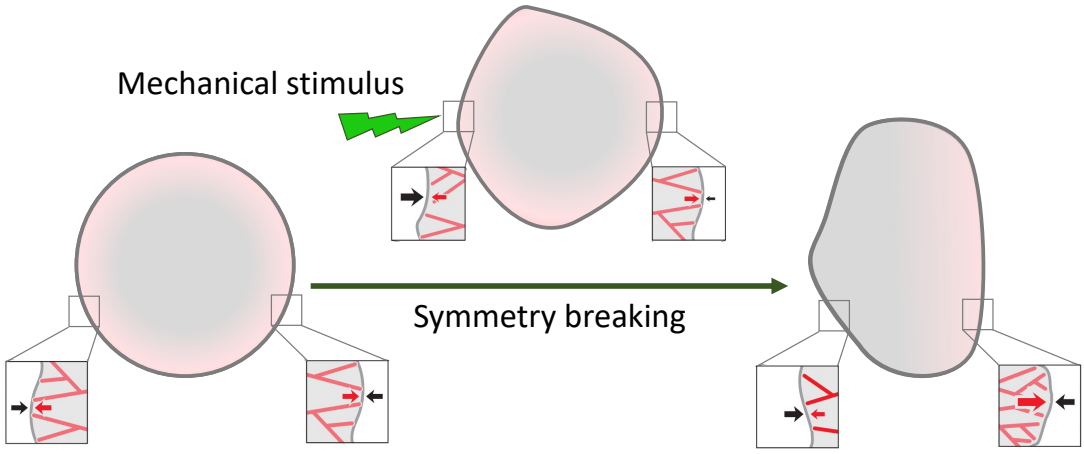

Figure 2. Symmetry breaking in mechanical, or reaction-diffusion systems. In an unperturbed state, the membrane tension (black arrow) of the cell is balanced by the internal

protrusive forces generated by actin polymerisation (red arrow) at the membrane. Asymmetry in polymerization can be induced through local amplification of protrusive signals, and maintained by biochemical or mechanical feedback that propagates the initial asymmetry. Based on Goehring and Grill. 2013.

Post symmetry breaking the signals pertaining to changes in the activity state of biochemical networks can be propagated in the cell through self-organized signal networks. These networks are thought to rely on feedback systems that involving local excitation coupled to global inhibition or mutual inhibition between signals that control front protrusion and back retraction. Establishment of directionality and its persistence is at least partially thought to be mediated by mechanisms that are based on mechanical and morphological cues. At the front, cells such as fibroblasts maintain directionality by forming new lamellipodia in close proximity to the preceding lamellipodia. In the rear of the cell, directionality can be maintained by establishment of a constant retraction force by treadmilling of integrin based-focal adhesions that are generated in the front and resolved in the rear (Stock and Pauli, 2021).

1.1.4 The molecular basis of cell migration

Studies based on two-dimensional *in vitro* culture systems have provided many details about the molecular basis of force generating cellular structures and how they are regulated and coordinated by regulatory proteins and signal networks. The morphodynamics of individual cells are primarily based on actin rich protrusions of different kinds, including lamellipodia, blebs, invadopodia and filopodia (Figure 3). These extensions are also supported by microtubules but have actin as their primary structural component (SenGupta et al, 2021). As coined by Michael Abercrombie in 1970, lamellipodia are sheet like extensions of a cell, usually located at the cell front (Abercrombie et al, 1970). Lamellipodia consist only of actin that polymerises and pushes the cell forward. Just behind the lamellipodia is a broader region that is called the lamellum. This structure consists of actin-myosin polymers, which assist in local contractility. In the lamellum, cell adhesion form which then get associated with stress fibres. The precise organization of actin filaments in the distinct subcellular domains is the structural basis of the distinct types of membrane protrusions, such as, blebs, filopodia

and lamellipodia. Organization of actin filaments in bundles gives rise to filopodia, while branched actin networks generate lamellipodia (Ydenberg et al, 2011).

The dynamicity of the actin filament network stems from its rapid turnover, which is known as actin treadmilling. The turnover of actin is dependent on the on/off kinetics of the ATP bound vs ADP bound actin proteins at the plus end and minus end of actin filaments. A rapid polymerization at the plus end by the virtue of fast, high-affinity driven association of ATP-bound monomers and low-affinity driven release of the ADP-bound monomers at the minus end leads to this treadmilling behaviour, which can be observed as a retrograde flow of the filament network. If this flow is impeded, for example by linkage to the cell substrate, the rapid polymerization at the plus end can generate a pushing force at the leading edge of the cell which leads to protrusions. Actin polymerization is assisted by various molecules like Profilin, ADF/cofilin, formins and Eva/VASP. Profilin can bind to actin monomers and catalyse the exchange of ADP to ATP. ADF/cofilin possess a severing function and promotes actin depolymerization. Formins and Ena/VASP complexes anchor barbed end of actin filaments at the plasma membrane, assist in filament elongation by recruiting actin-profilin complexes and by competing with capping proteins from binding and terminating barbed end elongation. Formins can also nucleate new actin filaments and thereby stimulate the rate-limiting step in subsequent actin polymerization. Actin filaments nucleated by formins are organized into parallel bundles and therefore typically are associated with filopodia. The Arp2/3 complex is another nucleating factor, which generates new filaments that branch off from a mother actin filament at a 70^{o} angle. Arp2/3 remains associated to the filaments after it has initiated a new actin filament branch. The resulting dendritic filament network is typically associated with lamellipodia. *In vitro* studies have shown that Arp2/3 proteins interact with WASP proteins via their C-terminal acidic domain. WASP activates Arp2/3, in turn promoting its nucleating activity (Rottner and Schaks, 2019).

Inside cells, actin filaments interact with non-muscle myosin to generate highly organized bundles and less organized actin-myosin networks. These structures exert contractile tensions at the plasma membrane. The most prominent bundles are called stress fibers. These structures are composed of actin bundles with unevenly spaced stacks of bipolar myosin II filaments. Stress fibers are attached to the plasma membrane via specialized structures called focal adhesions. Focal adhesions link stress fibers to the extracellular

space by several intermediate components that ultimately bind to integrin transmembrane receptors. In addition to these highly organized stress fibers, cells also form less organized actin-myosin networks which cover the entire plasma membrane and are typically referred to as the actin cortex (Svitkina, 2018). By its contractile nature, the cortex generates surface tension and mediates internal pressure. The cortex forms a continuous structure with other actin-based systems, including the lamellipodia, and is thought to play important roles in directing cell migration (Svitkina, 2018). All of these processes are regulated by signal networks, which include small GTPases as central components.

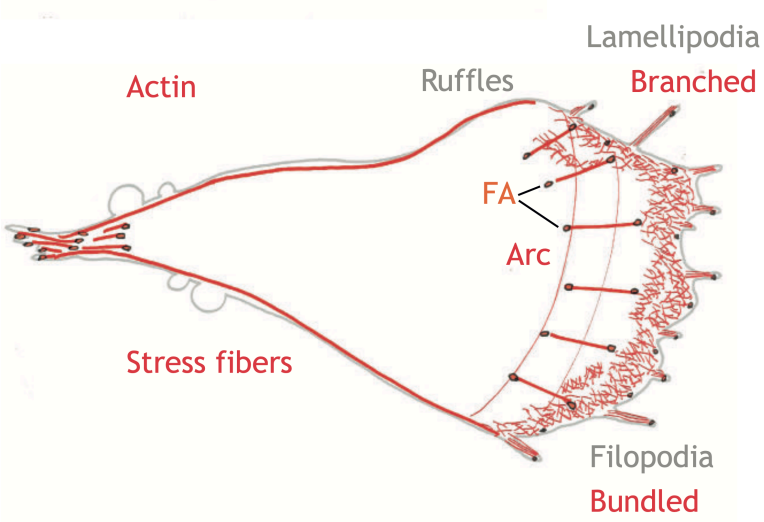

Figure 3. Actin cytoskeleton in a migrating cell. Actin cytoskeleton forms the subcellular structures like lamellipodia, filopodia and ruffles. FA: Focal adhesions. Vaidžiulytė et al, 2019.

1.1.5 Control of cell dynamics by small GTPases

Small GTPases of the Rho and Ras/Rap families are central players in the signal networks that control cell migration (Figure 4). They have a low molecular weight of about 20kDa. Depending on the bound nucleotide they either exist in an active GTP-bound or inactive GDP-bound state. The switch between the active and inactive forms occurs mostly at the plasma membrane. Their activation is triggered via the exchange of GDP to GTP, which is catalysed by guanine nucleotide exchange factors (GEFs). GTPases have very similar affinity for GTP and GDP molecules. The preferential binding of GTP after the exchange reaction occurs due to the higher cytosolic concentration of GTP compared to GDP (Stevens and Der, 2010).

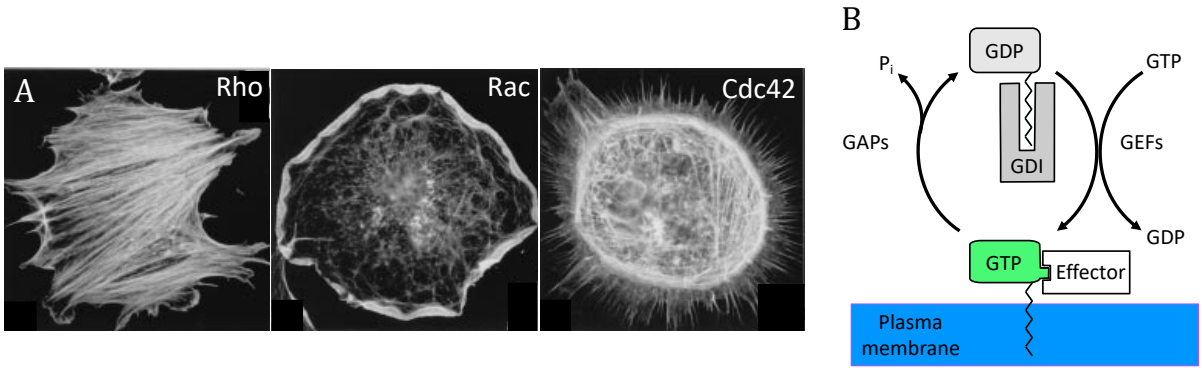

Figure 4. **Rho GTPase are central regulators of cytoskeletal organization.** A: Injection of dominant positive RhoA, Rac1, and Cdc42 induces stress fibres, lamellipodia and filopodia respectively (Hall, 1998). B: Cyclic exchange between GTP bound active GTPase and GDP bound inactive GTPase regulated by GDIs, GEFs, and GAPs. GTP: Guanosine triphosphate GDP: Guanosine diphosphate GDI: Guanosine nucleotide dissociation inhibitor GAP: GTPase activating proteins GEF: guanine nucleotide exchange factors (Stevens and Der, 2010).

Rho GTPases have a GTP binding domain or G-domain at the N-terminus, an effector binding region with switch I and switch II domains, and a hypervariable domain and CAAX (C=cysteine, A=aliphatic, X = terminal residue) box containing membrane targeting motif at the C-terminus. The CAAX motif is responsible for posttranslational modifications which control the subcellular localization of GTPases. Posttranslational modification in Ras GTPases involves addition of a C15 farnesyl isoprenoid lipid to the cysteine residue of the CAAX motif by farnesyltransferase. This follows cleavage of AAX residue via Ras converting enzyme (Rce1). Finally, the farnesylated cysteine residue is carboxymethylated via isoprenylcysteine carboxylmethyltransferase (ICMT). Most Rho GTPases undergo a different modification, which is characterized by addition of a C20 geranylgeranyl isoprenoid lipid via geranylgeranyltransferase-I (Stevens and Der, 2010).

The intrinsic hydrolysis in small GTPases is typically very slow. It is stimulated by GTPase activating proteins (GAPs), which provide an essential arginine amino acid for the efficient hydrolysis of GTP to GDP, switching the GTPase into the inactive state. Another class of regulatory molecules, called guanine dissociation inhibitors (GDI) are critical for the proper function of small GTPases. The hydrophobic C-terminal prenyl group of Ras and Rho-type GTPases, which normally anchors these molecules at the plasma membrane, interacts with GDIs to solubilize them inside the cytosol. This solubilization is thought to

preferentially occur for the inactive GTPase. Thereby, a relatively large inactive cytosolic pool of the GTPase can be present in the cytosol for activation at the plasma membrane. The precise mechanism of how GTPase activation and its translocation from the cytosol to the plasma membrane are coupled is still poorly understood (Golding et al, 2019). One key feature that has now been observed in several GTPase signal networks is excitability (Figure 5), which is thought to play important roles in detecting chemotactic gradients (Iglesias and Devreotes, 2012) and in driving exploratory cell migration (Nalbant and Dehmelt, 2018).

1.1.5.1 Cell protrusion: The excitable Rac1/Scar signal system

The Rho GTPase family member Rac is a well-studied regulator of cell protrusion. The active form of Rac mediates actin nucleation, primarily by activating the WAVE regulatory complex (WRC). In its canonical form, the WRC consists of WAVE, CYFIP1, Nap1, ABI2, and HSPC300. Each WRC has two binding sites for Rac, and two WRC complexes or four Rac molecules are required for an effective actin nucleation, mediated through activation of the Arp2/3 complex (Chen et al, 2017). Following actin nucleation via the Wave complex, actin polymerization can generate a pushing force that generates lamellipodial cell protrusions. In neutrophils, the WRC component Nap1 is exchanged by the homologous Hem-1 subunit. In polarized cells, bursts and wave-like dynamics of Hem-1 activity are observed, with the majority of Hem-1 activity near the cells leading edge. These dynamics are thought to emerge from a dual role of actin in relation to the WRC: On the one hand, actin polymerization is stimulated by WRC, and on the other hand, actin polymerization inhibits the WRC. Thus, based on this model, actin acts both downstream and upstream of the WRC. In addition, the WRC is thought to activate itself via autocatalysis. Thereby, WRC and actin can form an excitable system downstream of Rac1 activity, which can explain the observed wave-like activity patterns (Weiner et al, 2007).

1.1.5.2 Cell protrusion: The excitable Ras/Rap system

Ras family GTPases were also proposed to play a role in stimulating cell protrusion. In certain cell types, including *Dictyostelium* amoeba and epithelial cells, activity dynamics of Ras-related GTPases was detected in the form of travelling waves (Miao et al, 2017;

Zhan et al, 2020). Active Ras is thought to be controlled by positive and negative feedback loops, which involve phosphoinositides and their regulators. Similar to the Hem-1/Actin system, these feedback loops can generate an excitable system, which can explain the wave-like and burst like activities. From these studies it is unclear, which isoform of the Ras/Rap subfamily of GTPases is involved in these activity dynamics (Miao et al, 2017; Zhan et al, 2020). Ultimately, the Ras family GTPases are thought to activate Rac to stimulate cell protrusion (Campa et al, 2015).

1.1.5.3 Cell contraction and retraction: The excitable GEF-H1/Rho/Myosin system

The small GTPase RhoA is known to control contractile forces by stimulating acto-myosin assembly. Depending on the spatio-temporal organization of these forces, and how they are linked to the cell substrate, this can either lead to increased tension or to cell retraction. Recent studies revealed that Rho activity is also highly dynamic and can generate burst-like and wave like activity patterns that are typical for excitable systems. To generate these patterns, active Rho amplifies its activity at the membrane via enriching its own activator GEF-H1 in a Rho activity dependent manner. Downstream, active Rho stimulates non-muscle Myosin-IIa, which then with a delay inhibits Rho activity dynamics by blocking GEF-H1 mediated Rho amplification. This system therefore also combines positive and negative feedback loops to generate excitable system dynamics. Additional negative feedback mechanisms exist that can generate pulses of higher frequency, which are mediated by fast acting effectors, such as the GAP Myo9b (Graessl et al, 2017). The frequency of Rho activity pulses was found to be modulated by the stiffness of the cell substrate, showing that this system is able to transduce mechanical into biochemical signals (Graessl et al, 2017). In various developmental processes, similar processes that involve excitable cell contraction dynamics might be involved. For example, during *Drosophila* germband extension, pulsatile contractions were proposed to arise from a positive amplification of Rho resulting from advection from myosin flow, and a negative regulation from the subsequent acto-myosin assembly (Munjal et al, 2015). In studies of *Xenopus* oocytes, the Rho GEF Ect2 was proposed to regulate positive amplification of Rho, with actin filaments contributing as a negative feedback regulator (Bement et al, 2015).

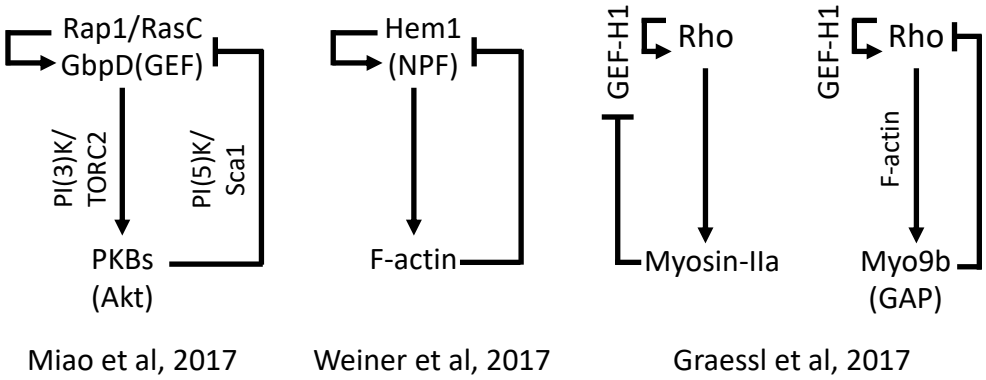

Figure 5. Signal networks underlying cell protrusion and contraction excitability. Network components of excitable systems involving cell protrusion signals: Ras/Rap/Rac and cell contraction signal: Rho.

1.1.6 Regulation and role of dynamic cell shape changes underlying cell migration.

As shown in Figure 1, cells can migrate via various modes (ameboid, mesenchymal, or directionally persistent keratocyte like), all of which are characterized by the coordination of two fundamental features of cell dynamics: protrusions and retractions. The coordination between protrusions and retractions is central for the directionality of cell migration. On the one hand, a stable segregation of protrusion and retraction leads to highly directional migration, while very transient cycles of protrusion and retraction lead to less directional migration, which can allow cells to efficiently explore their surrounding environment for external cues (Nalbant and Dehmelt, 2018). As summarized in sections *1.1.5.1-1.1.5.3,* various excitable systems associated with cytoskeletal remodelling have been suggested to play a role in the control of protrusions and retractions. The question then arises, how protrusions and retractions are coordinated in cells in space and time.

Earlier models for directional cell migration were based on the idea, that signals that control protrusion and retraction are mutually inhibitory. Such a system could lead to spontaneous symmetry breaking and the generation of mutually exclusive regions of these activities in cells (Wildenberg et al, 2006). Previous experiments in the Dehmelt lab directly investigated crosstalk between the major canonical GTPases of the Rho family: Rac1/RhoA/Cdc42 by combining acute perturbations with readouts of the signal network response. These experiments confirmed RhoA induced Rac inhibition at the plasma

membrane. However, interestingly Rac1 activation was found to strongly activate Rho at the plasma membrane. Although the Rac1 induced Rho activation is contradictory to previously proposed models, a Rac induced Rho activation could explain the dynamic coupling of protrusion and retraction during exploratory cell shape changes that are observed in mesenchymal cell migration. Deciphering the mechanism, how Rac can activate Rho would be critical for a better understanding how the excitable protrusion and retraction signals are linked to each other and how protrusion-retraction dynamics are coordinated during cell migration (Figure 6).

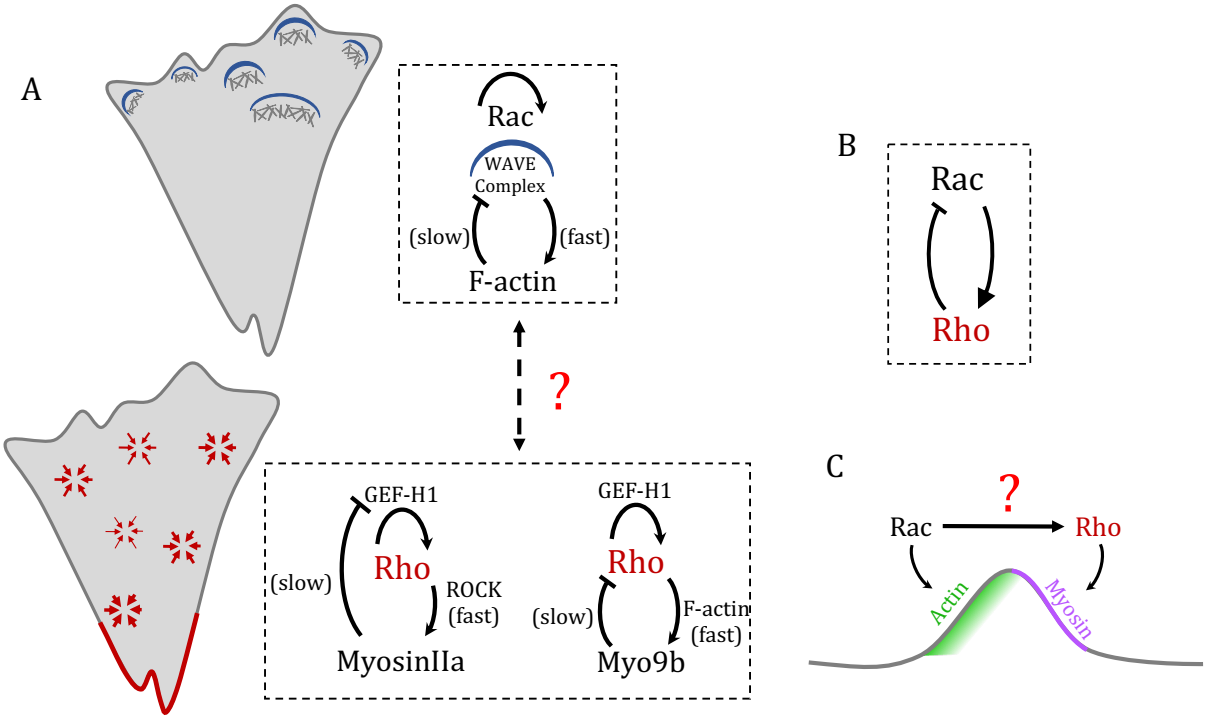

Figure 6. Regulators of dynamic cell shape changes underlying cell migration. A: Rac and Rho are components of excitable signal networks, which regulate protrusion and contraction dynamics. B: Recent investigations in the Dehmelt group showed that Rac can activate Rho, which in turn can inactivate Rac. C: Rac and Rho control actin polymerization and actomyosin contraction, respectively. A link between Rac and Rho activity could couple these two processes in space and time.

1.1.7 Methods to measure small GTPase activity state in cells.

As shown in Figure 4B, the activity state of small GTPases of the Rho family is controlled by the combined action of GEFs, GAPs and GDIs. To monitor the activity patterns of these

GTPases inside cells, several approaches were developed. Most studies were based on Foerster resonance energy transfer (FRET) between fluorescent dyes that were attached to the GTPase itself and an effector domain, which only recognizes the active form of the GTPase. Approaches that either use two separate protein chains, or single chain sensors were developed, which detect a conformational change between the fluorophores that is driven by the interaction between the activated GTPase and the effector domain. Due to their design, these FRET sensors do not directly measure the activity state of the endogenous GTPase, but rather measure the ratio between local GEF and GAP activity that acts on the sensor construct (O'Shaughnessy et al, 2016; de Seze et al, 2023). The first FRET based biosensors that was designed to measure Rac1activity was based on the well-established GTPase binding domain (GBD) of Pak1, which is known to selectively interact with the active form of Rac1. FRET was measured between a fluorescent dye, covalently tagged to Pak1-GBD and GFP-tagged Rac1 (Kraynov et al, 2000). Using the same principle, genetically encoded biosensors were then later developed for Rap1 and Ras by measuring FRET between genetically encoded fluorescent proteins instead of fluorescent dyes (Ohba et al, 2003).

A different approach to measure small GTPase activity in cells is based on so-called translocation sensors, which simply consist of the GBD of an effector fused to a fluorophore, as shown in Figure 6. As the active form of Rho GTPases is localized at the plasma membrane, these sensors will translocate from the cytosol to areas of the plasma membrane which contain increased levels of the active GTPase. Importantly, in this approach, the GTPase is not altered or overexpressed, and the sensor therefore measures the activity state of the endogenous GTPase in its physiological localization inside cells. Various well-characterized GBDs exists, that are used to detect various Rho GTPase family members, including domains derived from Anilin or Rhotekin (Rho), p67Phox, Abi1 (Rac) and WASp, (Cdc42). These GBDs differ from each other for their affinity to their specific GTPases (Mahlandt et al, 2023).

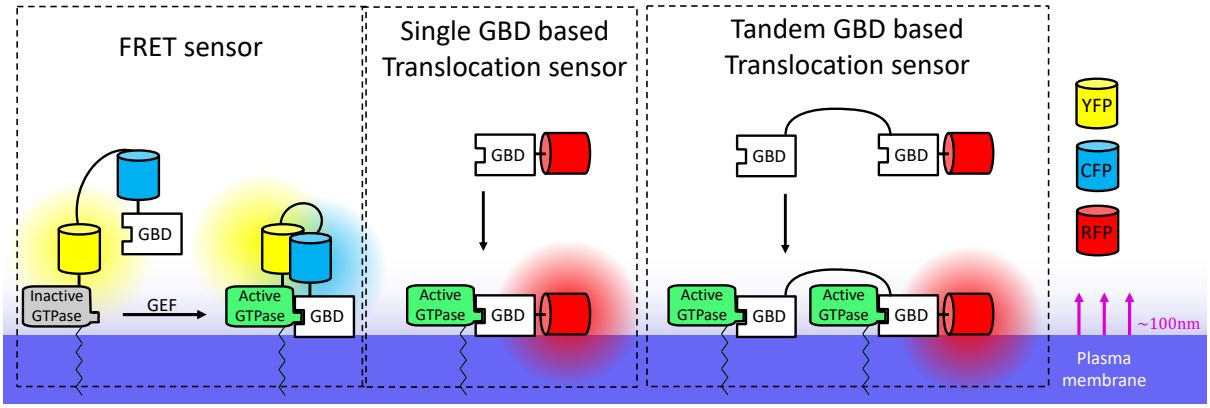

Figure 6. GTPase activity sensors. Sensor designs for GTPase activity sensors based on FRET, or GTPase binding domain-based translocation sensors. Tandem repeats of GTPase binding domains in the sensor construct could increase avidity of the sensor making it more sensitive.

1.1.8 Acute optogenetic perturbation of GTPase activity in cells

Advances in cell biology rely upon visualisation of dynamic interactions between signal network components inside the cell. Processes that are relevant for cell migration, such as cytoskeletal rearrangements are embedded into complex regulatory systems and occur at a time scale of seconds to minutes. Due to adaptation mechanisms, long-term perturbations, such as genetic gene knockdown or overexpression only enable very limited insight into these highly dynamic processes. Combining optogenetic methods, which enable precise spatio-temporal perturbations of signal networks, with monitoring of the signal network response using sensor constructs, enables more direct investigations into the mechanisms that mediate cellular signal processing (Wittmann et al, 2020; Kamps and Dehmelt, 2017).

Several optogenetic methods have been developed that enable precise perturbations of GTPases. Most of these methods rely upon genetically encoded proteins that change their conformation upon illumination with light of a specific wavelength. The blue light responding Light-oxygen-voltage domain of oat phototropin 1, LOV2, is widely used in this regard. One of the first examples of successful activity control of small GTPases is the genetically encoded light activated Rac1 GTPase, PA-Rac1 (Wu et al, 2009). In PA-Rac1, the LOV2 domain is fused to the N-terminus of dominant positive Rac1. In the dark state, the LOV2 domain sterically blocks the access to the effector binding site of Rac1. Upon photo-stimulation the extended Jα helix of LOV2 domain relaxes, which releases the LOV2

domain allowing dominant positive Rac1 to interact with its effector proteins. A Ca^{2+} binding site between the LOV2 domain and dominant positive Rac1, which was discovered later, makes this photoactivable mechanism unique to Rac GTPase (Winkler et al, 2015).

1.2 Objectives

In previous experiments that investigated activity crosstalk between the major Rho family GTPases Rac1, Cdc42 and RhoA, a surprising activation of Rho by Rac1 was observed.
The objective of this section of the thesis was to deduce a better understanding of this crosstalk between these regulators, and to evaluate its potential role in regulating protrusion-retraction cycles in mesenchymal cell migration. To address these questions, highly sensitive translocation-based sensors were developed to measure the activity dynamics of Rac and Rho in protrusion-retraction cycles. Potential mediators of this crosstalk were investigated based on a candidate approach, and their role in regulating the spatio-temporal coordination of protrusion-retraction cycles in migrating cells was studied.

1.3 Results

1.3.1 Monitoring Small GTPase activity in A431 cells

To monitor the activity dynamics of GTPases, effector-binding-domain-based translocation sensors were previously developed in the lab to monitor the dynamics of GTP bound active GTPases via total internal reflection fluorescence microscopy (TIRF-M). In this thesis the previously developed sensors for Rac, Rho and Cdc42 were first improved. Furthermore, TIRF activity sensors for Ras and Rap GTPases were developed based on well-established effector proteins.

1.3.1.1 c-Raf-GBD based Ras activity sensors.

The small GTPase Ras is very well-studied regulator of cell proliferation, growth and morphodynamics. c-Raf is a well-established effector protein of Ras. c-Raf interacts strongly and selectively with the GTP bound, active form of Ras via a well-defined GTPase binding domain (GBD). The c-Raf GBD is therefore commonly used in various studies of Ras activity, including the well-known Raichu-Ras FRET sensors which were developed to monitor Ras activity in living cells (Oliveira et al, 2013). We employed the c-Raf GBD as a translocation-based sensor to detect Ras activity dynamics in cells by combining its expression at a very low level with highly sensitive detection via TIRF microscopy (Graessl et al, 2017; Watanabe and Mitchison, 2002). The activity sensor was composed of a fluorescent protein tagged to the C-terminus of the c-Raf GBD, expressed under the control of the very weak delCMV promoter. To improve the sensitivity of the activity sensor, tandem GBD based sensors were designed, to increase the avidity of the sensor constructs to the endogenous GTPase in living cells. delCMV-2xc-Raf-GBD-mCherry and delCMV-3xc-Raf-GBD-mCherry showed more sensitive dynamic plasma membrane activity patterns compared to a single GBD (data not shown).

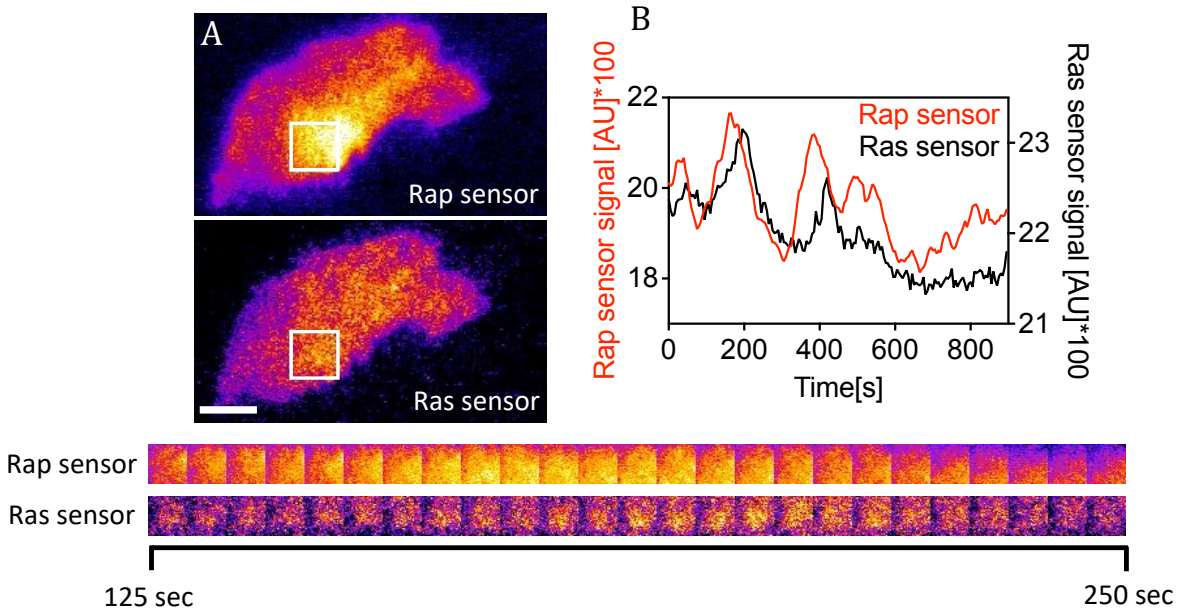

Figure 7. Ras and Rap activity sensors. A: Rap and Ras activity patterns in A431 cells. For both Rap and Ras, pulsatile and wave like activity patterns were observed at the plasma membrane. Near central attachment areas (white rectangle in top panels), bursts of Rap activity were typically followed by Ras activity at the cell centre (bottom panels that correspond to rectangle in top panels) B: Plot depicting activity sensor kinetics of Ras and Rap sensor signals over time, within the white rectangle area in A. Dynamic recruitment of Rap activity sensor was observed at the cell centre and at the cell periphery. The enrichment of the Ras sensor at the cell periphery was considerably weaker. Experimental conditions: Co-expression of delCMV-mCitrine-2xRalGDSRBD and delCMV-2xRafRBD-mCherry in A431 cells. Frame rate: 12/min. Scale bar: 10µm

1.3.1.2 RalGDS-GBD based Rap activity sensors.

The Ras-related small GTPase Rap was proposed to share many of the functions of Ras. In addition, Rap was proposed to play important roles in cell adhesion. RalGDS is a GEF for the Ral GTPase, and also a well-studied Rap effector. The GBD of RalGDS is frequently used in Rap activity assays, such as biochemical pull-down assays and in FRET sensors, such as Raichu-Rap (Ohba et al, 2003).

Analogous to the Ras translocation sensor described in *1.3.1.1*, we used the RalGDS GBD to generate a translocation sensor for Rap. The activity sensor was composed of a fluorophore tagged to the N-terminus of the RalGDS-GBD and expressed under the weak delCMV promoter. Similar to the Ras translocation sensor, the construct delCMV-mCitrine-2xRalGDS-GBD, which contains two copies of the GBD, was more sensitive to detect dynamic plasma membrane activity patterns. As shown in Figure 7, signals

recorded with the Ras and Rap sensors did partially overlap in space and time. Notably, the signals obtained using the Rap sensor were considerably stronger compared to the Ras sensor. Furthermore, Rap activity signals were strongly enriched at peripheral cell regions, in particular during actin-mediated cell protrusion (Figure 8).

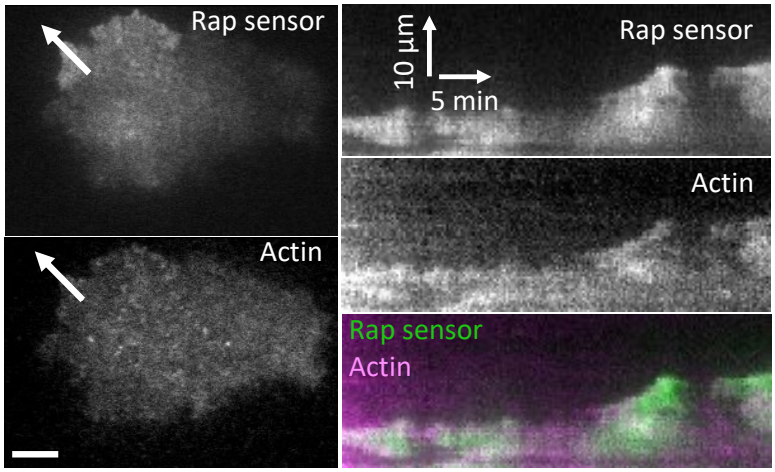

Figure 8. Co-enrichment of Rap activity with actin in A431 cells. Rap activity was observed to be present at the cell periphery during dynamic cell shape changes. Rap activity was particularly enriched in active protrusions which were characterized by a strong enrichment of actin. Experimental conditions: Co-expression ofdelCMV-mCitrine-2xRalGDSRBD and delCMV-mCherry-Actin in A431 cells. Frame rate: 12/min. Scale bar: 10µm

1.3.1.3 Improved Rac activity sensors

The small GTPase Rac is well known for its role in stimulation of actin polymerization and the formation of flat, sheet-like cell protrusions that are called lamellipodia (Machesky and Hall, 1997). As summarized in 1.1.7, various methods were developed to investigate Rac activity dynamics in living cells. In previously work of the lab, a translocation sensor based on the GBD of the Rac effector p67phox was established which responded strongly to optogenetic Rac perturbations via photoactivatable Rac1 (Graessl et al, 2017). Though the sensor responded to acute Rac perturbations, it was very weak to detect Rac activity dynamics in spontaneous cell protrusions. To improve the sensitivity of this sensor, a tandem GBD based approach was used to increase the number of effector GBDs in the sensor molecule, similar to the Ras and Rap sensors described above.

Two of these new Rac activity sensor designs that incorporate either two or three tandem repeats (delCMV-mCherry-2xp6phoxGBD, delCMV-Cherry-3xp67phoxGBD) showed much stronger responses to PA-Rac1 based Rac perturbations compared to the previously established delCMV-mCherry-1xp67phoxGBD sensor construct (Figure 9). Furthermore, in contrast to the sensors with one or two GBDs, the 3xp67phoxGBD based sensor was very sensitive to detect spontaneous Rac activity dynamics in the form of waves and pulses near central cell attachment areas.

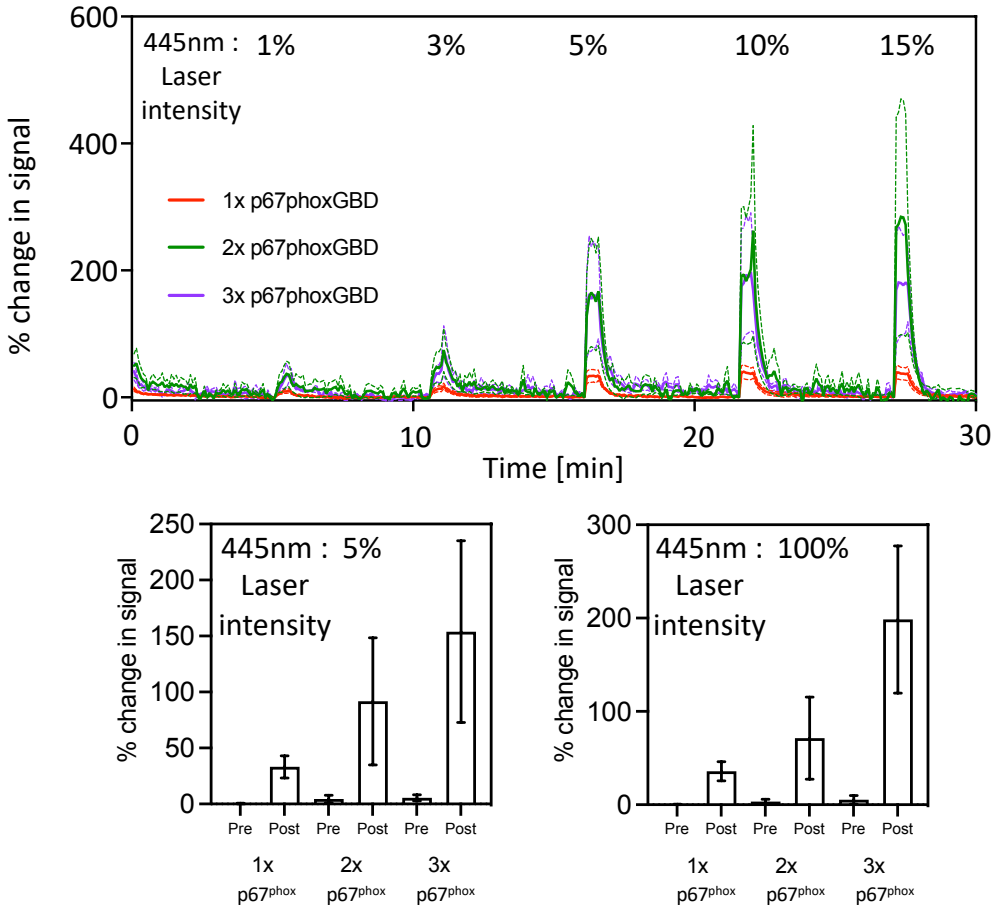

Figure 9. Characterization of improved translocation-based Rac activity sensors. Top panel: Rac activity sensors' response to stepwise increase in 445nm laser intensity. Bottom panel: Recruitment of Rac activity sensors at the plasma membrane 5 time points before and 5 time points after photoactivation with 5% or 100% 445nm laser. Several Rac activity sensor designs that differ in the number of GBD repeats of the Rac effector p67phox were generated and compared. In A431 cells, Rac sensors with multiple p67phoxGBDs showed a stronger enrichment during PA-Rac1 activation compared to the previously developed single GBD sensor. Experimental conditions: Co-expression of delCMV-mCherry-1xp67phoxGBD, 2xp67phoxGBD or 3xp67phoxGBD with CMV-mCerrulean-PA-Rac1 in A431 cells. %age represent laser intensity

percent used for perturbation. Error bars represents standard error of mean. n >5 cells. Single experimental repeat.

1.3.1.4 Improved Rho activity sensor

The small GTPase Rho is well known for its role in stimulating contractile forces in cells via myosin activation. Previously, a Rhotekin-GBD based Rho activity sensor was established in the lab, which reported strong Rho activity patterns after over-expression of Lbc-type GEFs (Graessl et al, 2017), and to acute local and global GEF-induced Rho activity perturbations (Kamps et al, 2020). Though the sensor responded to such perturbation, it only weakly detected spontaneous Rho activity dynamics in unperturbed cells. Similar to the approach described in the previous sections, constructs that incorporate multiple repeats of the Rhotekin-GBD were generated to improve the sensitivity of this sensor. Compared to the 1xRhotekinGBD based activity sensor, the 2xRhotekinGBD based sensor was more sensitive to detect Rho activity dynamics in dynamic cell retractions of migrating cells (Figure 10A). Furthermore, the 2xRhotekinGBD based sensor showed a stronger response to overexpression of the Lbc-type GEF Arhgef11 compared to the previous sensor design (Figure 10B).

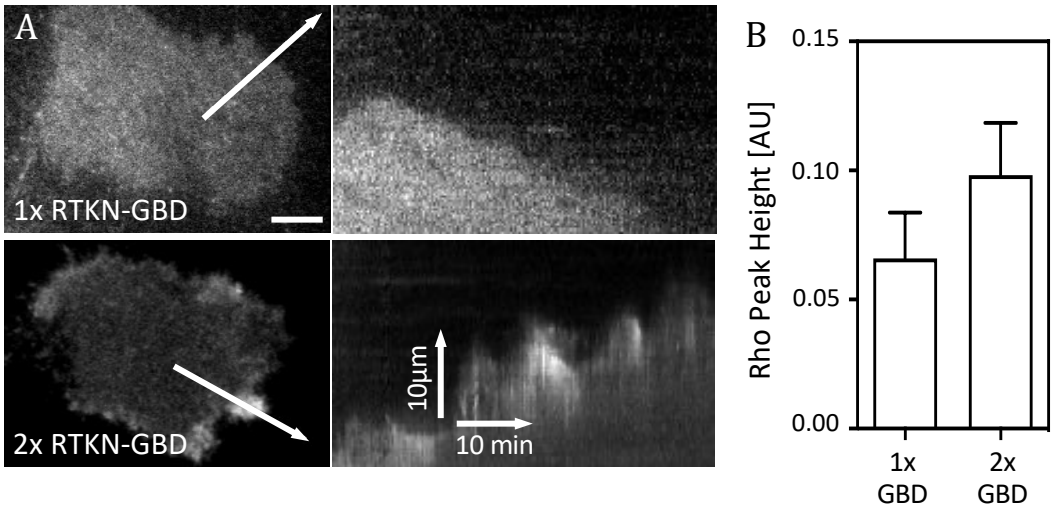

Figure 10. Characterization of an improved translocation-based Rho activity sensor. A: A sensor based on two repeats of the Rhotekin GTPase-binding domain (RTKN-GBD) was strongly enriched in dynamic retractions in A431 cells. Such enrichment was not observed using the previously established 1xRTKN-GBD based sensor. B: The improved Rho sensors with 2 GBDs showed a stronger enrichment of Rho sensor at the plasma membrane after Rho activity

amplification following Arhgef11 overexpression in MDCKII cells. Experimental conditions: A) Expression of delCMV-mCherry-1xRTKN-GBD or delCMV-mCherry-2xRTKN-GBD in A431 cells B) Co-expression of CMV-mCitrine-Arhgef11 and delCMV-mCherry-1xRTK-GBD or 2xRTKN-GBD in MDCK-II cells. n>10 cells. Single experimental repeat. RTKN: Rhotekin. Scale bar: 10μm. Error bars represents standard error of mean.

1.3.2 Direct investigation of Rho GTPase activity crosstalk in A431 cells

Previous studies in the lab employed chemically induced dimerization to study the crosstalk between the major Rho GTPase family members. This study revealed a strong activation of Rho in the neuroblastoma cell line N2a after the recruitment of dominant positive Rac1 to the plasma membrane (Abram Calderon, PhD thesis; Johannes Koch, PhD thesis; Than-Thuy Duong, personal communications). This unexpected Rac induced Rho activation was also supported by an alternate method, in which the photoactivable Rac1 (PA-Rac1) was employed (Abram Calderon, PhD thesis). In these experiments, Rac activation was stimulated with light, and the Rho activity response was measured via translocation-based sensors. In these studies, PA-Rac1 activation strongly and reversibly activated Rho in several commonly used cell lines, including N2a, HeLa, NIH3T3, N2A and U2OS cells (Johannes Koch, PhD thesis).

Investigations in this thesis focussed on dynamic cell protrusions and retractions, which are particularly pronounced in the keratocyte-derived A431 cell line. Detailed investigations into the Rac/Rho crosstalk in this thesis confirmed a strong, reversible Rho activity response during Rac1 photoactivation. Additionally, the response in A431 cells to PA-Rac1 activation was highly dynamic and characterized by a considerable level of cell-to-cell variability (Figure 11C). 67% of cells generated a reversible Rho activity response, while the remaining 33% showed either no response or a negative response. More specifically, 29% of cells showed a continuous Rho activation during PA-Rac1 photoactivation, while 38% showed a transient, pulse-like activity response. 25% of the cells showed no response to photoactivation of Rac1, and 8% of cells showed a negative response.

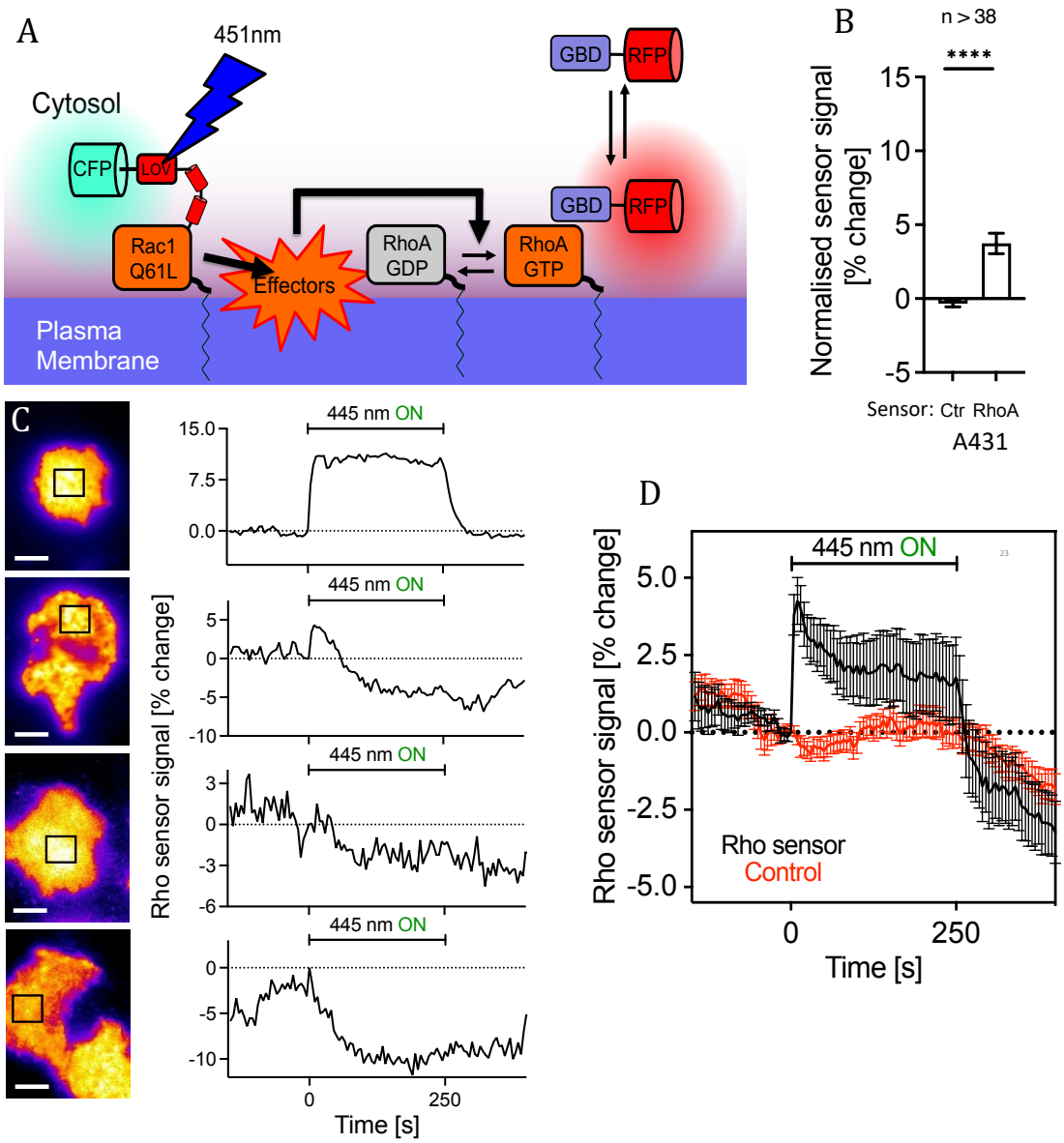

Figure 11. PA-Rac1 induced Rho activity response in A431 cells. A: Schematic of experimental strategy used to measure the Rac induced Rho activity response at the plasma membrane using TIRF microscopy. B: Compared to control, a strong activation of Rho was observed after Rac1 activation. C: Representative examples of the Rho activity response during PA-Rac1 activation. D: Average Rho activity response kinetics to PA-Rac1 activation. Experimental conditions in B-D: CMV-mCerrulean-PA-Rac1 was co-expressed with delCMV-mCherry (control) or delCMV-mCherry-1xRTKN-GBD (Rho sensor) in A431 cells. Photoactivation of Rac1 was performed using 30% of laser power with a 1000x neutral-density filter. n > 38 cells, Student's t-Test (*: P<0.05; **: P<0.01; ***: P<0.001; ****: P<0.0001;). Error bars represent standard error of the mean. Scale bars: 10µm.

The transient Rho activation dynamics to PA-Rac1 photoactivation in A431 cells indicated a presence of additional regulators that could modulate the Rac induced Rho activation responses. Such transient Rac-Rho crosstalk behaviour could play a role in mediating the transient protrusion-retraction cycles that are observed during exploratory migration of A431 cells. To address the possible role of the transient Rac-Rho crosstalk in regulating the transient protrusion-retraction cycles, A431 cells were established as a model system in the lab.

1.3.3 Cell system to study cell morphodynamics - A431 cells.

A431 cells are hypertriploid epidermoid carcinoma cells which exhibit a higher number of EGFR receptors (636 receptors/μm^2) compared to Hela cells (270 receptors/μm^2) (Zhang et al, 2015). A431 cells have an exploratory migration behaviour and exhibit highly dynamic cycles of cell protrusion and retraction during spontaneous cell migration (Clark et al, 2022). In this thesis, highly dynamic cycles during spontaneous migration on fibronectin coated glass surfaces was used as a standard condition (Figure 12). A431 cells were also shown to generate a single, highly dynamic protrusion/retraction cycle after the application of the growth factors EGF or HGF (Gagliardi et al, 2015).

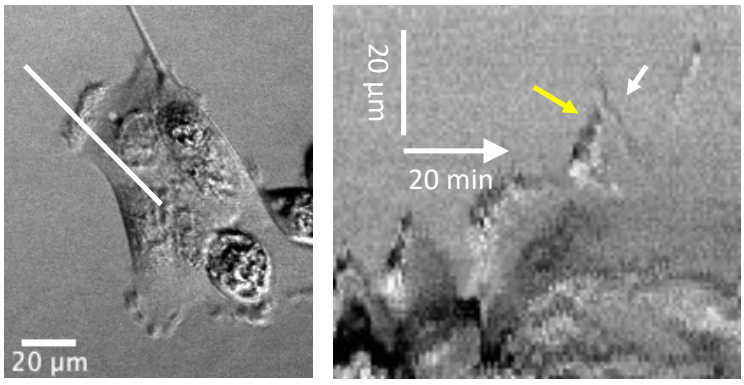

Figure 12. Spontaneous morphodynamics of A431 cells plated on fibronectin. Representative image obtained via DIC microscopy (left) and kymograph (right) corresponding to white line in left panel. Yellow and white arrows in the kymograph point to a local protrusion retraction cycle. Scale bar: 20µm.

1.3.4 Quantification of Rac and Rho activity dynamics in protrusion-retraction cycles.

As described in sections 1.1.5.1 and 1.1.5.3, effectors of Rac and Rho are well known stimulators of protrusive and contractile cell shape changes. Using the improved Rac and Rho sensors developed in this thesis, the exact spatio-temporal coupling of the activity dynamics of Rac and Rho with protrusion and retraction cycles were investigated in A431 cells. In spontaneously migrating A431 cells, Rac activity was found to be coupled very tightly with protrusion events, while Rho activity was very tightly coupled with retraction events.

To gain more quantitative insight into this relationship, an analysis approach was established based on the previously established ImageJ plugin ADAPT (Barry et al, 2015; Figure 13). To perform analysis via the ADAPT plugin, the boundaries of the cell have to be clearly defined, for example, by co-transfecting a soluble, fluorescent protein that can act as a cell filler (Figure 13A). This cell filler is then used for thresholding and segmentation of the cell border. Over time, the plugin is able to trace changes at the cell edge based on positive and negative changes in the position of gray values associated with the cell periphery. The positive and negative changes at the cell edge are then plotted by the plugin as a velocity map, which describes changes around the cell edge at defined positions on the Y-axis and over time in the X-axis (Figure 13B). In addition, the signal of interest is measured in a defined, narrow region close to the cell edge. based on these measurements, the plugin generates a signal map that describes the signal intensity around the cell edge over time analogous to the velocity map. The plugin further generates cross-correlation analysis plots to reveal spatio-temporal relationships between the signal map and the velocity map.

The original version of the plugin measures the signal intensity both inside and outside the cell border. This approach reduces the sensitivity and precision to measure the enrichment of the signal at the cell periphery. To improve this sensitivity, the plugin code was adjusted to restrict measurements inside the cell edge. Using this optimized plugin, the velocity map, signal map and velocity-signal cross-correlation functions were obtained. Visual inspection of the Rac activity signal and the cell edge velocity maps (Figure 13C) clearly indicates that cell protrusion (red color in velocity map) correlates with increased Rac activity (brighter regions in signal maps) both in space and in time. The signal cross-correlation functions that represent the average obtained from several

cells also showed a strong positive correlation between Rac activity signals and cell edge velocity (Figure 13D). In contrast, cross-correlation between Rho activity signals and cell edge velocity showed a negative correlation. A small positive time shift was observed for the maximum of the Rac–velocity crosscorrelation function and for the minimum of the Rho–velocity crosscorrelation function. However, overall, the correlation between the Rac/Rho activity signal and cell shape changes showed no substantial delay.

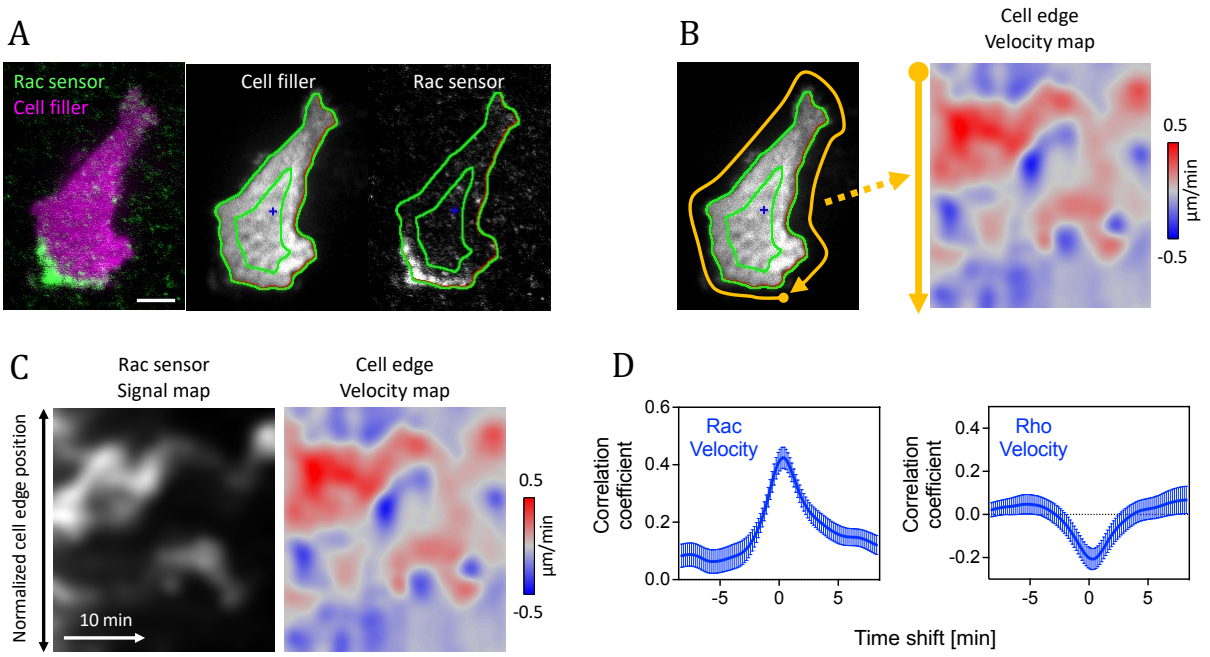

Figure 13. Quantification of sensor signal enrichment during dynamic cell shape changes. A modified version of the ADAPT plugin by Barry et al, 2015 was used to measure sensor signal enrichment at the cell periphery of spontaneously migrating A431 cells, which were plated on glass surfaces freshly coated with fibronectin. A: Representative A431 cell expressing a cytosolic cell filler (delCMV-mCitrine) and the improved Rac activity sensor (delCMV-mCherry-3xp67phoxGBD). B: Automated analysis of cell border movements via the ADAPT plugin. C: Maps generated by the ADAPT script that represent the spatio-temporal dynamics of the Rac sensor signal between the green lines in B (left) and of the cell edge velocity (right). Red areas in the velocity map correspond to local cell protrusions, blue areas to local cell retractions. D: Cross-correlation functions between cell edge velocity and signal intensity show a positive correlation for Rac activity and a negative correlation for Rho activity. Experimental conditions: A-D: delCMV-mCherry-3xp67PhoxGBD (Rac sensor) or delCMV-mCherry-2xRTKN-GBD (Rho sensor) were co-expressed with delCMV-mCitrine in A431 cells. n=3 independent experiments with >21 cells per condition. Error bars represent standard error of the mean. Scale bars: 10µm.

The crosscorrelation analyses shown above are limited in two major aspects: 1) They do not distinguish between signal changes that are associated with protrusion or retractions, and 2) they only quantify how similar the signal and velocity changes are, and do not report the extent or strength of the signal enrichment at protrusions or retractions. To dissect these questions a new analysis approach was developed in which signals from pixels corresponding to protrusion or retraction in the velocity map were extracted from the signal map (Figure 14). The signals were then normalized to the intensity in the whole cell attachment area to obtain a measure for the relative enrichment of signals during protrusion and retraction events. To define protrusions and retractions respectively, a threshold of +/- 0.075µm/min was used. To measure signal enrichment or depletion relative to the time-period of protrusion-retraction events, the signal measurements were shifted along the X-axis of the signal map.

This analysis revealed a strong enrichment of active Rac during protrusions, and a small but clearly detectable depletion during retractions (Figure 14F top). On the other hand, active Rho was strongly enrichment during retractions and strongly depleted during protrusion (Figure 14F bottom).

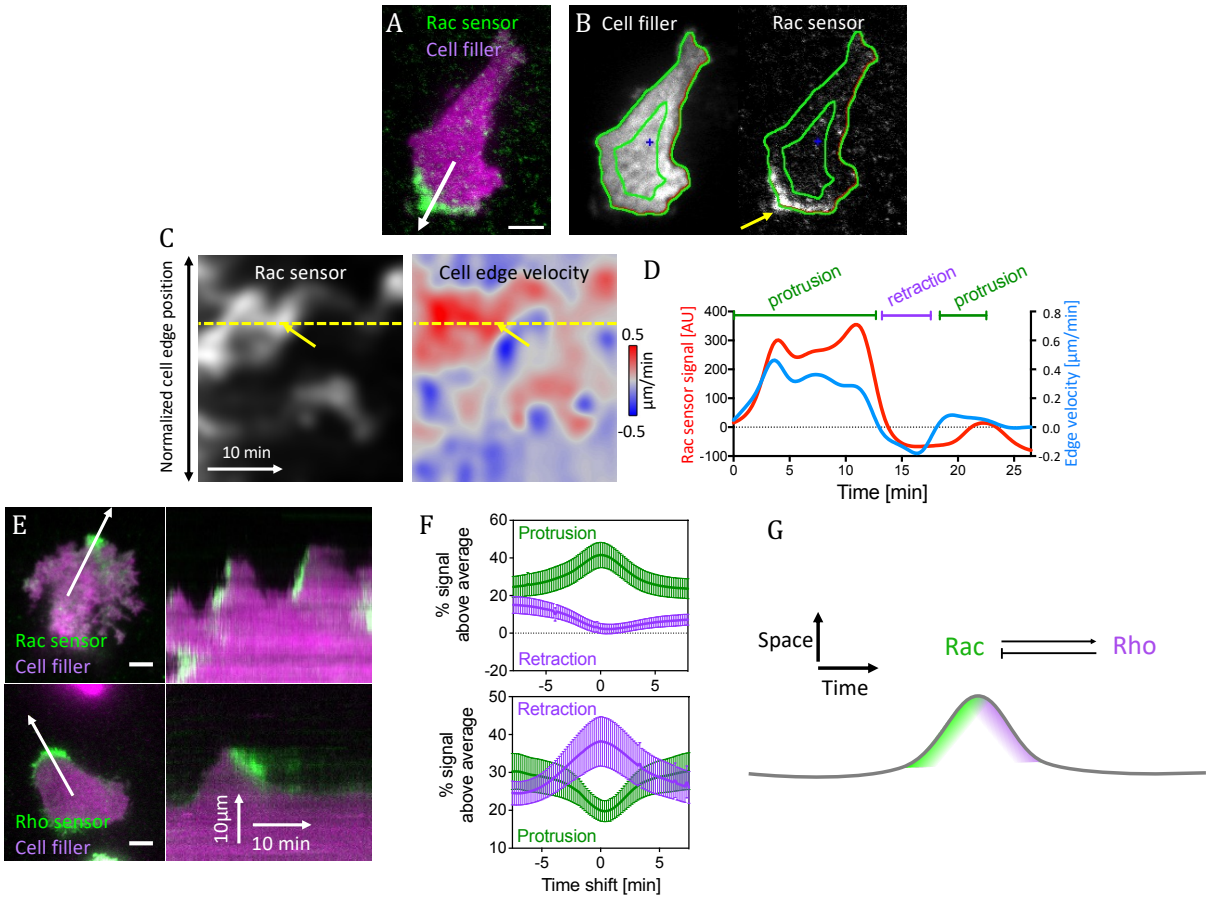

Figure 14. Sequential Rac and Rho activation is tightly coupled to cell protrusion-retraction cycles in space and time. A-B) Representative image of a A431 cell expressing the Rac activity sensor and a cytosolic cell filler, obtained via TIRF microscopy. The white arrow marks the direction of a local cell protrusion. C) Rac sensor and cell edge velocity map corresponding to the cell shown in B. Yellow arrows point to the local protrusion that occurs at the position of the cell area marked by the yellow arrow in B. D) Plot of Rac sensor signals and cell edge velocity corresponding to the yellow dotted line in C. E) Representative TIRF images (left) of A431 cells that express the Rac or Rho GTPase activity sensors and the cell filler. White arrows represent the protrusion direction. Kymographs (right) correspond to white arrows in TIRF images on left panels. F) Enrichment of Rac and Rho sensor signals in protrusions (>0.075µm/min) and retractions (<-0.075µm/min). Values are normalized to average control sensor enrichment measurements. n=3 independent experiments with >21 cells per condition. G) Schematic depicting observations regarding Rac and Rho activity enrichment in protrusion-retraction cycles. Experimental conditions: delCMV-mCherry-3xp67Phox (Rac sensor) or delCMV-mCherry-2xRTKN-GBD (Rho sensor) were co-transfected with delCMV-mCitrine in A431 cells. Frame rate 6/min. Error bars represent standard error of mean. Scale bars: 10µm.

1.3.5 Mechanism of Rac1-Rho crosstalk: Rac1-ROS mediated Rho activation

Various mechanisms how crosstalk between Rac and Rho could be mediated were reported in the literature (Guilluy et al, 2011). Most of these mechanisms focus on the idea that Rac can inhibit Rho, however, some studies also suggested an activation function. (Ridley et al, 1992). One potential mechanism could involve the activation of Rho by reactive oxygen species (ROS), which are thought to oxidize a cysteine residue in Rho leading to its activation. (Aghajanian et al, 2009; MacKay et al, 2017). Rac1 is well-known to activate NADPH oxidase and thereby induce ROS generation (Koga et al, 2003). To study if ROS production stimulated by active Rac could indeed activate Rho at the plasma membrane, we manipulated ROS production by inhibiting NADPH oxidases with DPI (Diphenyleneiodonium chloride) (Buck et al, 2019). We accompanied this pharmacological inhibition with photoactivation of Rac1 and monitoring of the Rho activity response via translocation sensors. However, pharmacological inhibition of NAPDH oxidases in Hela cells lead to an increase in PA-Rac1 induced Rho activation, which was contrary to the prediction if ROS was indeed involved in the Rac1 dependent Rho activation (data not shown).

1.3.6 Mechanism of Rac1-Rho crosstalk: Lbc GEF mediated Rac1-Rho crosstalk

Lbc type GEFs are a class of Rho GEFs that are known to activate RhoA. They belong to the larger Dbl family which is characterized by the presence of two major protein domains, a GEF activating Dbl homology (DH) domain and a regulatory pleckstrin-homology (PH) domain. The majority of Dbl GEFs are known to interact with phospholipids at the plasma membrane, which is thought to be an important part of their regulatory mechanism. The PH domains of Lbc type GEFs lack this phospholipid interaction, and they instead interact with active Rho via their PH domains. This can recruit these molecules to the plasma membrane, where they then in turn can activate more Rho, ultimately leading to Rho activity amplification. The Lbc GEF family includes Arhgef1, Arhgef2, Arhgef11, Arhgef12, AKAP13, Arhgef18, and Arhgef28 (Medina et al, 2013). Arhgef1, 11 and 12 are further known as RH GEFs for their interaction with G-protein coupled receptors (GPCRs) at the membrane via their RGS homology (RH) domains (Suzuki et al, 2003). In a previous study, Arhgef28 was shown to interact with active Rac1 via its PH domain. Furthermore

Arhgef11, Arhgef12, Arhgef13, Arhgef18 and Arhgef28 were shown to cause increase in activation of RhoA in presence of Rac1•GTPγS *in vitro* on phospholipid vesicles (Dada et al, 2018). This mechanism is similar to the well-established ability of Lbc type GEFs to amplify Rho activity and might play a role in Rac1 induced Rho activation (Figure 15A).

To narrow down the list of potential candidates, the Lbc GEFs were first overexpressed in randomly migrating A431 cells to investigate their subcellular localization (Figure 15B). Among the 7 Lbc GEFs, Arhgef11 and Arhgef12 were observed to be highly enriched at the cell periphery in protrusion-retraction cycles of A431 cells. Due to this localization, these two GEFs were strong candidates for mediating the Rac/Rho activity crosstalk.

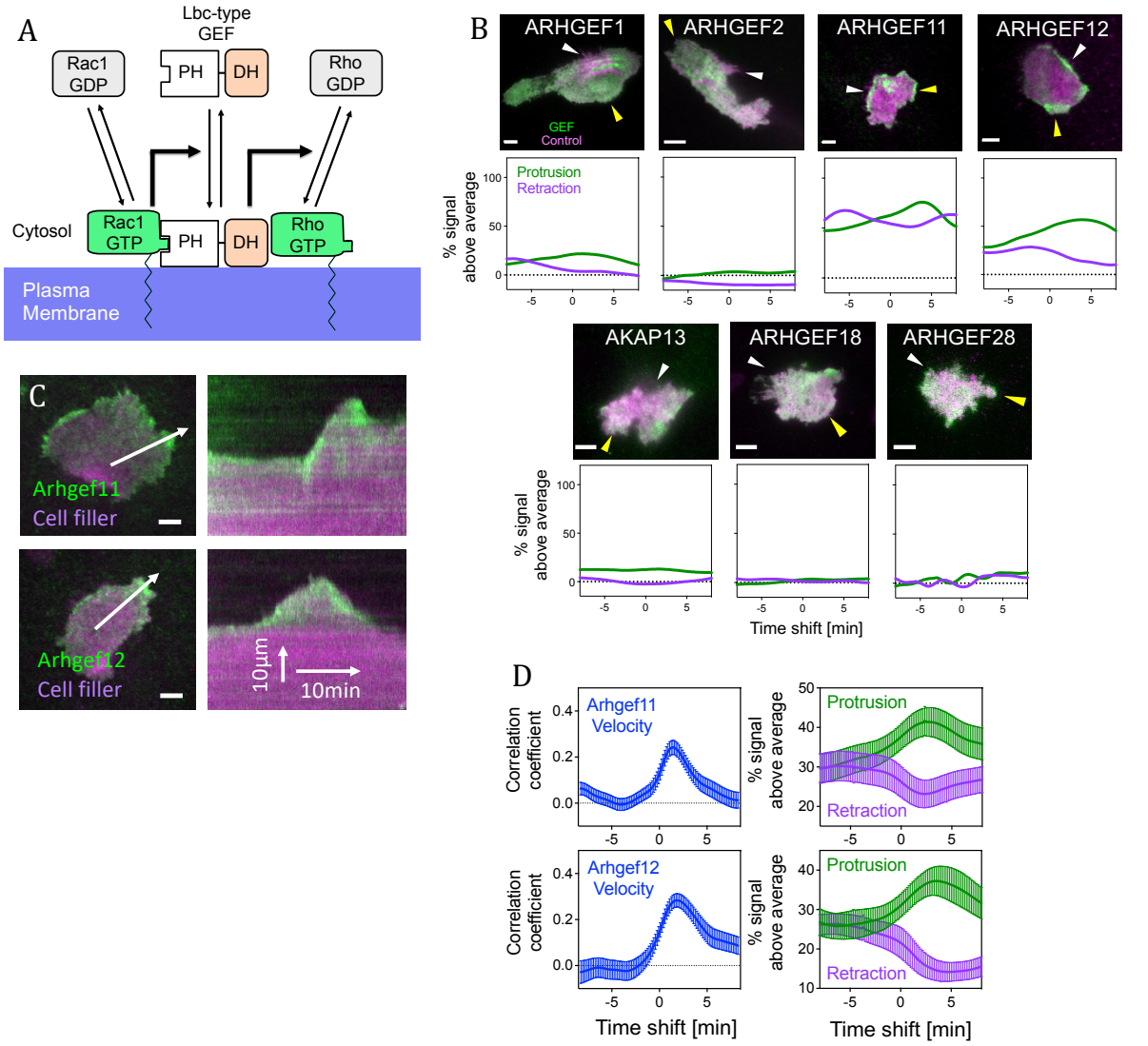

Figure 15. Enrichment of Arhgef11 and Arhgef12 in protrusion-retraction cycles at the cell periphery. A: Schematic representation of a hypothetical mechanism, by which Lbc-type GEFs could mediate Rac1/Rho activity crosstalk. B: TIRF microscopy images (top panels) and

protrusion-retraction enrichment functions (bottom panels) for representative cells that express Lbc-type GEFs (CMV-mCherry-GEF, green) and a cytosolic cell filler that acts as a control construct (delCMV-mCitrine, magenta). White and yellow arrows point to local cell retractions and protrusions, respectively. C: Representative TIRF images (left) of A431 cells that express Arhgef11 and Arhgef12 fused to mCherry and the cytosolic cell filler (mCitrine). White arrows represent the protrusion direction. Kymographs (right) correspond to white arrows in TIRF images. D: Crosscorrelation (left) between Arhgef11/Arhgef12 signals and cell edge velocity, and enrichment (right) of Arhgef11/Arhgef12 signals in protrusions and retractions. Arhgef11/Arhgef12 enrichment values were normalized to average control construct enrichment measurements. n=3 independent experiments with >22 cells per condition. Experimental conditions: B: CMV-mCherry-GEF constructs were co-expressed with delCMV-mCitrine in A431 cells. C-D) delCMV-mCherry-GEF constructs were co-expressed with delCMV-mCitrine in A431 cells. Error bars represent standard error of the mean. Scale bars: 10µm.

The cross-correlation function for GEF enrichment and cell edge velocity confirmed this association and showed a positive shift for both Arhgef11 and Arhgef12 (Figure 15 C-D). Furthermore, enrichment measurements showed a positive enrichment of Arhgef11 and Arhgef12 in protrusions with a positive time-shift. This suggests that the maximal enrichment of both GEFs at the plasma membrane occurs after maximal cell protrusion.

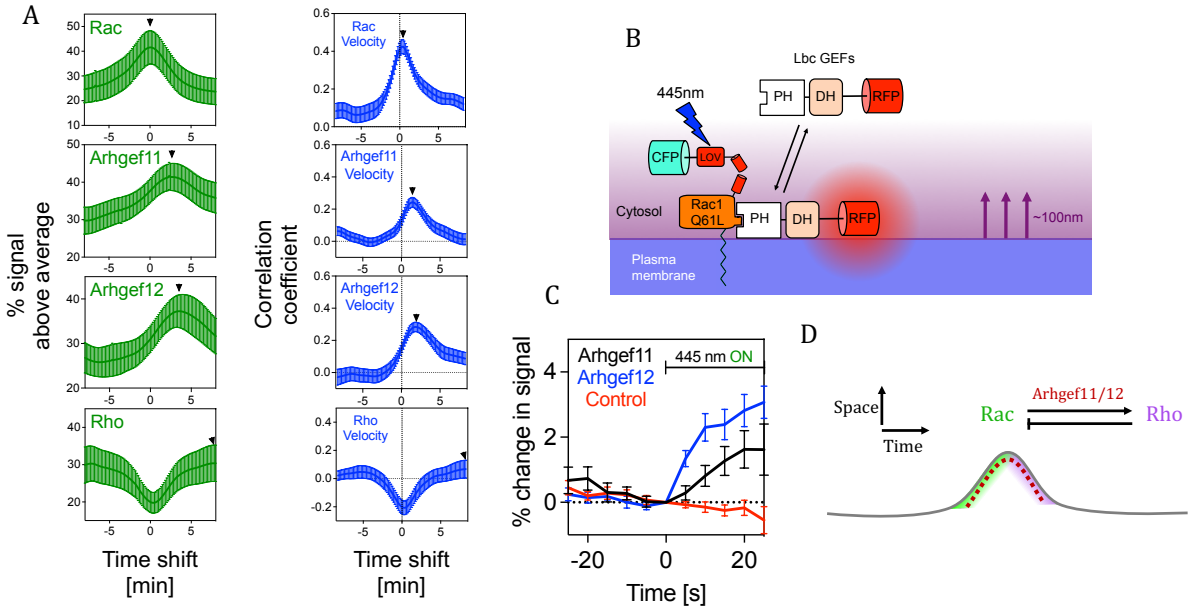

Figure 16. Identification of Arhgef11 and Arhgef12 as Rac effectors in local cell protrusion-retraction cycles. A: Direct comparison of signal enrichment of active Rac, Arhgef11, Arhgef12 and active Rho relative to the time-period of cell protrusion. Black arrows indicate the time point of maximal sensor or GEF enrichment. B: Schematic representation of the optogenetic strategy to

investigate Lbc-type GEF recruitment by active Rac1. C: Measurement of Lbc-type GEF and control construct recruitment during acute Rac activation starting at t=0s, n=3 independent experiments with >35 cells per condition. D: Schematic for enrichment of active Rac, active Rho and Arhgef11/12 in protrusion-retraction cycles. Experimental conditions: A: delCMV-mCherry-GEF constructs, delCMV-mCherry-3xp67Phox (Rac sensor) or delCMV-mCherry-2xRTKN-GBD (Rho sensor) were co-expressed with delCMV-mCitrine in A431 cells. B-C: CMV-mCerrulean-PA-Rac1 and CMV-mCherry-GEF constructs were co-expressed in A431 cells. Photoactivation of Rac1 was performed using 30% of 445nm laser power with a 10,000x neutral density filter. Error bars represent standard error of the mean.

Direct comparison of the temporal sequence of enrichment events in protrusions shows that Rac is maximal in cell protrusions with a minimal delay (~0s), which was followed by enrichment of Arhgef11 (~160s) and Arhgef12 (~210s), and finally active Rho (>470s) (Figure 16 A). Cross-correlation functions between GTPase/GEF activity and cell velocity showed the same temporal sequence of events. These observations further supported the possible role of Arhgef11 and Arhgef12 in mediating Rac-Rho activity crosstalk in A431 cells.

To directly investigate the causal link between these molecules, PA-Rac1 mediated perturbation was combined with measurements of Arhgef11/12 plasma membrane recruitment in A431 cells (Figure 16B-C; Experiments performed in collaboration with PhD student Arya Sachan). During photoactivation of PA-Rac1 in A431 cells, a strong enrichment of both Arhgef11 and Arhgef12 was observed in A431 cells. These observations further suggests that Arhgef11/12 are able to mediate Rac-Rho activity crosstalk in A431 cells. This PA-Rac1 mediated GEF recruitment was also observed in U2OS cells, where Arhgef11, Arhgef12 and in addition AKAP13 were found to be recruited to the plasma membrane by active Rac (see Apendix 3.1).

1.3.7 Regulation of protrusion-retraction cycles by Arhgef11 and Arhgef12 in A431 cells

A431 cells generate frequent recurring protrusion-retraction cycles that result in an exploratory mode of migration. We hypothesized that the Arhgef11/12 mediated crosstalk between Rac and Rho could play a role in stimulating these protrusion-retraction cycle dynamics in A431 cells. To address this hypothesis we measured, how the

duration of protrusion-retraction cycles is altered by varying the expression levels of Arhgef11 and Arhgef12 in A431 cells (Figure 17).

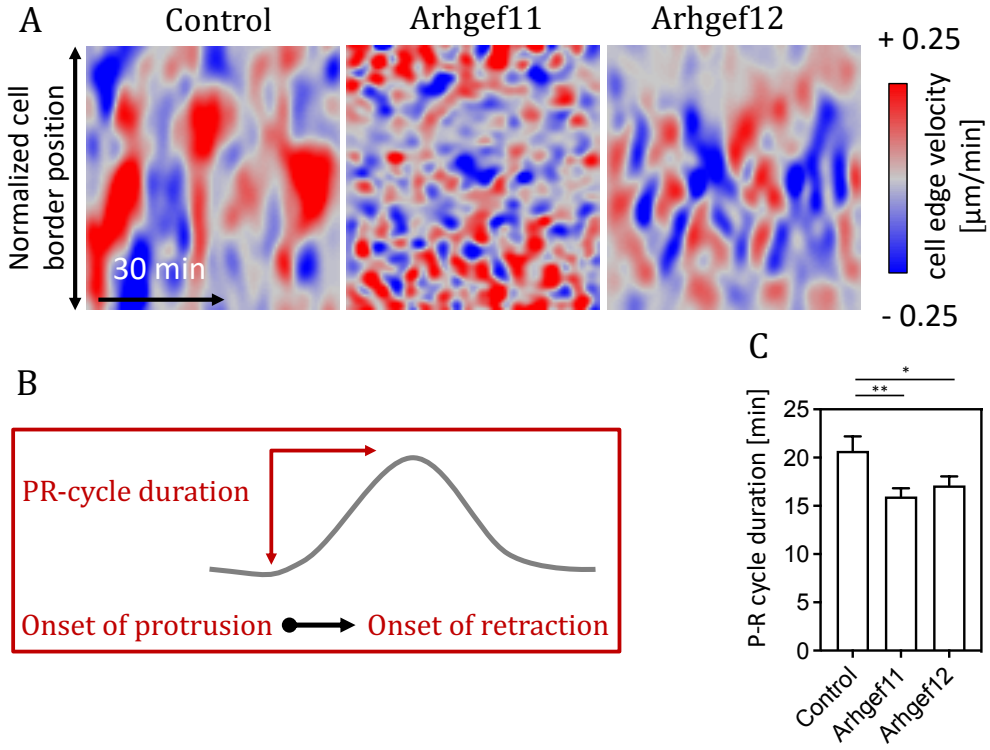

Figure 17. Arhgef11 and Arhgef12 stimulate Rac-dependent Rho activation and the spatio-temporal coordination of local cell protrusion-retraction cycles. A: Cell edge velocity maps of representative cells co-expressing a cell filler and Arhgef11/12 or mCherry control. B: For protrusion-retraction length measurement the duration from the onset of protrusion to the onset of retraction was measured. C: Quantification of P-R cycle length. Compared to mCherry control, a higher level of Arhgef11/12 induced by ectopic expression of these GEFs in A431 cells caused a shorter duration of protrusion-retraction cycles. Experimental conditions: delCMV-mCherry (control), CMV-mCherry-Arhgef11 or CMV-mCherry-Arhgef12 was co-expressed with delCMV-mCitrine in A431 cells. n=3 independent experiments with >26 cells per condition. Error bars represent standard error of the mean. (*: P<0.05; **: P<0.01; ***: P<0.001; ****: P<0.0001; One-way ANOVA). Images were recorded at a frame rate of 1.5/min.

Compared to the control condition, a higher level of Arhgef11/12 obtained via ectopic expression of these GEFs, lead to shorter protrusion-retraction cycles (Figure 17C). In contrast, reducing the endogenous Arhgef11/12 levels via siRNA mediated knockdown lead to an increase in protrusion-retraction duration (Figure18C). This suggests that

Arhgef11/12 can coordinate protrusion-retraction cycles in space and time by coupling Rac induced protrusion and Rho-induced retraction.

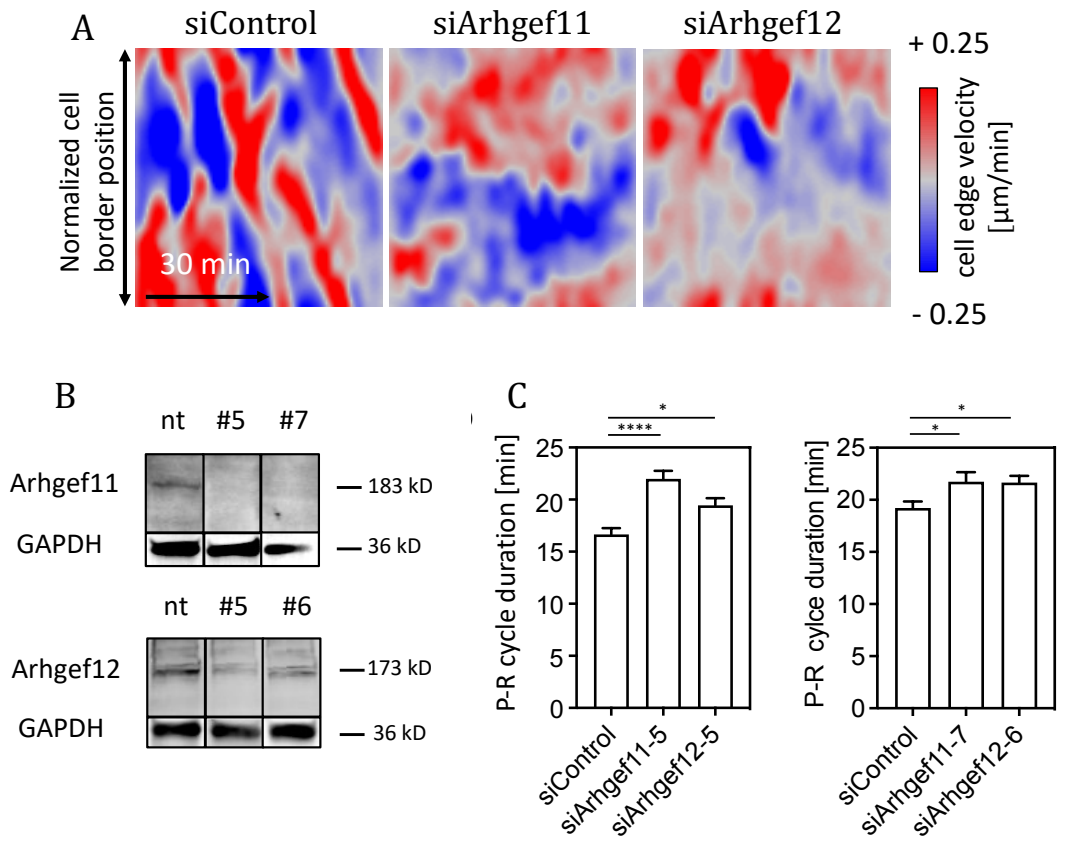

Figure 18. Arhgef11 and Arhgef12 are required for efficient Rac-dependent Rho activation and the spatio-temporal coordination of local cell protrusion-retraction cycles. A: Cell edge velocity maps of representative cells transfected with siRNA and expressing delCMV-mCherry. B: Quantification of Arhgef11/12 knockdown via Western blot analysis. A representative blot is shown (n=3 independent repetitions). Quantification of knockdown efficiency: 83±15% for Arhgef11-5, 75±11% for Arhgef12-5, 80±10.3% for Arhgef11-7 and 70±16.7% for Arhgef12-6 (percent ± standard error of the mean). C: Quantification of protrusion-retraction cycle duration based on cell edge velocity measurements of cells after knockdown of Arhgef11/12. n=3 independent experiments with >105 cells per condition. Error bars represent standard error of the mean. (*: P<0.05; **: P<0.01; ***: P<0.001; ****: P<0.0001; One-way ANOVA). Images were recorded at a frame rate of 1.5/min.

1.3.8 Regulation of directional cell migration by Arhgef11 and Arhgef12 in A431 cells

To investigate how Arhgef11/12 coordinated protrusion-retraction cycles regulate cell migration, individual migrating cells were tracked in combination with Arhgef11/12 knockdown in A431 cells (Figure 19). Measurements of the total migration distance revealed a significant decrease in migration distance after Arhgef11/12 knockdown. In contrast, measurements of cell displacement showed no significant effect of Arhgef12 knockdown. This suggests that migration directionality is increased, while the instantaneous movements of cells are not affected. Indeed, quantification of the directionality ratio showed a significant increase after Arhgef11/12 knockdown.

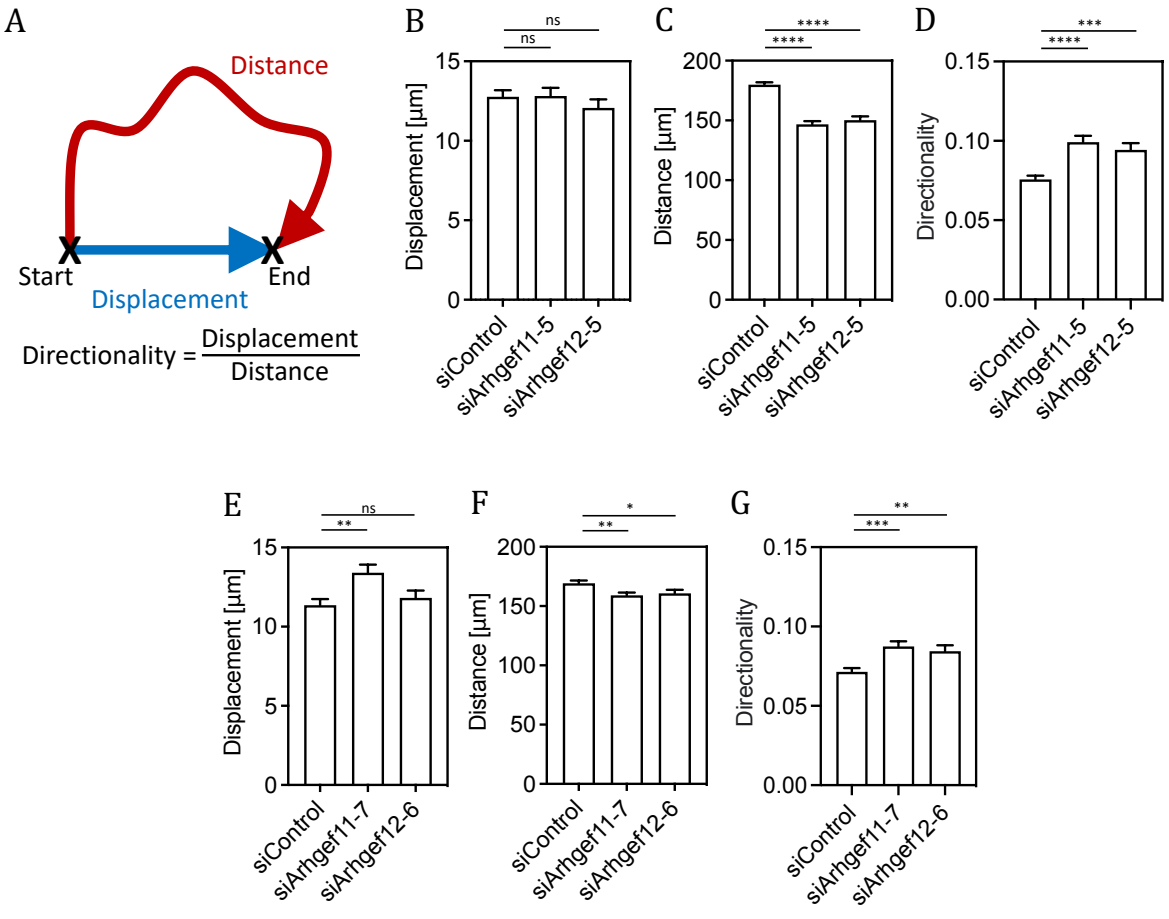

Figure 19. Arhgef11 and Arhgef12 are required for efficient exploratory migration of 431 cells. A: Schematic representation of distance (red) and displacement (blue) for typical spontaneous exploratory cell migration. The distance corresponds to the length of the cell migration trajectory which leads to the indicated displacement between the start and end locations. The directionality is defined as the ratio between these length measurements. B-G:

Quantification of displacement (B,E), distance (C,F) and directionality (D,G) of A431 cell trajectories over a 4h time period in control and Arhgef11/Arhgef12 depleted cells (n=3 independent experiments with >491 cells per condition). (*: P<0.05; **: P<0.01; ***: P<0.001; ****: P<0.0001; One-way ANOVA). Images were recorded at a frame rate of 1/min.

1.4 Discussion

Rac,1 RhoA and Cdc42 are three key GTPases studied for their role in remodeling of the cytoskeleton. As summarized in section 1.1.5.1-1.1.5-3 and Figure 5, these GTPases are central components of signal transduction excitation networks (STEN) that can generate pulses, burst and waves of activity inside cells. Such excitable networks are thought to be interconnected with other cellular systems to modulate cell function (Iglesias and Devreotes, 2012). Concerning cell protrusion, several excitable systems were proposed to be linked (Iglesias and Devreotes, 2012). Based on this idea, a cytoskeleton excitable network (CEN), in which the actin regulator Hem1 forms positive and negative feedback loops with filamentous actin is connected to a signal transduction excitable network (STEN) that involves Ras and/or Rap GTPases. Rac is thought to link the STEN to the CEN network. Modulation of the threshold of the STEN by upstream signals was proposed to regulate local cell morphodynamics during migration (Miao et al, 2019).

Concerning cell contraction, a similar system was uncovered, which combines features of the STEN and CEN in a single, relatively simple system: Here, the signal network component Rho forms positive and negative feedback loops with the cytoskeletal component myosin (Graessl et al 2017; Kamps et al, 2020). How the cell protrusion system interacts with cell contraction or retraction is less clear. In a screen of the Dehmelt lab for potential crosstalk between the major Rho GTPases, activation of the protrusion regulator Rac1 induced a strong activity response of the retraction regulator Rho. In this thesis, this crosstalk, and its potential role in the spatio-temporal coordination of cell protrusion and retraction in cell migration was investigated.

1.4.1 TIRF based translocation activity sensors for small GTPases.

To investigate the spatio-temporal pattering of the key GTPases in the STEN and CEN networks of mammalian cells, highly sensitive activity sensors were developed for Rac, Rho, Rap, and Ras. These small GTPases are very well known for their roles in cell migration, cell growth and proliferation. Various methods have been developed to study the localization and activity dynamics of these GTPases inside living cells. Although these methods can provide useful information, several discrepancies concerning GTPase

activity patterns were observed. For example, a sensor construct based on the Ras-binding domain of Raf that was developed by Bondeva et al, 2002 and Chiu et al, 2002 reported activity in perinuclear structures and in plasma membrane ruffles upon ectopic expression of H-Ras in CHO cells. Measurements based on the FRET-based Raichu probes showed Ras activity selectively at the plasma membrane and Rap activity selectively at the perinuclear sites in EGF treated COS cells (Mochizuki et al, 2001). Work done by Biovana et al, 2004 showed Rap activity selectively at the plasma membrane using a translocation based Rap1 sensor.

Several important points have to be considered for the design of useful GTPase activity sensor constructs. Currently, two distinct sensor design strategies are most frequently used: Single chain FRET sensors and translocation-based sensors. In the FRET sensor design, the wild type GTPase and an effector binding domain are fused together with two fluorophores in a single protein chain. The GTPase in the sensor construct is modulated by GEF and GAP activity inside cells, which leads to a change in its interaction with the effector domain and a conformational change of the sensor that alters FRET efficiency. Therefore, these sensors do not directly report the activity patterns of endogenous GTPases, but rather report the ratio between GEF and GAP activity inside cells. Furthermore, due to their complex multi-functional design and relatively large size, the subcellular localization of the sensors does not correspond to the localization of the wild-type GTPase. It was therefore suggested that some of the discrepancies between studies could be explained by FRET sensors being mis-localized to subcellular regions in which the endogenous GTPase is not found (de Seze et al, 2023). Expression of FRET constructs that contain the wild type GTPase can further create an intracellular imbalance in the ratio between GTPases and GDIs, which can skew the endogenous GTPase localization and activity patterns (de Seze et al, 2023). Translocation-based sensors on the other hand are simply based on the GTPase-binding domain of a specific GTPase effector linked to a fluorescent protein, and they report the local activity of GTPases by being translocated to its subcellular location from the cytosol. One potential problem in this approach is that the ectopic overexpression of the effector binding domain can compete with endogenous effectors and might thereby act as a dominant negative modulator of its function or affect its regulation in signal networks. To minimize this concern, Graessl et al, 2017 incorporated the use of the very weak delCMV promoter to express the GTPase binding domain at very low levels, along with highly sensitive monitoring of sensor translocation

to the plasma membrane via TIRF microscopy. The main advantage of this approach is that it enables measurements of endogenous GTPase activity patterns. A disadvantage is that activity patterns can only be investigated at the plasma membrane. In the case of Rho, Ras and Rap GTPases, the plasma membrane is however thought to be the major site of action, in particular concerning dynamic cell shape changes. Therefore, the combination of translocation-based sensors with weak expression and TIRF microscopy is particularly suitable to study GTPase activity patterns at the plasma membrane of living cells (Graessl et al, 2017). The design for GTPase sensors in this thesis therefore followed the same strategy.

These translocation-based sensors showed interesting activity patterns that were not previously observed in mammalian cells. The activity sensor for Rap showed two distinct activity patterns: First, activity waves and pulses near central cell attachment areas, and second, a local enrichment at the cell periphery during protrusion. The effector binding domain used for the Rap sensor, RalGDS-GBD, interacts with all isoforms of Rap, albeit with different affinities. The two different localized activity patterns that are reported by the sensor could therefore be specific to different isoforms of Rap or could arise from different modes of Rap activity regulation at central cell attachment areas and at cell periphery.

The cRaf-GBD based Ras activity sensors preferentially showed activity waves and pulses near central cell attachment areas and no noticeable enrichment at the cell periphery. This could either be due to a weak sensitivity of the Ras sensor for the endogenous Ras, or actually point to a difference in the function of Ras vs Rap GTPases. Ras is typically understood to play a central role in the regulation of cell proliferation, which is a function that affects the cell as a whole (Drosten et al, 2010). In contrast, Rap is thought to play important roles in the regulation of cell adhesion, which has to be controlled more locally, in particular during cell migration (Lin et al, 2010).

The new Rac and Rho activity sensors that include tandem GTPase binding domains, reported a strong enrichment of GTPase activity in protrusions and retractions, respectively. This was not observed with previous sensors that were based on single GTPase binding domains. Interestingly, the new Ras, Rap, Rac and Rho activity sensors all showed pulsatile activity patterns in central cell attachment areas, suggesting a general theme that might be associated with their proposed regulation via positive and negative feedback loops and the resulting excitable system dynamics.

1.4.2 Protrusion coupled Rac and retraction coupled Rho activity patterns in protrusion-retraction cycles.

Based on biochemical data that was collected for several decades, the mechanism, how Rac can stimulate actin polymerization during cell protrusion is very well understood. Conversely, many biochemical studies have established the mechanism for how Rho can stimulate myosin activation during cell retraction. According to this, several studies based on FRET sensors support the idea that Rac activity is associated with lamellipodial protrusion events (Fritz et al, 2015; Itoh et al, 2002; Komatsu et al, 2011; Miskolci et al, 2016; Moshfegh et al, 2014; Shcherbakova et al, 2018). Measurements based on FRET sensors also support a role of Rho in the trailing end of small migrating neutrophil cells (Wong et al, 2006). Nevertheless, studies of more dynamic protrusion-retraction cycles that were based on FRET activity sensors proposed unexpected activity dynamics of these GTPases that were in contradiction to the prior biochemical understanding. In particular, active Rho was found at lamellipodia and membrane ruffles at the cell front, which are typically associated with Rac activity (Kurokawa et al, 2005; Pertz et al, 2006). Furthermore, based on FRET sensor measurements, Machacek et al, 2009 reported that Rho activity was maximal during protrusion, and that Rac activity was maximal during retraction events, which is opposite to their biochemical function and opposite to the findings reported in this thesis (Figure 20).

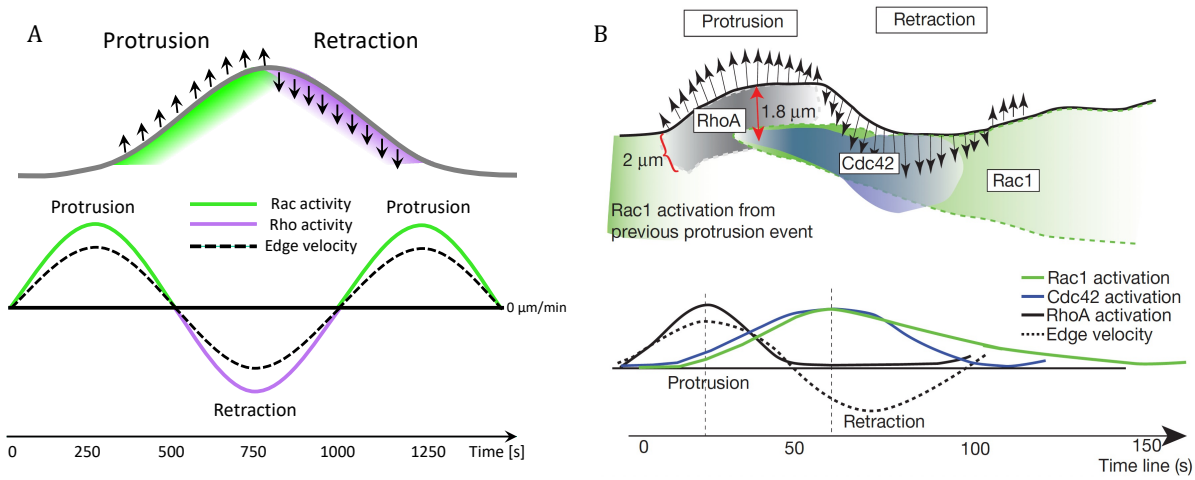

Figure 20. Spatio-temporal pattering of Rac and Rho activity in protrusion-retraction cycles. A: Spatio-temporal pattering of Rac and Rho and its tight coupling to cell protrusion and

retraction events. Bottom: Schematic representation of Rac and Rho activity, as well as cell edge velocity. B: Schemes corresponding to A, which summarize previous observations obtained via FRET sensors, which come to the opposite conclusion compared to this thesis. suggesting coupling of RhoA with that of protrusion events, and Cdc42 and Rac1 with that of retraction events (from Machacek et al, 2009).

Contrary to these unexpected observations in Machacek et al, 2009, the Rac and Rho activity patterns that were observed in this thesis were closely coupled with protrusion and retraction events, respectively. The activity dynamics that were observed in this thesis are therefore also in agreement with previous biochemical studies. The primary difference between the work presented in this thesis and that of Machacek et al, 2009 lies with the different sensors that were used to measure Rac and Rho activity in cells. Two major factors might play a role: First, the FRET sensors used by Machacek et al, 2009, detect the ratio between local GEF vs GAP activity, while the translocation sensors directly detect the localization of the active GTPase. Second, the FRET-based Rho activity sensor was recently suggested to be mis-localized in cells, which could lead to false signals (de Seze et al, 2023). While the endogenous GTPase is primarily localized to the cytosol and then translocated to the plasma membrane during its activation, the FRET sensor is already enriched at the plasma membrane, both during protrusion and retraction, even without activating signals. Thus, the FRET sensor is pre-enriched in cell protrusions, where it could detect a positive ratio of Rho GEFs vs Rho GAPs, while the endogenous, cytosolic GTPase might not be able to access these regulators.

1.4.3 Role of Arhgef11/12 in exploratory cell migration.

The tight coupling between Rac with cell protrusion and Rho with cell retraction suggested that crosstalk between these signal molecules could play a role in coordinating cell protrusion-retraction cycles. To investigate this idea, it was necessary to gain a deeper understanding of the mechanism, by which Rac is able to activate Rho in cells. Out of several candidates, members of the Lbc family of RhoGEFs were found to be strong candidates as mediators of this crosstalk. The Lbc family spans 7 family members, of which Arhgef11 and Arhgef12 were strongly enriched in protrusion-retraction cycles in migrating A431 cells. The maximal enrichment of Arhgef11 and Arhgef12 overlapped

both with maximal Rac and Rho enrichment in protrusions and retractions respectively, which further supports this idea. A causal relationship between Rac1 and these Rho GEFs was shown by combining perturbations using photoactivable Rac1 with measurements of Arhgef11 and Arhgef12 plasma membrane enrichment. Together with the well-known ability of these regulators to activate Rho, these findings strongly suggests that Arhgef11/12 can mediate Rac1 induced Rho activation.

Based on the original hypothesis proposed in this thesis, Arhgef11 (aka PDZ-RhoGEF) and Arhgef12 (aka LARG) could be recruited by active Rac1 by an interaction between the PH domain of the GEF and active Rac1 (Dada et al, 2018). However, Arhgef11 and Arhgef12 are multifunctional, multidomain proteins that could also be recruited to Rac1-stimulated cell areas via other mechanisms. For example, Arhgef11 and Arhgef12 are Rho GEFs containing an RGS homology (RH) domain (Figure 21) via which they can interact with the $G\alpha_{12/13}$ subunits of GPCRs at the plasma membrane (Suzuki et al, 2003). Furthermore, one study suggested that Arhgef11 contains an actin-binding domain (Banerjee et al, 2009). Thus, active Rac could also trigger signals that could participate in the recruitment and activation of Arhgef11 and Arhgef12 to the plasma membrane.

Results obtained in this thesis show that the expression levels of Arhgef11 and Arhgef12 are strongly coupled with protrusion-retraction dynamics in A431 cells. Higher levels of GEFs reduced protrusion-retraction cycle length, presumably by enhancing Rac-Rho crosstalk. Conversely, lower levels of these GEFs increased the protrusion-retraction cycle length, presumably by weakening Rac-Rho crosstalk. In addition, lower GEF levels lead to more directional cell migration, suggesting that Arhgef11/12 are essential for the highly dynamic exploratory cell migration of A431 cells.

These findings are supported by previous studies that investigated the association between Arhgef11 and Arhgef12 expression levels with developmental processes and cellular pathologies. Cell invasion in glioblastoma multiforme is associated with increased levels of both Arhgef11 (Ding et al, 2018) and Arhgef12 (Ding et al, 2020). Depletion of Arhgef11 or Arhgef12, or inhibition of RhoA or RhoC on the other hand inhibits glioma cell migration (Ding et al, 2018, 2020; Danen et al, 2005). A higher expression level of Arhgef11 has also been associated with metastatic hepatoma cell lines (Du et al, 2020), and other cancer related systems, such as colon cancer cells (Patel et al, 2014) and human

epithelial ovarian cancer (EOC) (Tocci et al, 2014). Taken together, these results suggests that these GEFs are associated with a random mode of cell migration during cell invasion.

In this thesis, we observed much stronger effects of Arhgef11 knockdown or overexpression on protrusion-retraction cycles, compared to that of Arhgef12. This difference is supported by previous studies, which show that Arhgef11 has significantly higher GEF activity for RhoA compared to Arhgef12 (Patel et al, 2014). Furthermore, ectopic expression of Arhgef11 also stimulated much stronger Rho activity dynamics compared to Arhgef12 in U2OS cells (see Appendix 3.1).

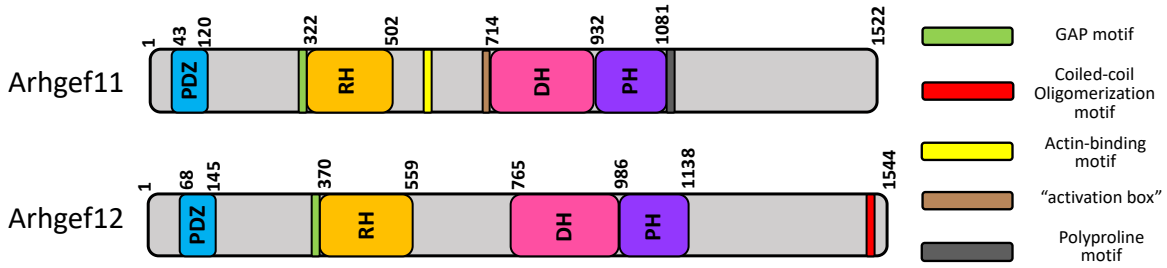

Figure 21. Domain structure of Arhgef11 and Arhgef12. Based on Aittaleb et al, 2014.

Both Arhgef11 and Arhgef12 are known to be regulated by a large-scale conformational change. In their inactive form, they are suggested to be in a closed conformation, unable to activate Rho, until they interact with Gα subunit at the plasma membrane via their RH domains. Binding to the Gα subunit allows for a conformational change that frees their DH domain and allows for Rho activation (Chen et al, 2008). It is therefore likely that additional signals are required to mediate Rac/Rho activity crosstalk in cells. How and if these signals are linked to Rac activity is unclear.

Arhgef11 and Arhgef12 are also known to form homo-oligomers and hetero-oligomers via their C-terminal sequences. Deletion of the c-terminal region significantly enhances their GEF activity *in vivo,* unleashing their full activity potential, suggesting that oligomerization maintains a lower GEF activity levels inside cells (Chikumi et al, 2004). The Arhgef11/Arhgef12 dimer was further shown to be present in a multi GEF complex involving another GEF PLEKHG4B. PLEKHG4B is a GEF for Cdc42. Binding of PLEKHG4B with Arhgef11/Arhgef12 dimers enhances its GEF activity for Cdc42. PLEKHG4B, when bound to Arhgef11/12, acts as an inhibitor to their GEF activity for Rho. PLEKHG4B also inhibits Rho activation via inhibiting interaction of Arhgef11 and Arhgef12 with $G\alpha_{12/13}$

subunits (Müller et al, 2020). As Cdc42 is primarily a regulator of cell protrusion, this mechanism might contribute to the switch-like change in cell protrusion and retraction and associated Rac and Rho signals observed in this study.

In conclusion, Arhgef11 and Arhgef12 were found to be enriched during cell protrusion-retraction cycles in migrating cells, where they can stimulate Rac1-Rho activity crosstalk and cell morphodynamics. Additional interactions of Arhgef11 and Arhgef12 with Cdc42 might play a role in the timing of Rac/Rho activity crosstalk. Furthermore, links to Ras and Rap GTPases and upstream signals might play a role in modulating the spatio-temporal organization of protrusion-retraction cycles to steer the direction of exploratory cell migration (Figure 22).

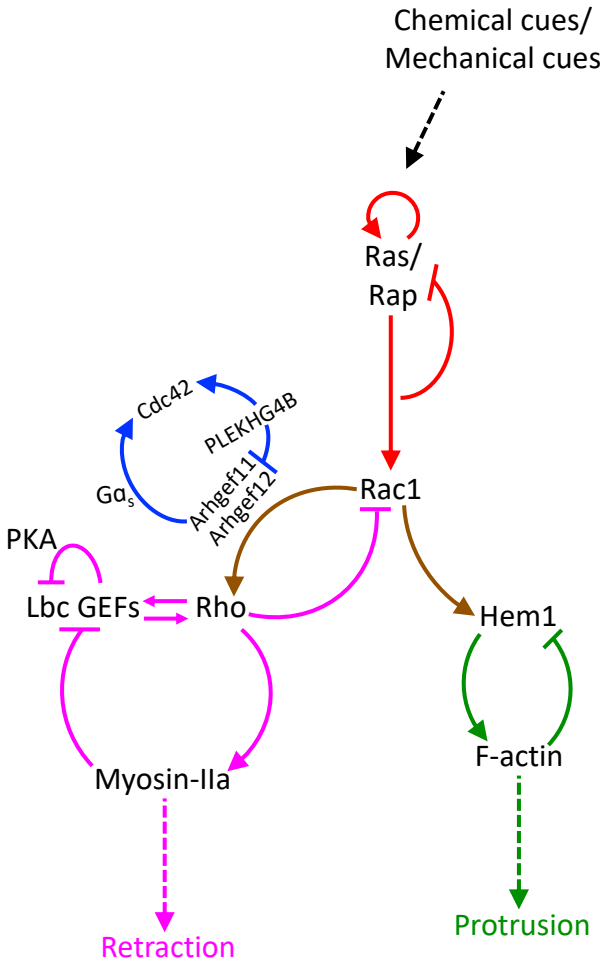

Figure 22. Signaling network underlying cell migration. **Rac** mediated interactions between **STEN,** **CEN** and contractility networks, with additional modulations of the crosstalk mediators, regulating protrusion and retraction events during cell migration.

2. Investigation of signal network dynamics at the plasma membrane of living cells using programmable RNA-based scaffolds.

2.1 Introduction

2.1.1 Complexity in signaling networks.

Intracellular signal proteins are central to many physiological processes in cells. For example, cells respond to various chemical or mechanical stimuli by activating signal molecules which relay information via effector molecules to generate an appropriate response. Signal molecules are typically interconnected via complex networks, which can process and integrate information to compute a measured response to complex, multi-modal input signals (Azeloglu and Iyengar, 2015).

Such signal networks can generate complex dynamics, which arise from multiple interdependent interactions between individual network components. Experimental investigations of such systems are therefore challenging, as a single component often does not adequately represent the state of the network. One way to approach the complex relationship between the signaling components is to first quantify simple binary relationships between two components, and to investigate their dynamic spatio-temporal interactions. Subsequently, several of these binary relationships can be combined to predict the dynamics of a larger and more complex system. Such a strategy can be particularly successful in the analysis of simple, hierarchical relationships between signal components, which correspond to simple cause and effect relationships. However, if feedback loops are present in such systems, cause and effect relationships are less clear, and individual components can act both downstream and upstream of each other. Such systems are less amenable to this simple approach (Weng et al, 1999). Methods that allow simultaneous readout of multiple relationships enable a more direct insight into the state of such interconnected signal networks (Kamps and Dehmelt, 2017).

An additional level of complexity is added to signal networks by compartmentalization and regional organization within cells. For example, many signal networks have components which can interact with the plasma membrane. Activity-dependent shuttling of these molecules between the cytosol and the plasma membrane, combined with diffusion, can generate local activity patterns that only affect sub-regions of cells. (Bhalla, 2004).

Analysis of such complex signaling networks has been facilitated by combining experimental investigations with theoretical approaches. Experimental measurements of protein interactions can provide critical knowledge about the activity state of signal network components and their relationships with other components (Weng et al, 1999). This information can then be used to generate models for how signal network components interact with each other. Computational simulations can be used to investigate the dynamic properties of such models. Reciprocal cycles of experimental investigations and theoretical analyses can lead to a better understanding of the system dynamics and how it is linked to cell function.

2.1.2 Relationship between Protein interactions and signal network activity state.

Molecular interactions inside cells are the basis to all cellular processes. Proteins play a particularly important role, as they perform the majority of specialized functions due to their versatile amino acid-based structure. In signal networks, proteins can change their state, which can then lead to a change in the structure of their conformation. Often, such state changes also lead to a modulation of interactions, which can then be measured experimentally. One example is the activity-dependent interaction of small GTPases with GTPase-binding domains of their effectors, which was extensively implemented in part 1 of this thesis to study the dynamics of Ras and Rho family small GTPases in cells. With protein-protein interactions being an essential aspects of signal transduction in signaling networks, various methods have been developed to study them (de Las Rivas and Fontanillo, 2010).

Such methods include *in vitro* methods like affinity purification, pull-down assays, and co-immunoprecipitation (co-IP), which rely on stable and strong interactions between proteins. They provide a snapshot of a probable interaction between two molecules inside the cell, disregarding their possible subcellular compartmentalization or their

regulation via transient interactions. A commonly used *in vivo* method to study protein-protein interaction is the yeast-two hybrid system. This system is based on the protein-interaction mediated reconstitution of a split transcription factor, which is read out as a survival signal (Young, 1998). The yeast-two hybrid system was used very successfully to identify previously known interactions via screening approaches. However, the method is also limited, as it is based on a rather artificial localization of the interaction to the yeast nucleus, which can differ quite significantly from the natural location of proteins of interest.

To study protein interaction more directly in their natural environment of mammalian cells, microscopy-based approaches were developed, which enable readout of protein interactions or protein conformational changes based on fluorescence intensity changes. This includes translocation sensors, analogous to those described in part 1 of this thesis, or methods in which the proximity of two fluorophores is monitored by measuring Förster resonance energy transfer (FRET) (Margineanu et al, 2016) (see also section 1.1.7).

2.1.3 Simultaneous monitoring of multiple protein interactions inside living cells

As discussed in section 2.1.1, it is difficult to investigate complex signal networks that contain feedback loops by measuring the activity state or the interaction dynamics of a single network component. By visualizing multiple protein interaction dynamics together in a living cell, complex feedback-mediated relationships can be deduced more directly. One experimental limitation of the commonly used translocation-based sensors or FRET approaches is due to the spectral properties of typical fluorescent proteins. To monitor multiple interactions in parallel, these approaches involve simultaneous imaging of multiple fluorescent proteins. Due to the broad excitation and emission spectra of these fluorophores, fluorescence-based methods like FRET imaging are limited in the choice of orthogonal donor-acceptor pairs (Shaner et al, 2007; Roquemore, 2020). Typical FRET approaches are based on only one donor-acceptor pair, which can be extended to two pairs with additional experimental effort (Roebroek et al, 2021).
To overcome such limitations, the Dehmelt lab developed a protein interaction array inside living cells, which enabled simultaneous measurements of multiple protein-

protein interaction using a limited number of spectrally available fluorophores. In this method, protein interactions were distinguished based on positional information in a defined regular pattern of intracellular proteins that were arranged by an extracellular pattern of ligands. This method relied on so-called bait presenting artificial receptor constructs, or bait-PARCs, which transferred the extracellular ligand pattern into a corresponding intracellular pattern of distinct bait proteins. The interaction of a fluorescently labeled prey protein with this bait protein pattern was monitored via TIRF microscopy. This method enabled measurements of the activation dynamics of multiple protein-kinase A isoforms in parallel inside a single living cell (Gandor et al, 2013). A drawback of the method was the challenging generation of a regular ligand array with subcellular dimensions, which required sophisticated techniques, such as Dip-Pen Nanolithography (DPN) and of DNA-directed immobilization. Furthermore, the development of distinct bait-PARCs that are functionalized with bait proteins of interest was more challenging than anticipated due to misfolding of artificial receptors during processing in the secretory pathway. In particular, scaling down the feature size of ligand patterns via DPN was challenging, which limited the number of protein-protein interactions that could be measured in parallel.

2.1.4 RNA scaffold-based multiplex sensors for protein interactions inside living cells

To overcome such limitations, the Dehmelt lab developed a related technique to monitor multiple protein-protein interactions in cells, based on a random array of RNA based scaffolds. The RNA scaffold molecules were designed to locally concentrate cytosolic bait proteins to monitor their interaction dynamics with a soluble prey molecule. The scaffolds were genetically encoded and contain recognition sequences for RNA biding proteins for their functionalization (Figure 23). They were immobilized at the plasma membrane via a variant of the bait-PARC artificial receptors to enable prolonged detection of the bait protein and its interaction with the prey over prolonged periods of time. To ensure their stability, RNA scaffolds were derived from a stable mRNA construct that includes a 5' UTR and a 3' UTR with an SV40 polyA signal. The RNA scaffolds contain a very short coding region to prevent interference of the ribosome with the scaffold functionalization in the 3' UTR of the RNA scaffold. The functionalization was based on several RNA binding motifs, which include the orthogonal RNA-protein binding pairs

MS2-MCP, PP7-PCP and PUM-NRE. 3 Novel pumilio proteins with 9 binding repeats (9RPUM), and associated binding sites, were generated to extend combinatorial functionalization, and to show that additional orthogonal biding motifs are feasible based on the programmable design of pumilio proteins.

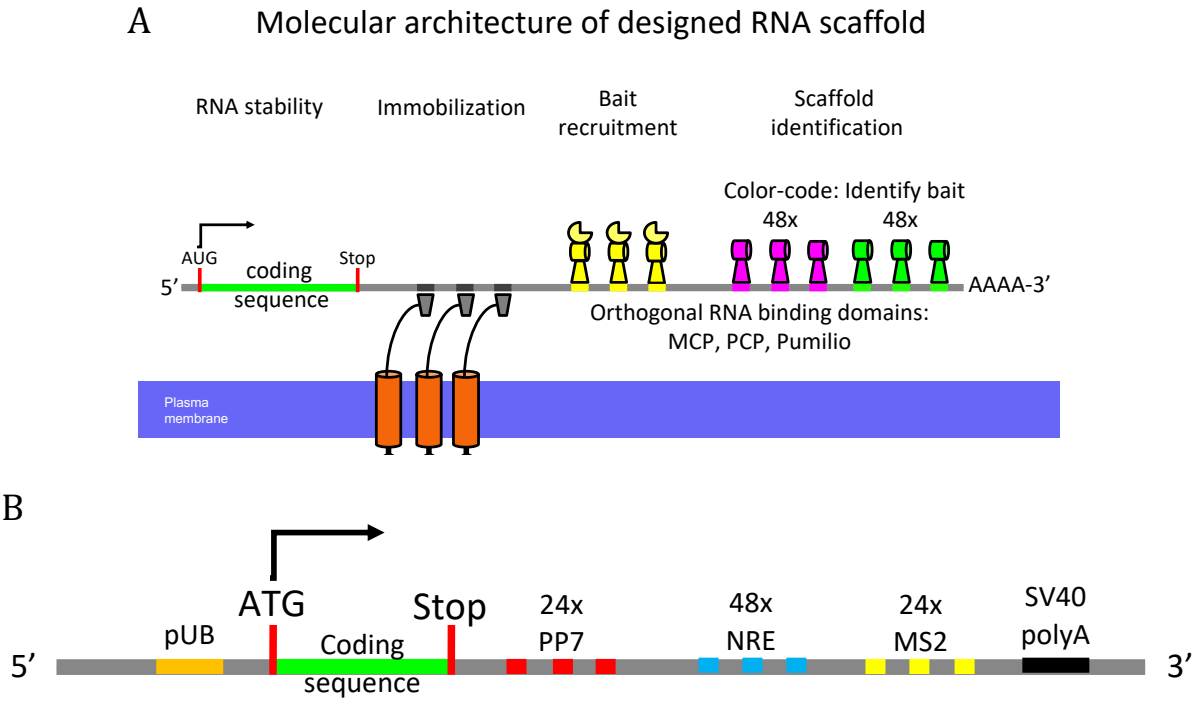

Figure 23. A: Molecular architecture of RNA scaffolds. Functionalized regions of the RNA scaffolds ensure stability, immobilization, bait recruitment and scaffold identification. B: Arrangement of orthogonal binding sites on the plasmid DNA which encodes the RNA scaffold molecule.

For analysis of protein interactions, up to 48 tandem repeats of RNA binding domains were introduced to ensure a high signal-to-noise ratio for measurement of fluorescent signals. The functionalized landmarks on the RNA scaffolds included binding sites for bait molecules, functionalized sites for bar-coding of scaffolds, and sites for immobilization of RNA scaffolds with artificial receptors for stable and long binding at the plasma membrane. The region for bar-coding enables the distinction between different scaffolds based on combinatorial fluorophore mixtures, which can exceed the number of fluorescent proteins that can typically be distinguished via standard microscopy techniques.

2.2 Objectives

This section of the thesis contributed to several aspects in the development of novel RNA scaffold-based multiplex activity sensors:

- Development of additional bar-coding methods for RNA scaffolds.
- Development of an RNA scaffold-based method to measure protein kinase A activity.
- Development of an RNA scaffold-based method to measure small GTPase activity dynamics.

2.3 Results

The RNA scaffold-based multiplex activity sensors were developed in a collaborative project together with the PhD student Dominic Kamps and Masters students Olga Jost, Stephanie Gossen, Eva-Maria Thüring, Jessica Spindler and Lukas Liven Grebe in the Dehmelt lab. The focus of the thesis of Dominic Kamps[1] was the development of orthogonal Pumilio-RNA binding motifs for extended scaffold functionalization and a proof of principle for distinguishing multiple RNA scaffolds via bar-coding. The focus of this thesis[2] was to extend the scope of bar-coding by capitalizing on additional features of fluorescently labeled RNA binding proteins, and to establish proof of principle sensors for monitoring the activity of protein kinase A or small GTPases Ras/Rap and Rac/Rho.

The general design of mRNA scaffolds was based on mRNAs that contain tandem PP7, MS2 and NRE binding sites. The initial construct was based on the TRICK sensor (Halstead et al, 2015), which already contained tandem PP7 and MS2 sites. The NRE binding repeats were introduced into a new RNA sequence, which was designed by the NUPACK algorithm (Fornace et al, 2022) to have minimal secondary structures. The RNA scaffolds used in this thesis were either strongly or weakly immobilized at the plasma membrane of cells via slowly diffusion artificial receptors or via more rapidly diffusing CAAX-box based membrane anchors.

2.3.1 Bar-coding of RNA scaffolds

The initial proof-of-concept for bar-coding of RNA scaffolds was based on combining two fluorescent molecules with distinct excitation/emission spectra. The initial experiments used mixtures of mTurquoise2 and mCherry to distinguish three different RNA scaffolds: those that contain only one of the two, or both fluorophores (PhD thesis of Dominic Kamps and Masters thesis of Eva-Maria Thüring). In theory, these two fluorophores can be used to distinguish 4 different scaffolds, and using a combination of three fluorophores would be sufficient to distinguish 9 different RNA scaffolds. At the current stage of the

[1] with support from Master's students Olga Jost, Stephanie Gossen and Eva-Maria Thüring
[2] with support from Master's students Jessica Spindler and Lukas Liven Grebe

project, only the presence or absence of fluorophores was used for bar-coding. By detecting different ratios of fluorophores, the number of RNA scaffolds that can be distinguished could be further increased. In this thesis, two alternative ways to increase this number were investigated, which are based on photoactivatable fluorophores and on the kinetics of RNA-binding protein domains.

2.3.1.1 Bar-coding of RNA scaffolds using photoactivable fluorophores

In principle, bar-coding of RNA scaffolds could use any detectable property that distinguishes two fluorescent proteins. The excitation and emission spectra are a particular obvious property. In addition, various fluorescent proteins were also developed which can change their spectral properties after illumination with a particular wavelength. This includes reversibly photo-switching of a single wavelength in proteins such as rsEGFP, photoconversion between two distinct wavelengths in proteins such as mEos3.1, or efficient photoactivation of a single wavelength in proteins such as PA-mCherry (Durisic et al, 2014). PAmCherry, derived from mCherry, contains a substitution of 10 amino acids and lacks fluorescence in its inactive OFF state (Subach et al, 2009). This makes it an interesting candidate to be used along with the normal mCherry fluorophore for bar-coding. In such a coding scheme, two RNA scaffolds could be distinguished based on a single wavelength, one of which only binds mCherry, and the other only PA-mCherry1, by virtue of controlled photoactivation. The challenge of this approach is the ability to detect individual scaffold molecules inside cells via the PA-mCherry fluorophore. Earlier experiments suggested that only those fluorophores work adequately in this assay which are particularly bright, fold very efficiently and do not tend to form oligomers. To test if RNA scaffolds can be functionalized with a photoactivatable fluorophore a PCP fused PA-mCherry1 construct was generated and used together with MCP fused to mCitrine. Here[3], both constructs were transfected together along with two RNA scaffolds, one of which only displayed MCP binding sites, and the other only displayed PCP binding sites. While the mCitrine functionalized scaffolds were visible from the start, the PA-mCherry functionalized scaffolds were only detected after activation of PA-mCherry by a short pulse of near UV light. These experiments therefore offer a proof-

[3] in experiments performed by Bachelor's student Alina Perne under my supervision

of-concept for a bar-coding strategy that incorporates photoactivatable fluorophores (Figure 24).

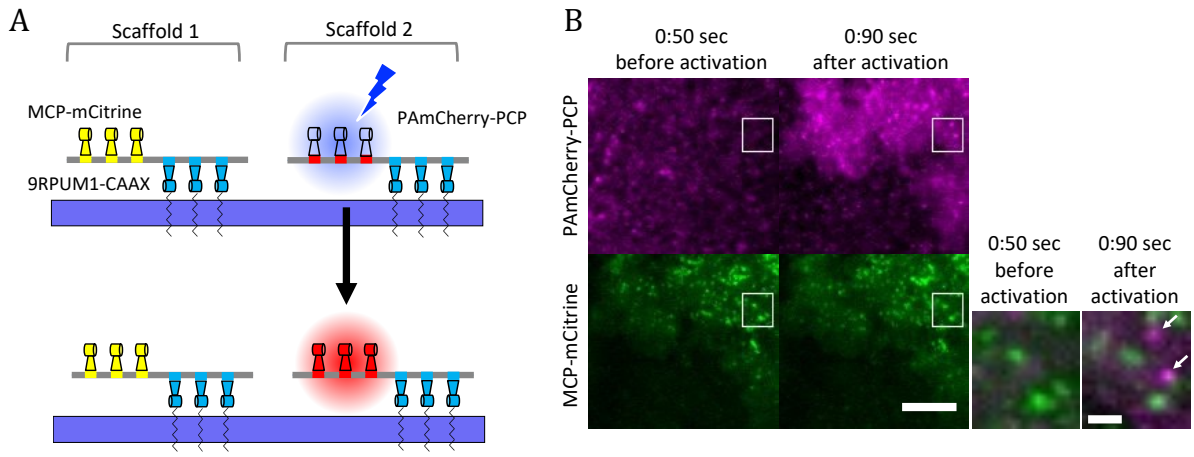

Figure 24. Proof-of-concept for bar-coding of RNA scaffolds via the photoactivatable fluorophore PA-mCherry. A: Schematic of the design of PA-mCherry-PCP based detection of two RNA scaffolds in parallel inside COS7 cells. B: Representative TIRF images depicting signals from MCP and PCP bound to two different RNA scaffolds. After photoactivation of PA-mCherry, the PCP containing RNA scaffolds were observed in the same cell as the MCP-mCitrine containing scaffolds. Experimental conditions: CMV-9RPUM1-CAAX, delCMV-PAmCherry-PCP, delCMV-MCP-mCitrine, pUB-STOP- 48x9xPUM-24xPP7-0xMS2 and pUB-STOP-48x9xPUM-0xPP7-24xMS2 were co-transfected into COS7 cells. Scale bar:10µm, 5 µm (inlet). Images were taken with a frame rate of 12/min.

2.3.1.2 Bar-coding of RNA scaffolds based on differences in the MCP/PCP RNA interaction kinetics.

MCP and PCP coat proteins share only 15% sequence identity. MCP binds to the cognate MS2 RNA hairpin structure with an affinity of ~ 5 nM (Carey et al, 1983), whereas PCP binds to the corresponding PP7 hairpin with an affinity of ~1nM (Lim et al, 2001). Although these binding affinities are quite similar, the interaction kinetics of these proteins with the RNA structure might differ. We hypothesized that such a difference might be detectable experimentally and could therefore be employed for bar-coding of RNA scaffolds. To test this idea, the fluorescence recovery after photobleaching (FRAP) was quantified for MCP and PCP on individual RNA scaffolds molecules.

The measurement of the recovery half-time of MCP-mCherry and mCherry-PCP revealed a surprisingly large difference in their interaction kinetics with RNA (Figure 27). With a half-time $t_{1/2}$=399.256s, the MCP-mCherry MS2 interaction was about 40 times more stable compared to the mCherry-PCP PP7 interaction ($t_{1/2}$=10.223s) (Figure 25). Furthermore, in the majority of measurements, this difference in the recovery kinetics was also detectable at the level of individual scaffolds. This shows that RNA scaffolds can indeed be bar-coded based on differences in the interaction dynamics of these RNA binding proteins.

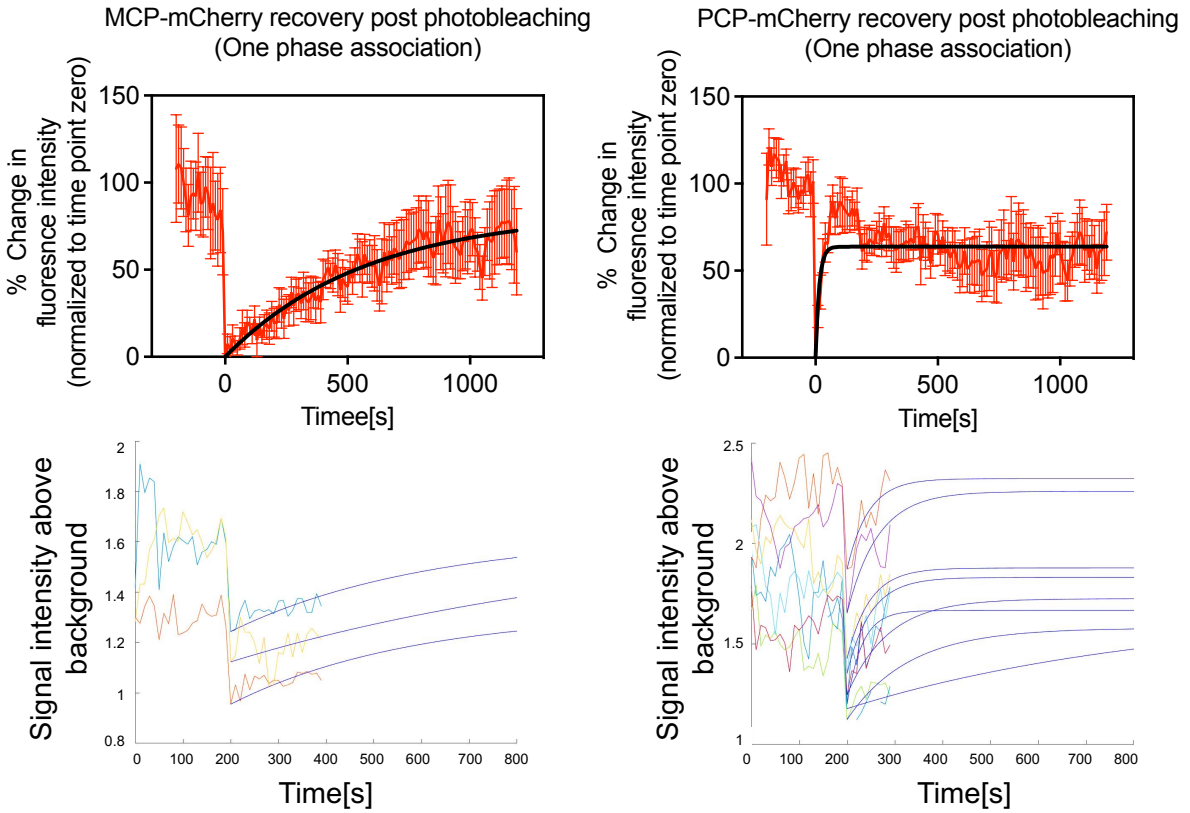

Figure 25. Bar-coding based on the interaction kinetics between RNA binding proteins and their cognate recognition motifs. Average profiles of mCherry-PCP and MCP-mCherry recruitment to RNA scaffolds after photobleaching. The half-time was determined by fitting an exponential one phase association function to the data. Experimental conditions: COS7 cells were co-transfected with pUB_STOP_12xPP7-48x(9-PUM-Repeats)-24xMS2, CMV-mTurquoise2-9R-PUM1-CAAX and either delCMV-mCherry-PCP or delCMV-MCP-mCherry. Cells were bleached with 100% laser intensity (561nm) at time point zero(0), followed by which the recovery of fluorophores on the scaffolds was recorded. Scaffolds were identified and tracked over time via mTurquoise2 fluorescence.

2.3.2 Monitoring of protein interactions via RNA scaffolds.

The main application of the programmable RNA scaffolds is to monitor the dynamics of protein interactions that report on the activity state of signal networks in cells. As a first proof-of-concept, the well-established interaction between the regulatory and catalytic subunits of the cAMP-dependent protein kinase A was implemented, which was already used in the previous multiplex sensors by Gandor et al, 2013. Subsequently, sensors for the Rho and Ras/Rap families of small GTPases were developed, which can be used to study the signal networks that control cell migration related to Part 1 of this thesis.

2.3.2.1 Monitoring Protein kinase-A activity dynamics via RNA scaffolds.

The cAMP-dependent protein kinase PKA is a serine/threonine kinase which is regulated by the local cellular concentration of the second messenger cAMP. Depending on its context within cells or tissues, PKA is involved in various functions, including regulation of long-term memory by the cAMP response element-binding protein CREB (Horiuchi et al, 2008), regulation of glycogenesis in myocytes (Palm et al, 2013), and regulation of protrusion-retraction cycles in migrating cells (Tkachenko et al, 2011).
The inactive PKA holoenzyme is a tetramer which consist of two regulatory subunits with binding sites CNB-A and CNB-B for two cAMP molecules, and two catalytic subunits. The catalytic subunits harbor the kinase activity. The regulatory subunit has a dimerization/docking (D/D) domain via which it forms homodimers. The D/D domain also interacts with A kinase anchoring proteins, which target PKA to specific subcellular regions. cAMP molecules interact with the regulatory subunits in a cooperative manner, leading to a conformational change of the holoenzyme and the release of catalytic subunit. Inside the cell, activity dynamics of PKA is regulated by cAMP concentration, which itself is regulated by adenylyl cyclase and phosphodiesterase. Adenylyl cyclase catalyzes cAMP production from ATP downstream of G-protein coupled receptors. cAMP production is limited by Phosphodiesterases, which convert cAMP to AMP (Torres-Quesada et al, 2017; Zhand et al, 2012).

To study the activity dynamics of PKA in cells, RNA scaffolds were designed to incorporate the regulatory subunit RII-β fused with MCP as the bait molecule. The

mCherry tagged Cat-α subunit was used as prey. PKA activation on the RNA scaffolds was controlled by pharmacological stimulation of cAMP production by stimulating adenylyl cyclase activity by Forskolin and inhibition of phosphodiesterases by IBMX (3-isobutyl-1-methylxanthine) (Chen et al, 1998). In resting cells, the RII-β presenting RNA scaffolds were observed to be bound to the mCherry fused catalytic subunit. Pharmacological stimulation of cAMP led to a rapid decrease in the Cat-α signal on RNA scaffolds. The interaction of the catalytic subunit was quickly recovered on the RNA scaffolds after Forskolin/IBMX washout (Figure 26).

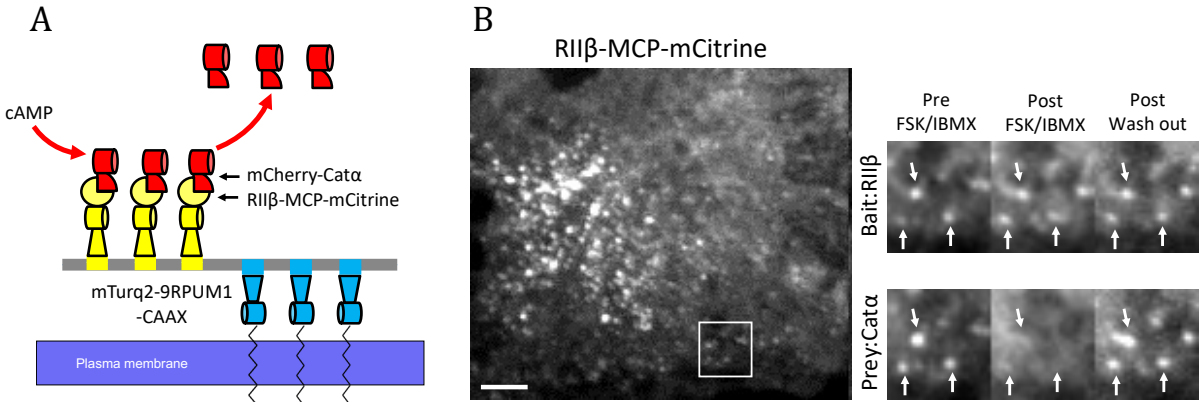

Figure 26. Protein kinase A activity dynamics on RNA scaffolds. A: Schematic for cAMP mediated PKA activation on RNA scaffolds. B: Representative TIRF image depicting signals from RIIβ-MCP-mCitrine bound to RNA scaffolds. Bait-prey interaction dynamics on RNA scaffolds in cells which were stimulated with 25uM forskolin and 100uM IBMX. Enlarged images (right panels) correspond to the white ROI (left panel) . Experimental conditions: CMV-mTurquoise-9R-PUM1-CAAX, delCMV-RIIβ-MCP-mCitrine, delCMV-mCherry-Cat-α and pUB_STOP_12xPP7-48x(9-PUM-Repeats)-24xMS2 were co-transfected in COS7 cells. Scale bar:10µm.

Several distinct isoforms of the PKA regulatory subunit exist, including RIα, RIIα, RIβ and RIIβ (Turnham and Scott, 2016). After establishing a proof-of-concept for monitoring the interaction dynamics for the catalytic subunit Cat-α and the RIIβ regulatory subunit[4], RNA scaffold based PKA sensors were adapted to measure interactions with multiple regulatory subunits in a single living cell. To do this, 9RPUM1 and MCP were used to recruit RIα and RIIβ subunits on two distinct RNA scaffolds, one with binding sites for 9RPUM1 and PCP and the other with binding sites for MCP and PCP (Figure 27A). PCP

[4] performed by Jessica Spindler, who conducted her Master's thesis under my supervision.

was used to immobilize both RNA scaffolds at the plasma membrane via a PCP fused artificial receptor.

The two different RNA scaffolds were distinguished via the two distinct fluorophores targeted to the RNA scaffolds. Pharmacological stimulation led to a rapid decrease in the Cat-α prey signal from both baits. Measurements of the activation kinetics for both the bait molecules showed a small difference in their activation kinetics.

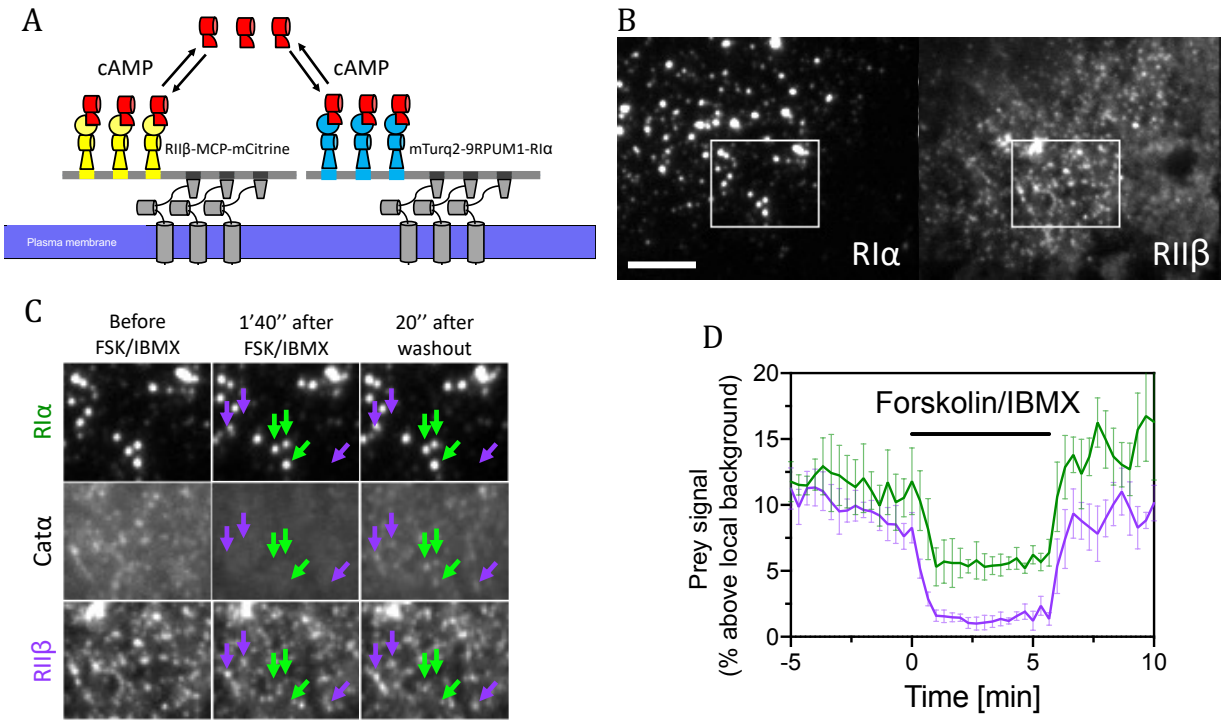

Figure 27. Protein kinase A activity dynamics based on RI and RIIβ measured in parallel on RNA scaffolds. A: Schematic description of cAMP mediated parallel measurement of the interaction kinetics of Cat-α with RIα and RIIβ on RNA scaffolds. B: Representative TIRF image depicting signals from RIIβ-MCP-mCitrine and mTurq2-9RPUM1-RIα bound to RNA scaffolds. C: Interaction dynamics of Cat-α with RIα and RIIβ on RNA scaffolds before, during and after stimulation with 25uM forskolin and 100uM IBMX. Panels correspond to the white ROI in B. D: Quantification of the interaction dynamics. Recruitment of Cat-α to RIIβ (t1/2=19.15s) was faster than to RIα (t1/2=23.85s). Experimental conditions: COS-7 cells were co-transfected with Dimerizer-PARC-CCL-moxBFP-PCP, delCMV-9R-PUM1-mTurq-hPRKAR1A_CAAX, delCMV-mCherry-hPRKACA, delCMV-hPRKAR2B-MCP-mCitrine, pUB_STOP-48x9RPUM1-24xPP7-0xMS2 and pUB_STOP_12xPP7-24xMS2. Scale bar:10µm

2.3.2.2 Monitoring GTPase activity dynamics via RNA scaffolds.

Small GTPases play a central role in various cellular processes. The members of the Ras/Rap subfamily are particularly well known for their role in cell growth regulation, while members of the Rho subfamily are well known for their role in cell morphodynamics. As shown in Part 1 of this thesis, the activity dynamics of these GTPases can effectively be studied via GTPase binding domains (GDBs) of effector molecules, which selectively interact with the active form of the GTPases. GBDs typically have a strong preference for the active GTPase, however, they often have similar affinity to highly related GTPases within subfamilies.

2.3.2.2.1 RNA scaffold-based sensors for Ras/Rap family GTPases.

Various Ras and Rap GTPases share some of their effector molecules, including cRaf, albeit with different binding affinities (Raaijmakers and Bos, 2009). For certain applications, this lack of specificity can also be an advantage. We therefore tested if the cRaf-GBD can be used to measure activity dynamics of Ras or Rap isoforms on RNA scaffolds. First, sensors were developed to measure the activity dynamics of individual isoforms of Ras or Rap on RNA scaffolds. MCP fused mCitrine was used to recruit the Ras isoform HRas as a bait protein to the RNA scaffolds. In the experiments, it was not necessary to add a separate functionalization to RNA scaffolds for their immobilization at the plasma membrane. Instead, RNA scaffold immobilization was based on the CAAX box of the wt GTPase molecules, which are present in the C-terminus of these molecules. In this configuration, Ras and Rap isoforms are expected to localize to the plasma membrane like their endogenous counterparts. To increase the affinity of the cRaf-GBD for small GTPases, a tandem GBD sensor with two GBDs fused to mCherry was used. The cRaf-GBD sensor was used as prey together with HRas on scaffolds as bait. Post stimulation of overnight starved COS7 cells with 100ng/ml EGF, a rapid increase in the prey recruitment to HRas was observed on RNA scaffolds (Figure 28).

Analogously, the Rap isoform Rap1a was used as a bait molecule on RNA scaffolds using MCP fused to mCitrine. Stimulation of COS7 cells with 25uM forskolin and 100uM IBMX, which is known to activate the cAMP-dependent Rap GEF Epac1, showed a strong

recruitment of prey molecules onto the RNA scaffolds (Figure 28). These experiments show that RNA scaffolds can be used to measure activity dynamics of Ras and Rap GTPases inside cells, using 2xcRaf-GBD-mCherry as the prey molecule.

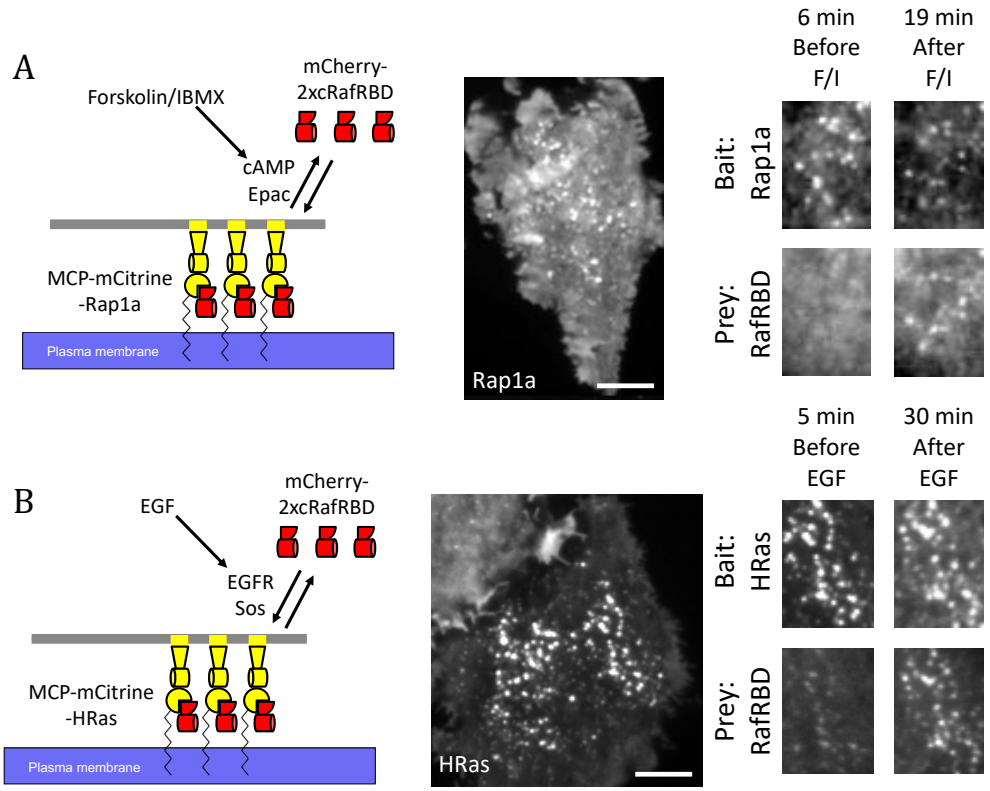

Figure 28. RNA scaffold-based Rap/Ras activity sensors. A and B: Schematic of FSK+IMBX (F/I) or EGF stimulated Rap and Ras activation on RNA scaffolds. For HRas activation, cells were starved for 16 hours before imaging. The cells were then treated with 100ng/ml of EGF during imaging. For Rap1 activation, cells were also starved or 16 hours and treated with 100uM of ddA (Sigma) before imaging to reduce basal cAMP levels. During imaging, cells were stimulated with 25uM forskolin and 100uM IBMX. Ra or Ras served as bait and were enriched on scaffolds via MCP fused to mCitrine. mCherry fused to two tandem repeats of the cRafGBD (2xcRafGBD) was used as prey. COS7 cells were stimulated either with EGF to activate Ras or with cAMP modulating pharmacological compounds to activate Rap. Experimental conditions: COS7 cells were co-transfected with pUB_STOP_12xPP7-48x(9-PUM-Repeats)-24xMS2, delCMV-2xcRafGBD-mCherry and delCMV-MCP-mCitrine-Rap1a (A) or delCMV-MCP-mCitrine-HRas (B). Scale bar:10µm

2.3.2.2.1 RNA scaffold-based sensors for Rho family GTPases.

The Rhotekin-GBD and p67phox-GBD described in Part 1 of this thesis are well studied effector domains of Rho family GTPases. Rhotekin-GBD is able to bind to the three very closely related genes RhoA, RhoB, RhoC, all of which share similar effectors and therefore play very similar roles in cells by stimulating cell retraction and contraction (Eckenstaler et al, 2022). Conversely, the p67phox-GBD is able to bind to the closely related genes Rac1, Rac2 and Rac3 (Haataja et al, 1997), which stimulate cell protrusion.

Knowledge about the selectivity of these domains for the respective GTPases was primarily derived from biochemical studies, which do not necessarily reflect the interaction specificity in cells. Here[5], RNA scaffolds were used to directly investigate the interaction specificity of these GBDs with distinct small GTPases. In a proof-of-concept, RNA scaffolds were designed to recruit the dominant positive GTPase mutants RhoA(Q63L) and Rac1(Q61L) that act as bait. Effector domains specific to either Rho or Rac were co-expressed to act as prey, and their interaction with RhoA and Rac1 functionalized scaffolds was measured in living cells (Figure 29). As expected, these measurements confirmed the specific interaction of the GBD derived from the Rac1 effector p67phox with active Rac1 and not with active RhoA.

[5] performed by Lukas Liven Grebe, who conducted his Master's thesis under my supervision.

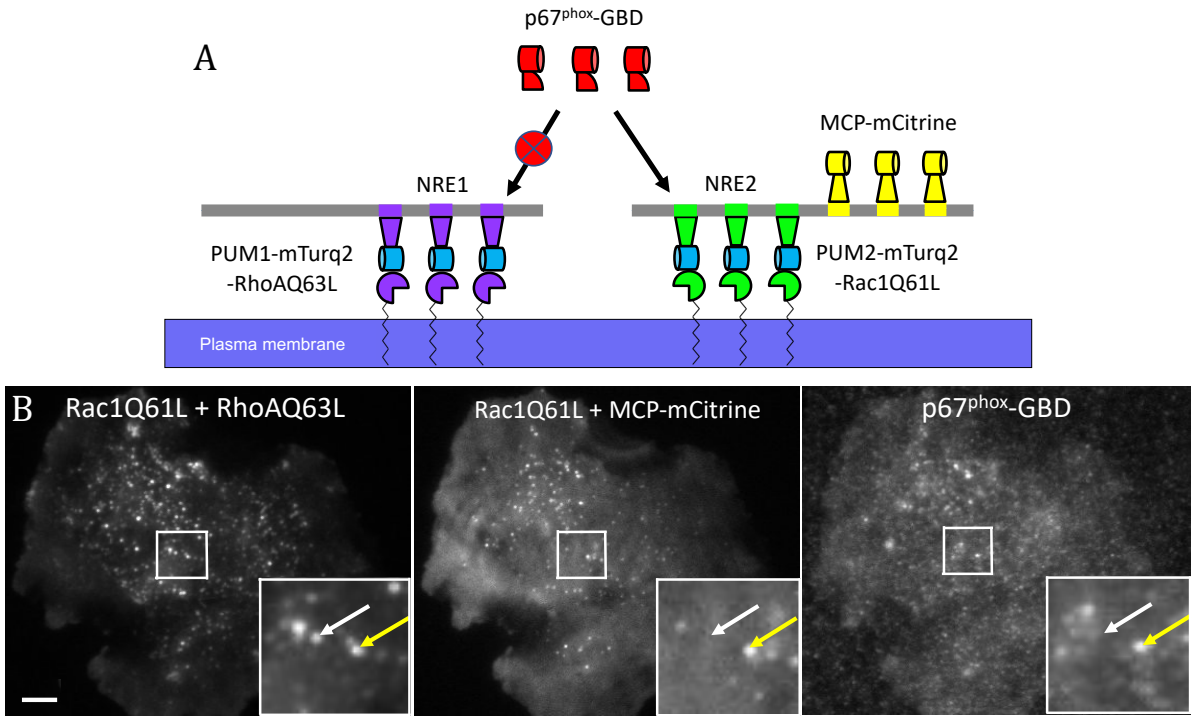

Figure 29. Representative TIRF images of bait protein recruitment on scaffolds. Scaffolds functionalized with mTurq2-RhoA(Q63L) were distinguished from scaffolds functionalized with mTurq2-Rac1(Q61L) based on colocalization of MCP-mCitrine, which served as a bar-code. p67Phox-GBD showed a strong enrichment on scaffolds functionalized with Rac1(Q61L). Experimental conditions: COS7 cells were co-transfected with delCMV-MCP-mCitrine, delCMV-mCherry-2xp67Phox, pUB-STOP_12xPP7_48xPUMDK3_24xMS2, delCMV-PUMDK3-mTurq-Rac1-Q61L, delCMV-9RPUM1-mTurq-RhoA-Q63L and pUB_STOP-48x(9-PUM-Repeats)-24xPP7. Scale bar:10µm

As this effector is well studied, this result was not very surprising. However, the specificity of many other regulators is far less well established. For example, the three isoforms of Rho, RhoA/B/C all interact with the effector Rhotekin, although their affinities were slightly different based on *in vitro* measurements (Eckenstaler et al, 2022; Ito et al, 2018). Here[6], the specificity the Rhotekin GBD was investigated via RNA scaffolds and found that this GBD interacts more strongly with RhoB compared to RhoA (Figure 30). This was contrary to the previous suggestions that Rhotekin would prefer interactions with RhoA and RhoC rather than RhoB (Ito et al, 2018).

[6] performed by Lukas Liven Grebe, who conducted his Master's thesis under my supervision.

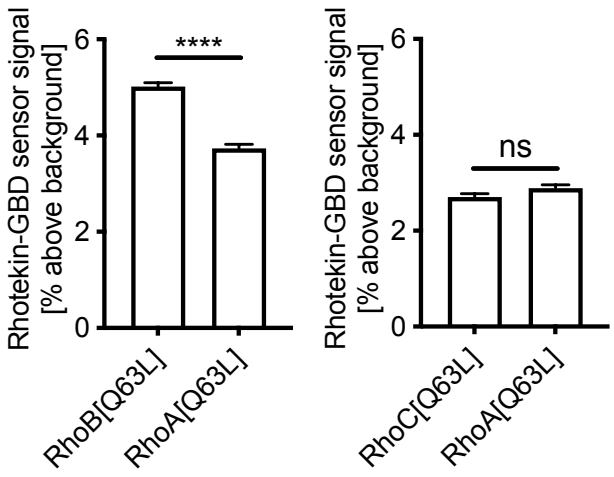

Figure 30. Investigation of preferential binding of the Rhotekin-GBD to distinct Rho isoforms. Plots represent fluorescence signal of the 2xRBD-mCherry recruitment on distinct RNA scaffolds bearing dominant positive form of RhoB and RhoA, or distinct RNA scaffolds bearing dominant positive form of RhoC and RhoA. Experimental conditions: COS7 cells were co-transfected with pUB_STOP_12xPP7-48xPUM1-0xMS2, pUB_STOP_12xPP7-48xPUMDK3-24xMS2 , delCMV-mCherry-2xRhotekin(RBD), delCMV-MCP-mCitrine, delCMV-9RPUM3-mTurq2-RhoAQ63L and delCMV-9RPUM1-mTurq2-RhoBQ3L/delCMV-9RPUM1-mTurq2-RhoCQ3L. Student's t-Test, ns: not significant; *: p<0.05; **: p<0.01; ***: p<0.001; ****: p<0.0001. n=3 independent repeats. Error bars represent standard error of mean.

2.4 Discussion

The RNA scaffold-based method presented in this work provides a proof-of-concept to measure multiple protein-protein interactions in parallel inside a single living cell. The present design of RNA scaffolds involves functionalization using MCP, PCP, 9RPUM1, 9RPUM2 and 9RPUM3 as orthogonal RNA binding proteins. This set could further be extended by incorporating additional RNA binding proteins, for example other 9-repeat pumilio variants, or the N-peptide/boxB system (Chattopadhyay et al, 1995) to increase the number of orthogonal functionalizations that can be incorporated into a single RNA scaffold.

2.4.1 Bar-coding of RNA scaffolds

Bar-coding of RNA scaffolds was previously established in the lab based on two fluorescent proteins with distinct spectral properties, to enable the visualization of three distinct RNA scaffolds inside a single cell (PhD Thesis of Dominic Kamps and Masters Thesis of Eva-Maria Thüring). In this thesis, a photoactivable protein was used to extend the bar-coding options for RNA scaffolds, without the need of additional, distinct spectral properties. Based on this strategy, it should be possible to distinguish RNA scaffolds that only gain fluorescence after a short pulse of UV light from those that are constitutively fluorescent. An additional bar-coding method based on differences in the turn-over rate of the MCP and PCP proteins on RNA scaffolds was proposed that could be read out with measurements of fluorescence recovery after photobleaching (FRAP). If the turn-over rate of other RNA-binding proteins such as the 9R Pumilio domains, is distinct from the MCP and PCP systems, the turnover of these molecules could also be used for bar-coding. In principle, RNA-fluorophore aptamer complexes such as “mango”, “spinach” and “broccoli” could also be employed for bar coding if their fluorescence intensity is high enough on individual RNA scaffold molecules (Braselmann et al, 2020).

2.4.2 Application of RNA scaffold based PKA activity sensors.

Proof-of-principle experiments demonstrate that RNA scaffolds can be used to measure the activation of multiple distinct regulatory PKA subunits together inside a single living

cell. The prey construct used a single catalytic subunit. Using multiple Cata-α units in the tandem could further improve the signal readout.

One potential application of the existing RNA scaffold based PKA sensors could address open questions related to the role of PKA in the regulation of Rho activity. Previous studies in the lab proposed that Rho activity dynamics at the plasma membrane are regulated by a combination of Rho activity amplification via Lbc GEFs like GEF-H1, and slow negative feedback via Myosin-IIa, which sequesters and inhibits GEF-H1 (Graessl et al, 2017). Due to the relatively slow activation of Myosin-IIa, this mechanism can generate Rho activity pulses at the time scale of minutes. As shown in Figure 34 of the Appendix, ectopic expression of AKAP13, another Lbc type GEFs, generates Rho activity pulses with much shorter duration, suggesting an additional mechanism for negative feedback regulation, which is not dependent on the slow Myosin-IIa component. AKAP13 is special among the Lbc type GEFs due to its direct interaction with the regulatory subunit of PKA (Kinderman et al, 2006). Previous studies suggested that PKA might inhibit Rho activity, for example by increasing GDI-mediated plasma membrane extraction either via phosphorylation of Rho GDI or phosphorylation of RhoA, which both increase their affinities for interreacting with each other (Lang et al, 1996; Tkachenko et al, 2011). Based on this idea, a model was proposed, in which negative feedback regulation of Rho activity is mediated by PKA (Tkachenko et al, 2011). However, in this model it is unclear, how PKA could be activated by RhoA. The RhoA activity dependent recruitment of AKAP13 to the plasma membrane might represent this missing link. RNA scaffolds could be used to measure PKA activation and Rho activity simultaneously inside a single living cell. Only three fluorophores would need to be monitored to achieve this: two fluorophores for measuring the cAMP-dependent interaction between RIIβ and Cat-α on RNA scaffolds and one fluorophore on a translocation-based sensor for active Rho. This approach would also offer additional information concerning PKA activity: The RNA scaffold recruitment of Cat-α is independent of endogenous AKAP activity, as it is based on the direct recruitment of the subunit via the RNA binding domain. Furthermore, a deletion of the dimerization domain in this construct also prevents AKAP binding to this bait protein. On the other hand, AKAP dependent recruitment of Cat-α can be monitored in parallel in regions that do not contain the RNA scaffolds. Parallel measurements of

these three activities can therefore help to dissect, how Rho activity, cAMP concentration and AKAP-based Cat-α plasma membrane recruitment are coordinated in space and time.

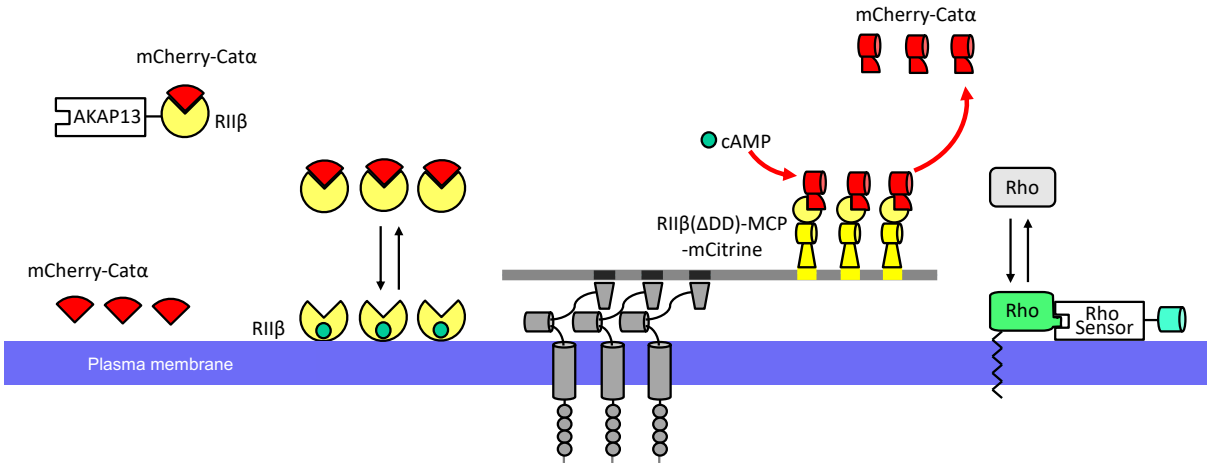

Figure 31. Schematic description for implementation of RNA scaffold for parallel measurements of Rho activity, cAMP concentration and AKAP-based Cat-α plasma membrane recruitment in living cells.

2.4.3 Application of RNA scaffold based GTPase activity sensors.

As a proof-of-principle, the application of RNA scaffolds to determine the specificity of GTPase binding domains (GBDs) of effectors for distinct GTPase family members was demonstrated for the specific binding of the Rac1 effector p67phox to active Rac1 and not to active RhoA, and Rhotekin was found to preferentially bind RhoB and not RhoA and RhoC. These observations confirm the strength of the RNA scaffolds-based method, in which two distinct competitive interactions can be monitored at the same time in the exact same individual cell. Such analyses are not possible with standard methods. For example, FRET based measurements would require two distinct fluorophore pairs. First, parallel imaging of four fluorophores and their FRET signals would be very challenging to perform, and second, the use of distinct fluorophores would make it very difficult to compare these interactions. The experiments performed in this thesis showed that the RNA scaffold method is relatively easy to adapt for new bait proteins. Therefore, measurements as those presented for the competitive interaction between the p67phox GBD and active Rac1 or RhoA would be very powerful for the development and characterization of new, specific translocation-based sensors.

2.4.4 Limitations and further improvements for RNA scaffolds-based sensor.

One limitation of the current design is the sensitivity of the system to observe prey/bait interactions. For the measurements of effector domain specificity, the prey molecules contained two GTPases binding domain (GBD) in tandem to improve sensitivity. Single GBDs showed only very weak signals of the prey molecule on the scaffolds and were therefore less suitable to evaluate smaller differences in selectivity (data not shown). For future implementations, the system could be further optimized. For example, more bait binding sites could be incorporated on the scaffold.

3. Appendix

3.1 Lbc type GEF mediated Rho activity amplification at the plasma membrane

The Lbc type GEFs, which include 7 family members, were previously proposed to amplify RhoA activity at the plasma membrane (Medina et al, 2013). Previous work performed by Grassel et al, 2017 and Kamps et al, 2020 showed that this amplification can lead to Rho activity pulses in the presence of a slower negative feedback and uncovered mechanistic details of Rho amplification at the plasma membrane by two Lbc type GEFs, Arhgef2 and Arhgef12. To further understand the role of these GEFs in modulating Rho activity dynamics, relationship between these GEFs and Rho activity was studied at the plasma membrane of U2OS cells using TIRF microscopy. U2OS cells express a low level of endogenous Lbc type GEFs, which makes them a suitable candidate system to study how their increased levels affect Rho activity dynamics. Overexpression of the Lbc GEFs had quite variable effects on Rho activity dynamics. Enrichment of the Rho activity sensors in activity pulses and waves was used to evaluate Rho amplification. Out of the 7 Lbc type GEFs, Arhgef1, Arhgef11 and Arhgef18 showed the strongest increase in Rho amplification at the plasma membrane (Figure 32).

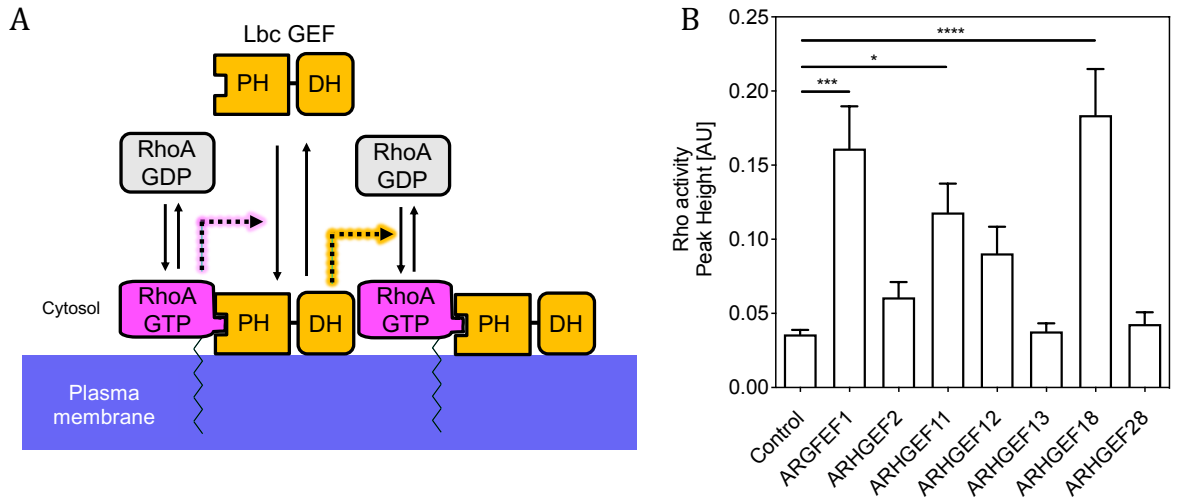

Figure 32. A: Mechanism of Rho activity amplification at the plasma membrane based on Medina et al, 2013. B: Enrichment of Rho activity sensor at the plasma membrane in activity pulses and waves, represented as Rho activity peak height. Experimental conditions: USOS cells were co-transfected with delCMV-mCherry-Rhotekin (GBD) and CMV-mCherry-Lbc-type-GEF. n> 22 cells

from 3 independent repeats. (*: P<0.05; **: P<0.01; ***: P<0.001; ****: P<0.0001; One-way ANOVA). Error bars represents standard error of mean.

To further investigate the relationship between the spatio-temporal patterning of Lbc type GEF plasma membrane recruitment and Rho activity, cross-correlation functions were determined for these signals. All of the GEFs showed a positive correlation with Rho activity, with the Arhgef18-Rho showing the highest crosscorrelation. The majority of Lbc type GEFs generated activity dynamics that are similar to the pulses that were previously observed by Grassel et al, 2017 and Kamps et al, 2020. However, some GEFs induced quite distinct dynamics. For example, the Arhgef1 activity dynamics were characterized by relatively small peaks followed by activity nadirs (Figure 33). These dynamics suggest that Rho or associated mediators might inhibit Arhgef1 recruitment at the plasma membrane. This can also be seen in the Arhgef1-Rho cross-correlation function, which shows correlation at negative time shifts and an anti-correlation with positive time shifts.

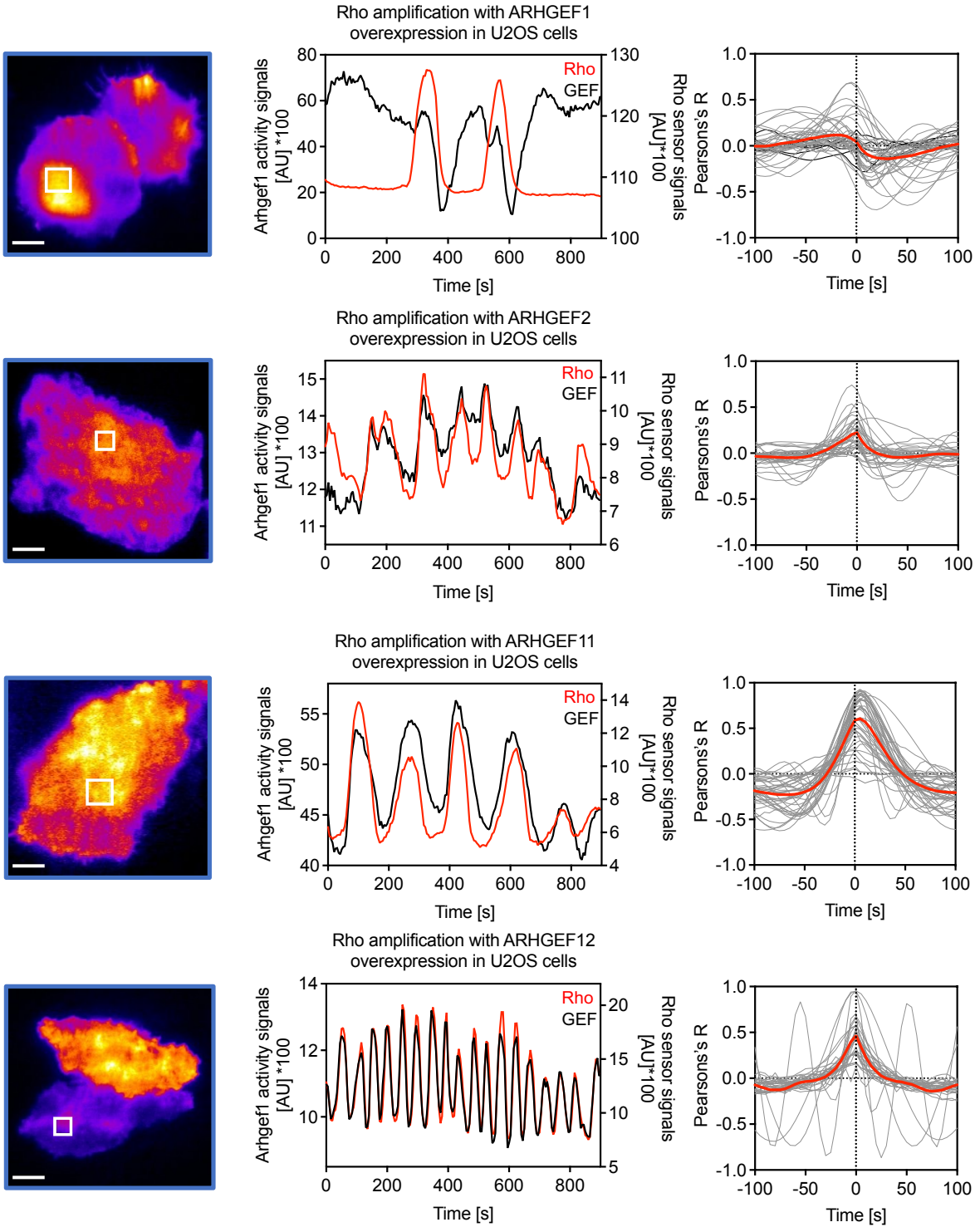
Rho amplification with ARHGEF1 overexpression in U2OS cells
Arhgef1 activity signals [AU] *100
Rho sensor signals [AU]*100
Rho
GEF
Time [s]
Pearson's R
Rho amplification with ARHGEF2 overexpression in U2OS cells
Rho amplification with ARHGEF11 overexpression in U2OS cells
Rho amplification with ARHGEF12 overexpression in U2OS cells

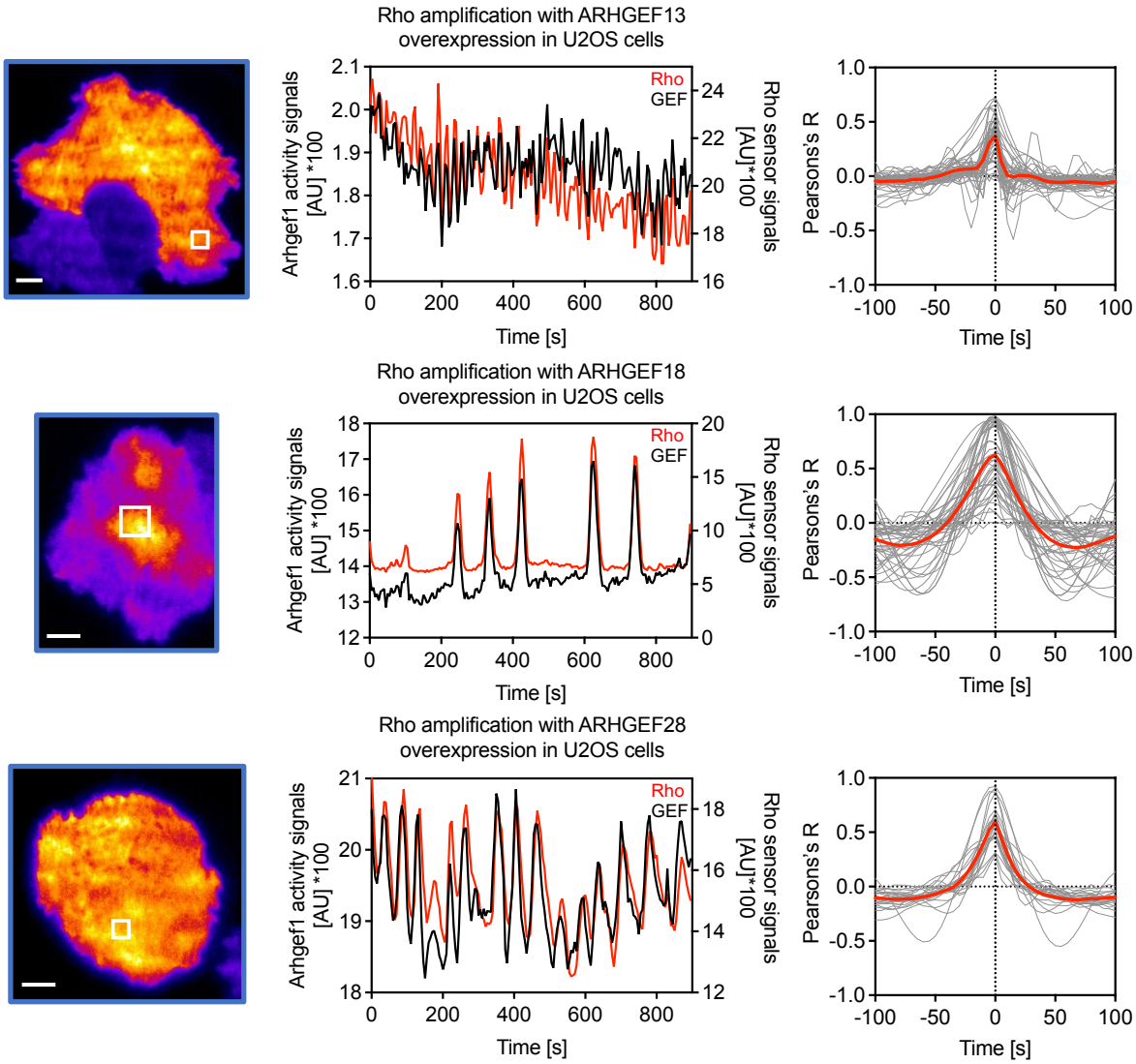

Figure 33. Stimulation of Rho activity dynamics by Lbc type GEFs. Left: Representative TIRF images of the Rho activity sensors in U2OS cells that overexpress individual Lbc type GEFs. Middle: Activity profiles of active Rho and the Lbc type GEF, corresponding to the while ROI in left panels. Right: Crosscorrelation functions with shown in red and data obtained from individual cells shown in grey. Compared to Arhgef11, a shorter peak interval was observed for Arhgef12 and Arhgef13. For Arhgef12, a portion of imaged cells showed very regular pulses in cross-correlation analysis. Furthermore, cross-correlation plots showed a delay in the dynamics for Arhgef11, which suggests a delayed release of Arhgef11 at the plasma membrane compared to Rho. This could occur due to additional interaction sites for Arhgef11 present at the plasma membrane, such as the RH domain which interacts with G-protein coupled receptors (Chen et al, 2008). Experimental conditions: USOS cells were co-transfected with delCMV-mCherry-Rhotekin (RBD) and CMV-mCherry-Lbc-type-GEF. n> 22 cells from 3 independent repeats. (*: P<0.05; **: P<0.01; ***: P<0.001; ****: P<0.0001; One-way ANOVA) Error bars represent standard error of mean.

AKAP13 generated particular short peak intervals. Previous work done by Grassel et al 2017 showed the presence of a delayed negative feedback between Arhegf2 and Myosin-IIa, is critical for the relatively long Rho activity pulse duration. In this work, AKAP13 only weakly amplified Rho activity at the plasma membrane, but nevertheless shows a strong correlation with Rho activity in most cells. The short interpeak interval seen in the AKAP13-simulated Rho activity dynamics suggests the presence of a rapid negative feedback loop that is specifically mediated by AKAP13 to inhibit Rho (see also section 2.4.2 of the Discussion).

4. Materials and Methods

4.1 Instruments and Equipment

Eppendorf research plus pipettes	Eppendorf
Centrifuge tubes (15ml/50ml)	Sarstedt
Nanodrop ND-2000	Thermofischer Scientific
Parafilm®	Bemis
Sarstedt serological pipettes	Sarstedt
Thermomixer compact	Eppendorf
"Vortex Genie 2" touch mixer	Scientific Industries
BioRad Power Pac 300	Bio-Rad Laboratories, Inc.
Centrifuge 5415R	Eppendorf
Centrifuge 5410R	Eppendorf
Odyssey Infrared Imager Clx	Li-Cor® Biosciences
Immobilon-FL PVDF	Millipore, Merck KGaA
8-well LabTek® chambers No. 1.0	ThermoFischer Scientific
35-mm MatTek petri dishes No. 1.5	MatTek Corporation
NUAIRE™ Celgard class II biological safety cabinet	Integra Biosciences
Cell culture dishes (35/60/100 mm)	Sarstedt
Thermocycler, Mastercycler 5341	Eppendorf
Vacusafe comfort Vacuum pump	IBS Integra Bioscience
Purelab flex, Water purification system	Veolia Water
SafeSeal microfuge tubes, 2 ml, 1.5 ml, 0.5ml, 0.1ml	Sarstedt
UVStar 312 nm Gel documentation system	Biometra
SDS – Polyacryl Amide gel electrophoresis system	Bio-rad
Agarose gel electrophoresis system	Bio-rad

Water bath	Kottermann
Mr. Frosty® Cryo 1°C freezing chamber	Thermo scientific
Vacuum pump	IBS Integra Bioscience
Cell culture Incubator	ThermoFischer Scientific

4.2 Biological and Chemical materials

4.2.1 Chemical reagents and kits

Gel Extraction Kit	Qiagen
PCR Purification Kit	Qiagen
Miniprep Kit / Maxiprep Kit	Qiagen
1 kb + DNA Ladder	New England Biolabs
Agarose	Thermofisher Scientific/Roth
dATP/dTTP/dCTP/dGTP	New England Biolabs
dNTP mix	New England Biolabs
DMEM (w Phenol Red)	PAN Biotech / Gibco
DMEM (w/o Phenol Red)	PAN Biotech
DPBS	PAN Biotech
OptiMEM	Gibco
FBS	PAN Biotech
L-Glutamine	PAN Biotech
Trypsin	PAN Biotech
Penicillin/Streptomycin Mix	PAN Biotech
Lipofectamine™ RNAiMAX	Invitrogen
Lipofectamine™ 3000	Invitrogen
Lipofectamine™ 2000	Invitrogen
Fibronectin	341631, Sigma-Aldrich
PEG-8000	Promega
DTT	Fluka Analytical

NAD	New England Biolabs
Q5 High-Fidelity DNA Polymerase	New England Biolabs
T4 DNA ligase	New England Biolabs
T5 Exonuclease	New England Biolabs
Phusion DNA polymerase	New England Biolabs
Taq DNA ligase	New England Biolabs
Restriction enzymes and associated buffers	New England Biolabs

4.2.2 Cell lines and bacterial strains

A431	Epidermoid carcinoma, *Homo sapiens*, ACC-91 (DSMZ)
U2OS	Osteosarcoma, *Homo sapiens*, HTB-96 (DSMZ)
COS-7	Kidney, *Cercopithecus aethiops*, ACC-60 (DSMZ)
Top 10 F– mcrA Δ(mrr-hsdRMS-mcrBC) Φ80lacZΔ M15 Δ lacX74 recA1 araD139 Δ(ara-leu) 7697 galU galK rpsL (StrR) endA1 nupG Λ-	Invitrogen
XL 10 Gold TetR Δ(mcrA)183 Δ(mcrCB-hsdSMR mrr) 173 endA1 supE44 thi-1 recA1 gyrA96 relA1 lac Hte [F' proAB lacIqZ Δ M15 Tn10(TetR) Amy CamR]	Stratagene

4.2.3 Reagent mixes

U2OS culture media	DMEM (Gibco), 10% FBS, 1% Pen/Strp
A431/COS7 culture media	DMEM (PAN Biotech), 10% FBS, 1% Pen/Strp, 1% L-Glutamine
Imaging media	DMEM (w/o Phenol Red), 10% FBS
Isothermal Buffer (5X)	25% PEG-8000, 500mM Tris-HCl (pH 7.5), 50mM MgCl2, 50mM DTT, 1mM dATP, 1mM dTTP, 1mM dCTP, 1mM dGTP, 5mM NAD, H2O
Gibson master mix	100µl Isothermal Buffer (5X), 2µl T5 Exonuclease (1.0 U/µl), 6.25 µl Phusion DNA Polymerase (2 U/µl), 50 µl Taq DNA Ligase (40 U/µl), 375µl H2O

4.2.4 Plasmids used in this thesis.

No.	Lab plasmid no.	Plasmid name	Source
1	100	delCMV-mCherry-Actin	Hannak
2	162	delCMV-mCherry	Abram Calderon
3	163	delCMV-mCitrine	Abram Calderon
4	199	delCMV-mCherry-p67phox	Abram Calderon
5	229	delCMV-mCherry-RTKN(RBD)	Abram Calderon
6	239	CMV-mCerrulean-PA-Rac1	Klaus Hahn
7	257	delCMV-mCitrine-RBD	Johannes Koch
8	325	pCMV5-EGFP-GEF-H1 wt	AG Nalbant
9	358	pTriEX-mCherry-Zdk1-RhoA Q63L	Addgene 81058
10	517	delCMV-MCP-mCitrine	Olga Jost
11	518	CMV-mCitrine-Arhgef11	Oliver Rocks
12	519	CMV-mCherry-Arhgef1	Oliver Rocks

13	520	CMV-mCherry-AKAP13	Oliver Rocks
14	521	CMV-mCherry-Arhgef18	Oliver Rocks
15	533	PARC-TFP-PCP	Olga Jost
16	539	Dimerizer-PARC-CCL-moxBFP-Halotag	Jens Niemann
17	551	CMV-mCherry-Arhgef11	Oliver Rocks
18	552	CMV-mCherry-Arhgef12	Oliver Rocks
19	553	CMV-mCherry-Arhgef28	Oliver Rocks
20	556	delCMV-mTurq2	Dominic Kamps
21	562	delCMV-mTurquoise2-PCP	Eva Thüring
22	614	delCMV-MCP-mCherry	Eva Thüring
23	615	pUB_STOP_12xPP7-24xMS2	Eva-Maria Thüring
24	626	pUB_STOP-48x9RPUM1-0xPP7-24xMS2	Alina Perne
25	667	delCMV-PAmCherry-PCP	Alina Perne
26	676	delCMV-9R-PUM1-mTurquoise2-CAAX	Stefanie Gossen
27	679	CMV-9R-PUM1-mTurquoise-CAAX	Stefanie Gossen
28	700	pUB_STOP-48x9RPUM1-24xPP7-0xMS2	Alina Perne
29	724	RafRBDmCherry	2108 (Abt 2) MPI
30	726	3xGFP-RalGDSRBD	1518 (Abt 2) MPI
31	727	EYFP-C1 Rap1A wt	2779 (Abt 2) MPI
32	729	mCit HRas wt	3291 (Abt 2) MPI
33	754	delCMV-mCit-PUMDK5	Dominic Kamps
34	786	pDONR223-PRKAR2B	Addgene 23667
35	787	pDONR223-PRKACA	Addgene 23495

36	789	pDONR223-PRKAR1A	Addgene 23741
37	830	delCMV-PUMDK3-mTurq-Rac1-Q61L	Lukas Grebe
38	833	pUB-STOP_12xPP7_48xPUMDK3_24xMS2	Lukas Grebe
39	836	delCMV-mCherry-Arhgef12	Lukas Grebe
40	871	pUB-STOP_12xPP7_48xPUMDK3_24xMS2	Lukas Grebe
41	873	delCMV_9RPUM1_mTurq_RhoBQ63L	Lukas Grebe
42	874	delCMV_9RPUM1_mTurq_RhoBQ63L	Lukas Grebe

4.2.5 Plasmids made in this thesis.

No.	**Lab no.**	**Plasmid name (Description)**	**Cloning method (Insert/Vector plasmids, Lab no.)**	**Oligo pair used**	**Enzymes used**
1	699	delCMV-mCherry-2xRTKN(RBD) (TIRF-M based improved Rho activity sensor)	Gibson assembly (229/229)	1	XhoI
2	730	delCMV-RafRBD-mCherry (TIRF-M based Ras activity sensor)	Restriction digestion and ligation (724/162)		NheI/AgeI
3	731	delCMV-mCitrine-RalGDSRBD (TIRF-M based Rap activity sensor)	Restriction digestion and ligation (726/257)		AccIII/MfeI
4	739	delCMV-MCP-mCitrine-HRaswt (MCP fused wt HRas bait construct)	Restriction digestion and ligation (729/517)		BsrgI/MfeI
5	740	delCMV-MCP-mCitrine-Rap1Awt (MCP fused wt Rap1A bait construct)	Restriction digestion and ligation (727/517)		BsrgI/MfeI

6	775	delCMV-mCherry-PCP (mCherry-PCP color code construct)	Restriction digestion and ligation (162/562)		AgeI/BsrgI
7	777	delCMV-mCherry-2xp67PhoxGBD (TIRF-M based improved Rac activity sensor)	Gibson assembly (199/199)	2	HindIII
8	778	delCMV-mCherry-3xp67PhoxGBD (TIRF-M based improved Rac activity sensor)	Gibson assembly (199/777)	3	EcoRI
9	779	delCMV-2xRafRBD-mCherry (TIRF-M based improved Ras activity sensor)	Gibson assembly (730/730)	4	AgeI
10	780	delCMV-mCitrine-2xRalGDSRBD (TIRF-M based improved Rap activity sensor)	Gibson assembly (731/731)	5	AccIII
11	784	delCMV_9RPUMDK3_mTurq (Orthogonal pumilio protein)	Gibson assembly (754/556)	6	EcoRI
12	801	delCMV-3xRafRBD-mCherry (TIRF-M based improved Ras activity sensor)	Gibson assembly (730/730)	7&8	AgeI
13	803	delCMV-9RPUM1-mTurq-RhoA-Q63L (9RPUM1 fused RhoAQ63L bait construct)	Gibson assembly (358/676)	9	BsrgI
14	810	delCMV-mCitrine-3xp67Phox (TIRF-M based improved Rac activity sensor)	Restriction digestion and ligation (163/778)		AgeI/AccIII
15	837	delCMV_9RPUM3_mTurq_RhoAQ 63L (9RPUM3 fused RhoAQ63L bait construct)	Restriction digestion and ligation (358/784)		BsrgI/MfeI
16	839	Dimerizer-PARC-CCL-moxBFP-PCP (PCP tagged artificial receptor construct)	Restriction digestion and ligation (533/539)		BsrgI/SacII

17	883	delCMV-mCherry-Arhgef1 (Lbc type GEF)	Gibson assembly (519/162)	10	BsrgI
18	884	delCMV-mCherry-Arhgef11 (Lbc type GEF)	Restriction digestion and ligation (551/883)		AscI/PacI
19	894	delCMV-9R-PUM1-mTurq-hPRKAR1A_CAAX (9RPUM1 fused RI-α bait construct)	Gibson assembly (789/676)	11	BsrgI
20	896	delCMV-mCherry-hPRKACA (Cat-α prey construct)	Gibson assembly (787/162)	12	
21	950	delCMV-hPRKAR2B-MCP-mCitrine (MCP fused RII-β bait construct)	Gibson assembly (786/517)	13	HindIII/XhoI
22	951	CMV-mCherry-hArhgef2 (Lbc type GEF)	Gibson assembly (325/519)	14	AscI/PacI

4.2.6 Oligo pairs used for clonings.

No.	Forward primer / Reverse primer
1	5'- TACAAGTCCGGACTCAGATCTCGAGAAGCTTCGAATTCCCTGG-3'/ 5'-AGGGAATTCGAAGCTTGAGCGAGTCCGGAGCCTGTCTTCTCCAGCAC-3'
2	5'- TACAAGTCCGGACTCAGATCTCGAGAAGCTTCGAATTCCCTGG-3'/ 5'-AGGGAATTCGAAGCTTGAGCGAGTCCGGAGCCTGTCTTCTCCAGCAC-3'
2	5'-GGACTCAGATCTCGAGCTCACATGTCCCTGGTGGAGGCCA-3'/5'-ACCAGGGACATGGAATTCGATCCACTTCCAGAACCCGTCGCCTTGCCTAGGTAATC-3'
3	5'- ACGGGTTCTGGAAGTGGATCGGTTCTCATGTCCCTGGTGGAGGC-3'/5'-GGCCTCCACCAGGGACATGGAATTCGATCCACTTCCAGAACCCGTCGCCTTGCCTAGGTAATC-3'
5	5'-CATGGACGAGCTGTACAAGTCCGGAGGTTCCGGAAGTGGATCCGCGCTGCCGCTCTACAAC-3'/5'-

	GCGCAGCTCGAGATCTGAGTCCGGATCCACTTCCGGAACCGGTCCGCTTCTTGAGGAC -3’
6	5’-TCCGCTAGCCTCAAGCTTCGAATTCGCCACCATGGGTTCCGGAAGTGGATCC-3’/5’-CTTGCTCACCATGGTGGCGACCGGTCCGGATCCACTTCCAGAACCCCCCAGGTCGACCCCATT-3’
7	5’-TAGATGTCGACGGGGATCCAGGTTCTGGAAGTGGATCCCCGAGTAAGACAAGCAAC -3’/ 5’- GGAGGATCCACTTCCAGAACCGTCGACATCTAGAAAATCTAC-3’
8	5‘-GGTTCTGGAAGTGGATCCTCCCCGAGTAAGACAAGCAAC-3’/5‘-CTTGCTCACCATGGTGGCGACCGGTGGATCCCCGTCGACATCTAGAAAATCTAC-3’
9	5’-ACTCTCGGCATGGACGAGCTGTACAGTTCCGGTGGTTCTGGTTCTGGTGGTACCATGGCTGCCATCCGGAAG-3’/5’-CCGGAACCGCCGGATCCACTTTACAAGACAAGGCACCCAG-3’
10	5’- CTCCACCGGCGGCATGGACGAGCTGTACAAGTCCGGACTCAGATCTC-3’/5’-TCTAGAGTCGCGGCCGCTTTACTTTTAGTTAATTAAAGTGCAGCCAG-3’
11	5’ACTCTCGGCATGGACGAGCTGTACAGTGGTTCTGGAAGTGGATCCGGTTCTGGAAGTATGGAGTCTGGCAGTACC-3’/5’-CCGGAACCGCCGGATCCACTGACAGACAGTGACACAAAAC -3’
12	5’-ACCGGCGGCATGGACGAGCTGTACAAGGGTTCTGGAAGTGGATCCGGTTCTGGAAGTATGGGCAACGCCGCCGCC -3’/ 5’-GAGTCGCGGCCGCTTTACTTCAAAAACTCAGAAAACTCCTTGCCACACTTCTCATTGATGGAG-3’
13	5‘-AGCGCTACCGGACTCAGATCTCGAGGCCACCATGAGCATCGAGATCCCG-3’/5‘-TGAGTAAAGTTAGAAGCCATACCGGATCCACTTCCAGAACCTGCAGTGGGTTCAACAATATC-3’
14	5’-AGTCCGGACTCAGATCTCGAGGGCGCGCCATGTCTCGGATCGAATCCC-3’/5’-GATCCGGTGGATCCTTAGTTAATTAAGCTCTCGGAGGCTACAGC-3’

4.3 Methods

4.3.1 Adherent cell culture and cryopreservation

All cell lines were handled in an aseptic environment inside a BSL-II biosafety cabinet. All the reagents used to culture cells were prewarmed at 37°C inside a water bath for 15-20 min. To start a culture, a frozen cryovial of cells was thawed in the water bath at 37oC for 3 min. The thawed cell suspension was then collected in a 15 ml tube and 5 ml of pre-warmed (37˚C) media was added to the vial. Using a 10 ml serological pipette the cell suspension was gently mixed and centrifuged at 1000 rpm for 5 min. Post centrifugation the media supernatant was discarded, and the cell pellet was resuspended in 10 ml of fresh warm media. The cell suspension was then plated in a 100 mm dish and stored in a 37°C incubator with 5% CO_2 to grow. Once the cells reached ~80% confluency, they were subcultured. To subculture the cells, the medium was removed from the culture plate. Then, 5 ml of prewarmed DPBS was added to the culture dish and the dish was gently swirled to wash the cells. The DPBS was removed, and 2 ml of prewarmed solution of Trypsin-EDTA was added to the cells. The cells were then incubated at 37°C for trypsinization for ~5 min. Once detached, the cells were collected in a 15 ml tube and 8 ml of prewarmed media was added to the tube. Using a 10 ml serological pipette the cells were resuspended, and 2 ml of cell suspension was transferred to a fresh 100 mm dish. 8 ml of fresh prewarmed media was added to the dish and the cells were resuspended and stored in a 37°C incubator with 5% CO_2 to grow.

For long-term storage, cells were cryopreserved in freezing media at -150°C. For cryopreservation 80-90% confluent cell culture plates were used. First the media was discarded, and cells were washed with prewarmed DPBS as mentioned above. The cells were then trypsinzed using prewarmed Trypsin-EDTA as mentioned above. The cells were then collected in a 15 ml tube and were resuspended with 8 ml of fresh prewarmed media and were counted using a counting chamber. The cells were then centrifuged at 1000 rpm for 5 min and the cell pellet was resuspended with 5% DMSO-media for a final concentration of 10^6 cells/ml. The cells were then aliquoted in 2 ml cryovials, with 1 ml of cell suspension in each. The cryovials were labelled and transferred into a Mr. Frosty® Cryo 1°C freezing chamber (with fresh Isopropyl alcohol). The freezing chamber was then

transferred to a -80°C freezer and stored overnight. Next day morning the frozen vials were transferred in a cardboard box and stored at -150°C for long term storage.

4.3.2 Single cell migration

SPY650-DNA dye (SPY™) was used to stain the nuclei to track migrating cells. 96 hours after siRNA treatment, 10,000 cells were seeded on an 8 well LabTek dish coated with 10µg/ml of fibronectin. 6 hours post seeding, the media was removed, and the cells were treated with SPY-650 (1:1000) in imaging medium and were incubated for 1.5 hours. The cells were then washed (1x) with fresh warm imaging media and were incubated again for 1 hour in fresh imaging media before imaging. Incubations of cells with imaging media were performed at 37˚C w/o CO_2.

4.3.3 Subcloning

Subcloning was performed with enzymes obtained from NEB. Wherever possible, high fidelity (HF) enzymes were used for digestion.

4.3.3.1 Subcloning with restriction digestion and ligation

For subcloning DNA fragments into vectors with compatible restriction sites, standard restriction enzymes were used from NEB for plasmid DNA digestion. 1 µl of restriction enzyme was used to digest 1 µg of plasmid DNA in a compatible buffer at the enzyme specific temperatures. In all the cases, the restriction digestions were performed for a minimum of 3 hours. For stricter temperature control, thermocyclers were used. Wherever possible, the enzymes were heat inactivated at the end of the digestion incubation. Post digestion, the digested fragments of interest were separated via agarose gel electrophoresis, using a suitable concentration of agarose. QIAquick Gel extraction kit (Qiagen) was then used to cut out and purify the fragment of interest.
To ligate the insert and a backbone with compatible sites, T4 DNA ligase (NEB) was used. Ligations were always set-up in a 20µl reactions with 1x ligase buffer. 1 µl of T4 ligase was used, along with insert and vector DNA fragments in 3:1 molar ratio. All ligation reactions were performed at 16°C for 16 hours in a thermocycler. At the end of the

reaction the T4 ligase was inactivated with a 65°C incubation for 10 min. 5µL of the ligation reaction was then used for bacterial transformation.

4.3.3.2 Gibson assembly

Gibson assembly was used wherever compatible restriction sites were unavailable for the desired DNA insert and vector backbone. It was done in two steps. First the insert, or both insert and backbone, were PCR amplified. Second, the DNA template in the PCR reaction mix was destroyed and the insert and backbone fragments were mixed with the Gibson master mix and incubated. Gibson assembly based cloning strategies were outlined using the online NEBuilder® assembly tool.

Polymerase chain reaction (PCR)

Q5® High-Fidelity DNA Polymerase from NEB was used for polymerase chain reactions. All PCR reactions were set-up in a 25µl reaction mixture, with 1x Q5 reaction buffer, 1x Q5 high GC enhancer, 200 µM dNTPs (NEB), 0.5 U of Q5® High-Fidelity DNA Polymerase, and 100 ng of DNA template.

The following conditions were used for a polymerase chain reaction:

	Temperature (°C)	**Time**
Initial denaturation	98	5’
Denaturation (30x)	98	10’’
Annealing (30x)	(Primer pair specific)	30’’
Extension	72	30’’/kb
Final extension	72	2’

The annealing temperature used for individual polymerase chain reactions was calculated using the online NEBT_m calculator. After each PCR reaction the PCR amplified product was checked for correct size using agarose gel electrophoresis. NEB DNA ladders (1kb plus/100 bp) were used as size controls.

After the PCR reaction, the template DNA in the PCR reaction mix was destroyed using a DpnI digestion. To do that, 0.5µl of DpnI was added to the PCR reaction mix. The reaction mix was then mixed and incubated at 37oC for 3 hr. At the end of the incubation, DpnI was inactivated with a further incubation of the reaction at 80˚C for 20 min.

To set-up a Gibson assembly, 15µL of the 1.5x lab made Gibson master mix was used. The reaction volume was fill up to 20 µL with DNA mix (3:1, insert: backbone) and nuclease free water. All the Gibson reactions were performed at 50˚C for 5 hours. 5µL of Gibson reaction mix was then used for bacterial transformation.

4.3.4 Bacterial transformation and plasmid DNA isolation

Chemically competent *E.coli* strains (XL-10 Gold and Top-10) were used for transformation of subcloned DNA constructs. A frozen aliquot of competent cells was obtained from -80°C storage and was thawed on ice for 5-10 min. Plasmid DNA was then added to the cells and mixed. The reaction tube was then incubated on ice for 30 min. After that, the cells were treated with a heat shock at 42˚C for 30 seconds. Immediately after that, the reaction tube was transferred back to ice, and was incubated on ice for 5 min. Then, 400µL of prewarmed (37˚C) S.O.C media was added to the cells, and the cells were incubated at 37°C for 1 hour, with shaking. For retransformation, 50 µL of cultured cell suspension was used and plated on an LB-Agar plate with appropriate antibiotics for selection. For transformations post cloning, the cell suspension was spun down at 10,000 rpm for 1 min, and the pellet was resuspended in 100 µl of media supernatant. The 100µl cell suspension was then plated on an LB-Agar plate with appropriate antibiotics for selection. LB-Agar plates were then incubated at 37˚C overnight.
To set-up a culture for plasmid isolation, 5 ml of LB media (with antibiotics for selection) in a 15 ml tube was inoculated with a single colony taken from a fresh LB plate with colonies. The colony was then allowed to grow in the media overnight at 37°C, with shaking. Plasmid DNA isolation was then performed from the overnight grown culture using a QIAGEN Miniprep kit.

To make a glycerol stock for long term storage of the bacterial culture, a fresh over day culture was set-up using the overnight grown culture. The over day culture was allowed

to grow for 5 hours post inoculation, after which 500µl of culture was aliquoted in a 2 ml cryovial. To the cryovial 500µl of 50% glycerol was added, and the cryovial was mixed gently. The vial was then labelled and transferred to -80˚C for long term storage.

4.3.5 Plasmid DNA transfection

Chemical transfection methods were used for plasmid DNA transfection into cells. Lipofectamine™ 2000 was used for plasmid DNA transfection into USOS and COS7 cells. Lipofectamine™ 3000 was used for plasmid DNA transfection into A431 cells. Lipofectamine™ 2000 was used in 1:2 ratio (1µg of plasmid DNA with 2µl of transfection reagent). For transfections with Lipofectamine™ 3000, P3000 was used in 1:2 ratio (1µg of plasmid DNA with 2µl of P3000) along with either 1µl Lipofectamine™ 3000 per well (8-well LabTek) or 1.6µl Lipofectamine™ 3000 per dish (3.5mm culture dish/MatTek).

4.3.6 RNA interference

ON Target Plus siRNA from Dharmacon™ was used for RNAi. Transfection of the siRNA was performed using 5µL of Lipofectamine RNAiMax© per transfection. siRNAs were used at 30 nM final concentration. The cells were treated with the siRNAs for 96 hours before they were processed for experimental evaluation or knockdown quantification.

4.3.7 SDS-PAGE and Western blotting

For SDS-PAGE, cell lysis was performed using cell lysis buffer from CST (9803, CST). Cells were washed one time with ice cold PBS then lysed with 1x cell lysis buffer for 5 min on ice. After 5 min, the cells were scrapped out and the lysed cells were collected in a chilled 1.5 ml tube. The tube was then centrifuged at 13000 rpm for 10 min at 4˚C, after which the supernatant was collected in a fresh chilled 1.5 ml tube, and the pellet was discarded. Protein concentration measurement were performed using the Bradford assay with the Pierce™ Coomassie Plus (Bradford) Assay Kit (23236). Wide-ranging concentrations (0.5 µg/ml, 1µg/ml, 2µg/ml, 3µg/ml and 5µg/ml) of BSA were used as standards to quantify protein concentrations in the cell lysate. Bradford reactions were prepared in a 2 ml micro tubes and absorbance measurements were performed at 595 nm.

SDS-PAGE was performed using a Mini-Protean Gel electrophoresis system from Bio-rad. 5x Laemmli sample buffer was used to prepare protein samples of equal concentrations. Samples were boiled at 95˚C for 5 min and were separated using a gradient polyacrylamide gel (4561086, Biorad). Pre-strained protein marker from Pan-Biotech (MB-2030050) was used as molecular weight standard. Electrophoresis was performed at a constant voltage of 100V for ~ 90 min.

Wet blot transfer was used to transfer proteins to a PVDF membrane (MERCK). Mini Trans-Blot system from Bio-rad was used for electroblotting. Electroblotting was done for 3 hours at a constant voltage of 70 V in the cold room. Intercept blocking buffer (927-60001, LI-COR) was then used to block the membrane for 60 min at room temperature. For primary antibody staining against Arhgef11 and Arhgef12, blots were incubated for 24 hr in primary antibody dilution at 4˚C, with shaking. For primary antibody staining against Rac1, blots were incubated overnight in primary antibody dilution at 4˚C, with shaking. Arhgef12 antibody was used at 1:1000 dilution, Arhgef11 antibody was used at 1:50 dilution, and Rac1 antibody was used at 1:1000 dilution. GAPDH antibody was used at 1:1000 dilution as loading control. The membranes were then washed with 1x TBS-T buffer and stained with secondary antibodies (IRDye®, Licor) for 60 min at room temperature. The blots were then washed again and were imaged using Odyssey® CLx imaging system (LI-COR).

4.3.8 Live cell imaging

4.3.8.1 Tracking single cell migration

SPY650 stained cells were imaged using an Olympus IX81 microscope with a UPlanSApo 10x objective. The imaging system was equiped with a Hamamatsu C10600-10B-H camera and a Lumencor SpectraX (Olympus) light source. The wide-field images were acquired using a 651 nm LED lamp. CellSense software (Olympus) was used to automate the sequences of image acquisition. The imaging set-up was equipped with a temperature-controlled incubation chamber for imaging the samples at 37°C. Images were acquired in phenol red free medium with HEPES buffer, supplemented with 10% FBS.

4.3.8.2 Total internal reflection fluorescence (TIRF) microscopy

TIRF imaging was performed using an Olympus IX81F-3 microscope with a TIRF 60x oil objective (N.A 1.45). The imaging system was equipped with a Hamamatsu Image EM CCD-C9100-13 Camera and a ZDC autofocus device. TIRF images were acquired using a 4 laser set-up with excitation wavelengths of 405 nm, 445 nm, 514 nm, and 561 nm. Wide-field images were acquired using either a Lumencor SpectraX (Olympus), or via an MT20 light source (Olympus). Either the Cell^R software (Olympus) or the CellSense software (Olympus) was used to automate sequences of image acquisition. The TIRF set-up was equipped with a temperature-controlled incubation chamber for imaging the samples at 37°C. TIRF images were acquired with samples in a phenol red free media with HEPES buffer, supplemented with 10% FBS.

4.3.8.2.1 Imaging A431/U2OS cells on an 8 well Labtek

For imaging cells on an 8-well Labtek, the dishes were treated with either 0.01% collagen (U2OS) for 1 hour at 37°C, or 10µg/ml Fibronectin (A431) for 45 min at room temperature. On day 1 the cells were seeded (14k cells/well) on the coated dishes. On day 2 the cells were transfected with either Lipofectamine™ 2000 (U2OS) or Lipofectamine™ 3000 (A431). For transfection 1µL of Lipofectamine™ 2000 was used per well (U2OS) or 1µL of Lipofectamine™ 3000 + 2µL of P3000™ per well (A431), along with 25µL of OptiMEM media and the required amount of plasmid DNA. The OptiMEM + DNA + Lipofection reagents mix was incubated at room temperature for 20 min before adding to the wells. Post transfection, on day 3 the cells were imaged with TIRF-M.

4.3.8.2.2 Imaging migrating A431 cells on a 35 mm MatTek.

For imaging A431 migration on 35 mm MatTek, the cells, on day 1, were first seeded on 35mm culture dish (140k cells/dish, red label). On day 2 the cells were transfected. For transfection Lipofectamine™ 3000 (1.6µl of Lipofectamine™ 3000 + 2µL of P3000™ per 35mm dish) was used, along with 250µL OptiMEM per dish and the required amount of plasmid DNA. The OptiMEM + DNA + Lipofection reagents mix was incubated at room temperature for 20 min before adding to the dishes. For imaging, on day 3, the cells were

reseeded on 35 mm MatTek which was coated with 10µg/ml Fibronectin overnight at 4°C before use. 1.5 hours post seeding, the cells were observed for proper attachment. Once properly attached, the cells were then taken for imaging with TIRF-M.

4.3.8.3 Differential interference contrast (DIC) microscopy

For DIC microscopy, the cells were seeded on an 8-well Labtek (10k cells/well) or a 35 mm MatTek (15k cells in the centre) which was coated with 10µg/ml Fibronectin overnight at 4°C before use. 1.5 hours post seeding, the cells were observed for proper attachment. Once properly attached, the cells were then taken for imaging. The cells were imaged using an Olympus IX81 microscope with a UPlanSApo 10x DIC objective.

4.3.9 Data analysis

Image analysis was performed using Fiji (ImageJ). Custom built ImageJ scripts were used to automate image analyses. Microsoft PowerPoint was used to compile figures. Plots were generated using GraphPad Prism.

4.3.9.1 Measuring change in sensor signals in TIRF post Rac1 optogenetic perturbations.

The cells were imaged first with a pre-run of 150 s. The cells were then stimulated with a perturbation cycle of 445 nm laser perturbation for 5 seconds followed by image acquisition. The perturbations were cycled for 245 s, after which images were recorded for 255 s to measure the recovery period. 30% of 445nm laser was used for perturbations, with either a 1000x neutral-density filter for Rho sensor measurements, or a 10,000x neutral-density filter for GEF recruitment measurements.
To analyse the effect of perturbation, videos were compiled, and background corrected based on the average intensity recorded of the background from a ROI of 10x10. Individual cells were then isolated from the videos. Cells were eroded to remove fluctuations at the cell periphery and were scaled down by a factor of 25 to reduce noise. A threshold was then applied to the bright pixels in the cell centre. Ignoring the fluctuating pixels at the cell periphery, the temporal changes in signal were measured using the applied threshold, with a walking average of 5 seconds.

4.3.9.2 Temporal cross correlation measurements between two signals

To measure temporal cross-correlation between two signals, the videos were first processed as described above, and a mask video was generated using the applied threshold. Custom built MATLAB scripts were then used to deduce the temporal cross-correlation.

4.3.9.3 Measurement of signal enrichment in protrusion-retraction cycles in migrating cells.

Enrichment of signals in the protrusion retraction cycles and the cell edge velocity of migrating cells were measured using a modified version of the ADAPT plugin in ImageJ. The signal enrichment at the cell periphery was measured within a defined segment inside the cell edge. Using a cytosolic filler, the signal channel was thresholded for cell segmentation and signal measurements.
A smoothing filter radius of 5 pixels was used for segmentation of the videos. For videos recorded with higher frame rate (6/min), a temporal filter radius of 50 seconds was used, whereas for videos recorded with a lower frame rate (1.5/min), a temporal filter radius of 80 seconds was used. To measure the signals at the cell periphery a cortex depth of 3 μm was used. Using the velocity map, signal map, and velocity-signal cross-correlation maps from the default output files generated by the ADAPT plugin, signal enrichment in protrusions and retractions were deduced, via a custom-built ImageJ script.

The velocity map was also used to define regions of cell periphery to be either in protrusion or in retraction. Defined number of pixels corresponding to either protrusion or retraction, defined for a threshold based positive or negative speed, were used to measure the signal intensity at the corresponding time points in the signal map. The signal enrichment was then calculated as the ratio of the intensity of threshold defined regions divided by the average intensity of the whole cell over the whole time-period of the video. A time shifted local enrichment was then generated by shifting the threshold defined regions on the signal map along the temporal axis of the map.
To calculate the length of protrusion-retraction cycles, first average protrusion and average retraction velocities were calculated from the velocity map. Only threshold

defined protrusion/retraction pixels were used.. The duration of protrusion-retraction cycles was then calculated as the time between the onset of a protrusion and the onset of the following retraction.

4.3.9.4 Measurement of migration parameters of single cell migration.

Quantification of velocity and directionality was performed using the TackMate plugin in ImageJ. SPY-650 stained nuclei were selected and segmented using an intensity threshold and size filter in TrackMate. Cell tracks that run out of the field of view were filtered out. The tracks generated using TrackMate were used to compute velocity and directionality measurements using a chemotaxis plugin (Ibidi GmbH, Martinsried, Germany) for ImageJ.

4.3.9.5 Measurement of signal intensity and kinetics of prey molecules on RNA scaffolds.

For measuring the signal intensity on each scaffold, a home-made jython based macro was used in Fiji. Using 'TrackMate' in Fiji, scaffolds were identified for a threshold of 0.25uM diameter. The signal intensity on the scaffolds was then measured by normalising the intensity observed on the scaffold, with that of the local background. The intensity on each scaffold was calculated by the ratio of the background corrected median of signal intensity of the pixels in inner ring to that of the background corrected median of the signal intensity of the pixels in the outer donut.

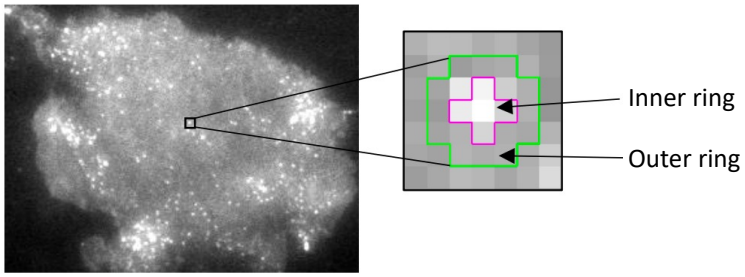

$$\text{Fluorescnece signal above local background} = \frac{\text{Background Corrected Median (inner circle)}}{\text{Background Corrected Median (outer docut)}}$$

For analysis of dynamic interactions between a bait and its prey, the bait channel was used as a reference channel to track each scaffold for the whole-time span of the movie

and the corresponding local intensity was measure in the prey channel to obtain a dynamics change in signal intensity on the scaffolds. For each frame, the mean of the fluorescence signal of each scaffold was accounted as one value for it's corresponding time-point.

5. References

1. Abercrombie, M., Heaysman, J. E. M., & Pegrum, S. M. (1970). The locomotion of fibroblasts in culture I. Movements of the leading edge. Experimental Cell Research, 59(3), 393–398. https://doi.org/10.1016/0014-4827(70)90646-4
2. Aghajanian, A., Wittchen, E. S., Campbell, S. L., & Burridge, K. (2009). Direct Activation of RhoA by Reactive Oxygen Species Requires a Redox-Sensitive Motif. PLOS ONE, 4(11), e8045. https://doi.org/10.1371/JOURNAL.PONE.0008045
3. Aman, A., & Piotrowski, T. (2010). Cell migration during morphogenesis. Developmental Biology, 341(1), 20–33. https://doi.org/10.1016/J.YDBIO.2009.11.014
4. Azeloglu, E. U., & Iyengar, R. (2015). Signaling Networks: Information Flow, Computation, and Decision Making. Cold Spring Harbor Perspectives in Biology, 7(4), a005934. https://doi.org/10.1101/CSHPERSPECT.A005934
5. Banerjee, J., Fischer, C. C., & Wedegaertner, P. B. (2009). The amino acid motif L/IIxxFE defines a novel actin-binding sequence in PDZ-RhoGEF. Biochemistry, 48(33), 8032. https://doi.org/10.1021/BI9010013
6. Barry, D. J., Durkin, C. H., Abella, J. v, & Way, M. (2015). Open source software for quantification of cell migration, protrusions, and fluorescence intensities. J Cell Biol, 209(1), 163–180. https://doi.org/10.1083/jcb.201501081
7. Bement, W. M., Leda, M., Moe, A. M., Kita, A. M., Larson, M. E., Golding, A. E., Pfeuti, C., Su, K. C., Miller, A. L., Goryachev, A. B., & von Dassow, G. (2015). Activator-inhibitor coupling between Rho signalling and actin assembly makes the cell cortex an excitable medium. Nature Cell Biology, 17(11), 1471–1483. https://doi.org/10.1038/NCB3251
8. Bhalla, U. S. (2004). Signaling in Small Subcellular Volumes. I. Stochastic and Diffusion Effects on Individual Pathways. Biophysical Journal, 87(2), 733. https://doi.org/10.1529/BIOPHYSJ.104.040469
9. Blaser, H., Eisenbeiss, S., Neumann, M., Reichman-Fried, M., Thisse, B., Thisse, C., & Raz, E. (2005). Transition from non-motile behaviour to directed migration during early PGC development in zebrafish. Journal of Cell Science, 118(17), 4027–4038. https://doi.org/10.1242/JCS.02522

10. Bondeva, T., Balla, A., Várnai, P., & Balla, T. (2002). Structural Determinants of Ras-Raf Interaction Analyzed in Live Cells. Molecular Biology of the Cell, 13(7), 2323. https://doi.org/10.1091/MBC.E02-01-0019
11. Braselmann, E., Rathbun, C., Richards, E. M., & Palmer, A. E. (2020). Illuminating RNA Biology: Tools for Imaging RNA in Live Mammalian Cells. Cell Chemical Biology, 27(8), 891–903. https://doi.org/10.1016/J.CHEMBIOL.2020.06.010
12. Buck, A., Sanchez Klose, F. P., Venkatakrishnan, V., Khamzeh, A., Dahlgren, C., Christenson, K., & Bylund, J. (2019). DPI Selectively Inhibits Intracellular NADPH Oxidase Activity in Human Neutrophils. ImmunoHorizons, 3(10), 488–497. https://doi.org/10.4049/IMMUNOHORIZONS.1900062
13. Campa, C. C., Ciraolo, E., Ghigo, A., Germena, G., & Hirsch, E. (2015). Crossroads of PI3K and Rac pathways. Https://Doi.Org/10.4161/21541248.2014.989789, 6(2), 71–80. https://doi.org/10.4161/21541248.2014.989789
14. Carey, J., Uhlenbeck, O. C., Cameron, V., & de Haseth, P. L. (1983). Sequence-Specific Interaction of R17 Coat Protein with Its Ribonucleic Acid Binding Site. Biochemistry, 22(11), 2601–2610. https://doi.org/10.1021/BI00280A002/ASSET/BI00280A002.FP.PNG_V03
15. Castillo-Kauil, A., García-Jiménez, I., Cervantes-Villagrana, R. D., Adame-García, S. R., Beltrán-Navarro, Y. M., Gutkind, J. S., Reyes-Cruz, G., & Vázquez-Prado, J. (2020). Gαsdirectly drives PDZ-RhoGEF signaling to Cdc42. Journal of Biological Chemistry, 295(50), 16920–16928. https://doi.org/10.1074/JBC.AC120.015204/ATTACHMENT/F8658DD4-1367-4B5B-920F-899371685E0C/MMC2.PDF
16. Chattopadhyay, S., Garcia-Mena, J., Devito, J., Wolska, K., and Das, A. (1995). Bipartite function of a small RNA hairpin in transcription antitermination in bacteriophage A. Proc. Natl. Acad. Sci. U S A 92, 4061–4065.
17. Chen, B., Chou, H. T., Brautigam, C. A., Xing, W., Yang, S., Henry, L., Doolittle, L. K., Walz, T., & Rosen, M. K. (2017). Rac1 GTPase activates the WAVE regulatory complex through two distinct binding sites. ELife, 6. https://doi.org/10.7554/ELIFE.29795
18. Chen, T., Hinton, D., Zidovetzki, R., & Hofman, F. (1998). Up-regulation of the cAMP/PKA pathway inhibits proliferation, induces differentiation, and leads to

apoptosis in malignant gliomas. Laboratory Investigation; a Journal of Technical Methods and Pathology.

19. Chen, Z., Singer, W. D., Danesh, S. M., Sternweis, P. C., & Sprang, S. R. (2008). Recognition of the Activated States of Gα13 by the rgRGS Domain of PDZRhoGEF. Structure, 16(10), 1532–1543. https://doi.org/10.1016/J.STR.2008.07.009
20. Chikumi, H., Barac, A., Behbahani, B., Gao, Y., Teramoto, H., Zheng, Y., & Gutkind, J. S. (2004). Homo- and hetero-oligomerization of PDZ-RhoGEF, LARG and p115RhoGEF by their C-terminal region regulates their in vivo Rho GEF activity and transforming potential. Oncogene, 23(1), 233–240. https://doi.org/10.1038/SJ.ONC.1207012
21. Chiu, V. K., Bivona, T., Hach, A., Sajous, J. B., Silletti, J., Wiener, H., Johnson, R. L., Cox, A. D., & Philips, M. R. (2002). Ras signalling on the endoplasmic reticulum and the Golgi. Nature Cell Biology, 4(5), 343–350. https://doi.org/10.1038/NCB783
22. Clark, A. G., Maitra, A., Jacques, C., Bergert, M., Pérez-González, C., Simon, A., Lederer, L., Diz-Muñoz, A., Trepat, X., Voituriez, R., & Vignjevic, D. M. (2022). Self-generated gradients steer collective migration on viscoelastic collagen networks. Nature Materials 2022 21:10, 21(10), 1200–1210. https://doi.org/10.1038/s41563-022-01259-5
23. Cortese, B., Palamà, I. E., D'Amone, S., & Gigli, G. (2014). Influence of electrotaxis on cell behaviour. Integrative Biology, 6(9), 817–830. https://doi.org/10.1039/C4IB00142G
24. Dada, O., Gutowski, S., Brautigam, C. A., Chen, Z., & Sternweis, P. C. (2018). Direct Regulation of p190RhoGEF by Activated Rho and Rac GTPases. Journal of Structural Biology, 202(1), 13. https://doi.org/10.1016/J.JSB.2017.11.014
25. Danen, E. H. J., van Rheenen, J., Franken, W., Huveneers, S., Sonneveld, P., Jalink, K., & Sonnenberg, A. (2005). Integrins control motile strategy through a Rho-cofilin pathway. Journal of Cell Biology, 169(3), 515–526. https://doi.org/10.1083/JCB.200412081/VIDEO-7
26. de Las Rivas, J., & Fontanillo, C. (2010). Protein–Protein Interactions Essentials: Key Concepts to Building and Analyzing Interactome Networks. PLOS Computational Biology, 6(6), e1000807. https://doi.org/10.1371/JOURNAL.PCBI.1000807

27. de Seze, J., Gatin, J., & Coppey, M. (2023). RhoA regulation in space and time. FEBS Letters, 597(6), 836–849. https://doi.org/10.1002/1873-3468.14578
28. Ding, Y., Xu, L., Jovanovic, B. D., Helenowski, I. B., Kelly, D. L., Catalona, W. J., Yang, X. J., Pins, M., & Bergan, R. C. (2007). The Methodology Used to Measure Differential Gene Expression Affects the Outcome. Journal of Biomolecular Techniques : JBT, 18(5), 321. /pmc/articles/PMC2392989/
29. Ding, Z., Dhruv, H., Kwiatkowska-Piwowarczyk, A., Ruggieri, R., Kloss, J., Symons, M., Pirrotte, P., Eschbacher, J. M., Tran, N. L., & Loftus, J. C. (2018). PDZ-RhoGEF Is a Signaling Effector for TROY-Induced Glioblastoma Cell Invasion and Survival. Neoplasia, 20(10), 1045–1058. https://doi.org/10.1016/J.NEO.2018.08.008
30. Ding, Z., Dong, Z., Yang, Y., Fortin Ensign, S. P., Sabit, H., Nakada, M., Ruggieri, R., Kloss, J. M., Symons, M., Tran, N. L., & Loftus, J. C. (2020). Leukemia-Associated Rho Guanine Nucleotide Exchange Factor and Ras Homolog Family Member C Play a Role in Glioblastoma Cell Invasion and Resistance. American Journal of Pathology, 190(10), 2165–2176. https://doi.org/10.1016/j.ajpath.2020.07.005
31. Drosten, M., Dhawahir, A., Sum, E. Y. M., Urosevic, J., Lechuga, C. G., Esteban, L. M., Castellano, E., Guerra, C., Santos, E., & Barbacid, M. (2010). Genetic analysis of Ras signalling pathways in cell proliferation, migration and survival. The EMBO Journal, 29(6), 1091–1104. https://doi.org/10.1038/EMBOJ.2010.7
32. Du, J., Zhu, Z., Xu, L., Chen, X., Li, X., Lan, T., Li, W., Yuan, K., & Zeng, Y. (2020). ARHGEF11 promotes proliferation and epithelial-mesenchymal transition of hepatocellular carcinoma through activation of β-catenin pathway. Aging (Albany NY), 12(20), 20235. https://doi.org/10.18632/AGING.103772
33. Durisic, N., Laparra-Cuervo, L., Sandoval-Álvarez, Á., Borbely, J. S., & Lakadamyali, M. (2014). Single-molecule evaluation of fluorescent protein photoactivation efficiency using an in vivo nanotemplate. Nature Methods 2013 11:2, 11(2), 156–162. https://doi.org/10.1038/nmeth.2784
34. Eckenstaler, R., Hauke, M., & Benndorf, R. A. (2022). A current overview of RhoA, RhoB, and RhoC functions in vascular biology and pathology. Biochemical Pharmacology, 206, 115321. https://doi.org/10.1016/J.BCP.2022.115321
35. Fornace, M. E., Huang, J., Newman, C. T., Porubsky, N. J., Pierce, M. B., & Pierce, N. A. (2022). NUPACK: Analysis and Design of Nucleic Acid Structures, Devices, and Systems. https://doi.org/10.26434/CHEMRXIV-2022-XV98L

36. Friedl, P., & Wolf, K. (2010). Plasticity of cell migration: a multiscale tuning model. The Journal of Cell Biology, 188(1), 11–19. https://doi.org/10.1083/JCB.200909003
37. Fritz, R. D., Menshykau, D., Martin, K., Reimann, A., Pontelli, V., & Pertz, O. (2015). SrGAP2-Dependent Integration of Membrane Geometry and Slit-Robo-Repulsive Cues Regulates Fibroblast Contact Inhibition of Locomotion. Developmental Cell, 35(1), 78–92. https://doi.org/10.1016/j.devcel.2015.09.002
38. Gagliardi, P. A., Puliafito, A., di Blasio, L., Chianale, F., Somale, D., Seano, G., Bussolino, F., & Primo, L. (2015). Real-time monitoring of cell protrusion dynamics by impedance responses. Scientific Reports, 5. https://doi.org/10.1038/SREP10206
39. Gandor, S., Reisewitz, S., Venkatachalapathy, M., Arrabito, G., Reibner, M., Schröder, H., Ruf, K., Niemeyer, C. M., Bastiaens, P. I. H., & Dehmelt, L. (2013). A Protein-Interaction Array Inside a Living Cell. Angewandte Chemie International Edition, 52(18), 4790–4794. https://doi.org/10.1002/ANIE.201209127
40. George, S., Martin, J. A. J., Graziani, V., & Sanz-Moreno, V. (2023). Amoeboid migration in health and disease: Immune responses versus cancer dissemination. Frontiers in Cell and Developmental Biology, 10. https://doi.org/10.3389/FCELL.2022.1091801
41. Goehring, N. W., & Grill, S. W. (2013). Cell polarity: mechanochemical patterning. Trends in Cell Biology, 23(2), 72–80. https://doi.org/10.1016/J.TCB.2012.10.009
42. Golding, A. E., Visco, I., Bieling, P., & Bement, W. M. (2019). Extraction of active rhoGTPases by rhoGDI regulates spatiotemporal patterning of rhogtpases. ELife, 8. https://doi.org/10.7554/ELIFE.50471
43. Graessl, M., Koch, J., Calderon, A., Kamps, D., Banerjee, S., Mazel, T., Schulze, N., Jungkurth, J. K., Patwardhan, R., Solouk, D., Hampe, N., Hoffmann, B., Dehmelt, L., & Nalbant, P. (2017). An excitable Rho GTPase signaling network generates dynamic subcellular contraction patterns. The Journal of Cell Biology, 216(12), 4271–4285. https://doi.org/10.1083/JCB.201706052
44. Haataja, L., Groffen, J., & Heisterkamp, N. (1997). Characterization of RAC3, a Novel Member of the Rho Family. Journal of Biological Chemistry, 272(33), 20384–20388. https://doi.org/10.1074/JBC.272.33.20384

45. Hall, A. (1998). Rho GTPases and the actin cytoskeleton. Science (New York, N.Y.), 279(5350), 509–514. https://doi.org/10.1126/SCIENCE.279.5350.509
46. Halstead, J. M., Lionnet, T., Wilbertz, J. H., Wippich, F., Ephrussi, A., Singer, R. H., & Chao, J. A. (2015). An RNA biosensor for imaging the first round of translation from single cells to living animals. Science, 347(6228), 1367–1370. https://doi.org/10.1126/SCIENCE.AAA3380/SUPPL_FILE/HALSTEAD.SM.PDF
47. Halstead, J. M., Wilbertz, J. H., Wippich, F., Lionnet, T., Ephrussi, A., & Chao, J. A. (2016). TRICK: A Single-Molecule Method for Imaging the First Round of Translation in Living Cells and Animals. Methods in Enzymology, 572, 123–157. https://doi.org/10.1016/BS.MIE.2016.02.027
48. Harrison, R. G. (1906). Observations on the living developing nerve fiber. Https://Doi.Org/10.3181/00379727-4-98, 4(1), 140–143. https://doi.org/10.3181/00379727-4-98
49. Horiuchi, J., Yamazaki, D., Naganos, S., Aigaki, T., & Saitoe, M. (2008). Protein kinase A inhibits a consolidated form of memory in Drosophila. Proceedings of the National Academy of Sciences of the United States of America, 105(52), 20976–20981. https://doi.org/10.1073/PNAS.0810119105/SUPPL_FILE/0810119105SI.PDF
50. Huang, C. H., Tang, M., Shi, C., Iglesias, P. A., & Devreotes, P. N. (2013). An excitable signal integrator couples to an idling cytoskeletal oscillator to drive cell migration. Nature Cell Biology 2013 15:11, 15(11), 1307–1316. https://doi.org/10.1038/ncb2859
51. Huang, S. (2016). Where to Go: Breaking the Symmetry in Cell Motility. PLOS Biology, 14(5), e1002463. https://doi.org/10.1371/JOURNAL.PBIO.1002463
52. Iglesias, P. A., & Devreotes, P. N. (2012). Biased excitable networks: how cells direct motion in response to gradients. Current Opinion in Cell Biology, 24(2), 245–253. https://doi.org/10.1016/J.CEB.2011.11.009
53. Ito, H., Morishita, R., & Nagata, K. I. (2018). Functions of Rhotekin, an Effector of Rho GTPase, and Its Binding Partners in Mammals. International Journal of Molecular Sciences, 19(7). https://doi.org/10.3390/IJMS19072121
54. Itoh, R. E., Kurokawa, K., Ohba, Y., Yoshizaki, H., Mochizuki, N., & Matsuda, M. (2002). Activation of rac and cdc42 video imaged by fluorescent resonance energy transfer-based single-molecule probes in the membrane of living cells. Molecular

and Cellular Biology, 22(18), 6582–6591. https://doi.org/10.1128/MCB.22.18.6582-6591.2002

55. Jamaluddin, M., Wang, S., Boldogh, I., Tian, B., & Brasier, A. R. (2007). TNF-α-induced NF-κB/RelA Ser276 phosphorylation and enhanceosome formation is mediated by an ROS-dependent PKAc pathway. Cellular Signalling, 19(7), 1419–1433. https://doi.org/10.1016/J.CELLSIG.2007.01.020
56. Kamps, D., & Dehmelt, L. (2017). Deblurring Signal Network Dynamics. ACS Chemical Biology, 12(9), 2231–2239. https://doi.org/10.1021/ACSCHEMBIO.7B00451/ASSET/IMAGES/MEDIUM/CB-2017-004514_0006.GIF
57. Kamps, D., Koch, J., Juma, V. O., Campillo-Funollet, E., Graessl, M., Banerjee, S., Mazel, T., Chen, X., Wu, Y. W., Portet, S., Madzvamuse, A., Nalbant, P., & Dehmelt, L. (2020). Optogenetic Tuning Reveals Rho Amplification-Dependent Dynamics of a Cell Contraction Signal Network. Cell Reports, 33(9). https://doi.org/10.1016/J.CELREP.2020.108467
58. Kinderman, F. S., Kim, C., von Daake, S., Ma, Y., Pham, B. Q., Spraggon, G., Xuong, N. H., Jennings, P. A., & Taylor, S. S. (2006). A Novel and Dynamic Mechanism for AKAP Binding to RII Isoforms of cAMP-dependent Protein Kinase. Molecular Cell, 24(3), 397. https://doi.org/10.1016/J.MOLCEL.2006.09.015
59. Kiyatkin, A., Aksamitiene, E., Markevich, N. I., Borisov, N. M., Hoek, J. B., & Kholodenko, B. N. (2006). Scaffolding protein Grb2-associated binder 1 sustains epidermal growth factor-induced mitogenic and survival signaling by multiple positive feedback loops. The Journal of Biological Chemistry, 281(29), 19925–19938. https://doi.org/10.1074/JBC.M600482200
60. Koga, H., Terasawa, H., Nunoi, H., Takeshige, K., Inagaki, F., & Sumimoto, H. (1999). Tetratricopeptide repeat (TPR) motifs of p67(phox) participate in interaction with the small GTPase Rac and activation of the phagocyte NADPH oxidase. The Journal of Biological Chemistry, 274(35), 25051–25060. https://doi.org/10.1074/JBC.274.35.25051
61. Komatsu, N., Aoki, K., Yamada, M., Yukinaga, H., Fujita, Y., Kamioka, Y., & Matsuda, M. (2011). Development of an optimized backbone of FRET biosensors for kinases and GTPases. Molecular Biology of the Cell, 22(23), 4647–4656.

https://doi.org/10.1091/MBC.E11-01-0072/ASSET/IMAGES/LARGE/4647FIG7.JPEG

62. Krause, M., & Gautreau, A. (2014). Steering cell migration: lamellipodium dynamics and the regulation of directional persistence. Nature Reviews Molecular Cell Biology 2014 15:9, 15(9), 577–590. https://doi.org/10.1038/nrm3861
63. Kraynov, V. S., Chamberlain, C., Bokoch, G. M., Schwartz, M. A., Slabaugh, S., & Hahn, K. M. (2000). Localized Rac activation dynamics visualized in living cells. Science (New York, N.Y.), 290(5490), 333–337. https://doi.org/10.1126/SCIENCE.290.5490.333
64. Kurokawa, K., & Matsuda, M. (2005). Localized RhoA activation as a requirement for the induction of membrane ruffling. Molecular Biology of the Cell, 16(9), 4294–4303. https://doi.org/10.1091/MBC.E04-12-1076/ASSET/IMAGES/LARGE/ZMK0090572960006.JPEG
65. Lang, P., Gesbert, F., Delespine-Carmagnat, M., Stancou, R., Pouchelet, M., & Bertoglio, J. (1996). Protein kinase A phosphorylation of RhoA mediates the morphological and functional effects of cyclic AMP in cytotoxic lymphocytes. The EMBO Journal, 15(3), 510. https://doi.org/10.1002/j.1460-2075.1996.tb00383.x
66. Levchenko, A., & Iglesias, P. A. (2002). Models of Eukaryotic Gradient Sensing: Application to Chemotaxis of Amoebae and Neutrophils. Biophysical Journal, 82(1), 50–63. https://doi.org/10.1016/S0006-3495(02)75373-3
67. Lim, F., Downey, T. P., & Peabody, D. S. (2001). Translational repression and specific RNA binding by the coat protein of the Pseudomonas phage PP7. The Journal of Biological Chemistry, 276(25), 22507–22513. https://doi.org/10.1074/JBC.M102411200
68. Lin, K. B. L., Freeman, S. A., & Gold, M. R. (2010). Rap GTPase-mediated adhesion and migration: A target for limiting the dissemination of B-cell lymphomas? Cell Adhesion & Migration, 4(3), 327. https://doi.org/10.4161/CAM.4.3.11114
69. Linghu, C., Johnson, S. L., Valdes, P. A., Shemesh, O. A., Park, W. M., Park, D., Piatkevich, K. D., Wassie, A. T., Liu, Y., An, B., Barnes, S. A., Celiker, O. T., Yao, C. C., Yu, C. C. (Jay), Wang, R., Adamala, K. P., Bear, M. F., Keating, A. E., & Boyden, E. S. (2020). Spatial Multiplexing of Fluorescent Reporters for Imaging Signaling Network Dynamics. Cell, 183(6), 1682-1698.e24. https://doi.org/10.1016/J.CELL.2020.10.035/

70. Liu, P., Calderon, A., Konstantinidis, G., Hou, J., Voss, S., Chen, X., Li, F., Banerjee, S., Hoffmann, J. E., Theiss, C., Dehmelt, L., & Wu, Y. W. (2014). A Bioorthogonal Small-Molecule-Switch System for Controlling Protein Function in Live Cells. Angewandte Chemie International Edition, 53(38), 10049–10055. https://doi.org/10.1002/ANIE.201403463
71. Lo, C. M., Wang, H. B., Dembo, M., & Wang, Y. L. (2000). Cell movement is guided by the rigidity of the substrate. Biophysical Journal, 79(1), 144–152. https://doi.org/10.1016/S0006-3495(00)76279-5
72. MacHacek, M., Hodgson, L., Welch, C., Elliott, H., Pertz, O., Nalbant, P., Abell, A., Johnson, G. L., Hahn, K. M., & Danuser, G. (2009). Coordination of Rho GTPase activities during cell protrusion. Nature, 461(7260), 99–103. https://doi.org/10.1038/NATURE08242
73. Machesky, L. M., & Hall, A. (1997). Role of Actin Polymerization and Adhesion to Extracellular Matrix in Rac- and Rho-induced Cytoskeletal Reorganization. The Journal of Cell Biology, 138(4), 913. https://doi.org/10.1083/JCB.138.4.913
74. MacKay, C. E., Shaifta, Y., Snetkov, V. v., Francois, A. A., Ward, J. P. T., & Knock, G. A. (2017). ROS-dependent activation of RhoA/Rho-kinase in pulmonary artery: Role of Src-family kinases and ARHGEF1. Free Radical Biology & Medicine, 110, 316–331. https://doi.org/10.1016/J.FREERADBIOMED.2017.06.022
75. Mahlandt, E. K., Kreider-Letterman, G., Chertkova, A. O., Garcia-Mata, R., & Goedhart, J. (2023). Cell-based optimisation and characterisation of genetically encoded, location-based biosensors for Cdc42 or Rac activity. BioRxiv, 2022.09.12.507573. https://doi.org/10.1101/2022.09.12.507573
76. Manser, E., Leung, T., Salihuddin, H., Zhao, Z. S., & Lim, L. (1994). A brain serine/threonine protein kinase activated by Cdc42 and Rac1. Nature, 367(6458), 40–46. https://doi.org/10.1038/367040A0
77. Margineanu, A., Chan, J. J., Kelly, D. J., Warren, S. C., Flatters, D., Kumar, S., Katan, M., Dunsby, C. W., & French, P. M. W. (2016). Screening for protein-protein interactions using Förster resonance energy transfer (FRET) and fluorescence lifetime imaging microscopy (FLIM). Scientific Reports 2016 6:1, 6(1), 1–17. https://doi.org/10.1038/srep28186

78. McCarthy, J. B., Palm, S. L., & Furcht, L. T. (1983). Migration by haptotaxis of a Schwann cell tumor line to the basement membrane glycoprotein laminin. Journal of Cell Biology, 97(3), 772–777. https://doi.org/10.1083/JCB.97.3.772
79. Medina, F., Carter, A. M., Dada, O., Gutowski, S., Hadas, J., Chen, Z., & Sternweis, P. C. (2013). Activated RhoA is a positive feedback regulator of the Lbc family of Rho guanine nucleotide exchange factor proteins. The Journal of Biological Chemistry, 288(16), 11325–11333. https://doi.org/10.1074/JBC.M113.450056
80. Merino-Casallo, F., Gomez-Benito, M. J., Hervas-Raluy, S., & Garcia-Aznar, J. M. (2022). Unravelling cell migration: defining movement from the cell surface. Cell Adhesion & Migration, 16(1), 25–64. https://doi.org/10.1080/19336918.2022.2055520
81. Miao, Y., Bhattacharya, S., Banerjee, T., Abubaker-Sharif, B., Long, Y., Inoue, T., Iglesias, P. A., & Devreotes, P. N. (2019). Wave patterns organize cellular protrusions and control cortical dynamics. Molecular Systems Biology, 15(3). https://doi.org/10.15252/MSB.20188585
82. Miao, Y., Bhattacharya, S., Edwards, M., Cai, H., Inoue, T., Iglesias, P. A., & Devreotes, P. N. (2017). Altering the threshold of an excitable signal transduction network changes cell migratory modes. Nature Cell Biology 2017 19:4, 19(4), 329–340. https://doi.org/10.1038/ncb3495
83. Michaelson, D., Silletti, J., Murphy, G., D'Eustachio, P., Rush, M., & Philips, M. R. (2001). Differential Localization of Rho Gtpases in Live Cells: Regulation by Hypervariable Regions and Rhogdi Binding. The Journal of Cell Biology, 152(1), 111. https://doi.org/10.1083/JCB.152.1.111
84. Miskolci, V., Wu, B., Moshfegh, Y., Cox, D., & Hodgson, L. (2016). Optical Tools To Study the Isoform-Specific Roles of Small GTPases in Immune Cells. Journal of Immunology (Baltimore, Md. : 1950), 196(8), 3479–3493. https://doi.org/10.4049/JIMMUNOL.1501655
85. Mochizuki, N., Yamashita, S., Kurokawa, K., Ohba, Y., Nagai, T., Miyawaki, A., & Matsuda, M. (2001). Spatio-temporal images of growth-factor-induced activation of Ras and Rap1. Nature, 411(6841), 1065–1068. https://doi.org/10.1038/35082594

86. Moshfegh, Y., Bravo-Cordero, J. J., Miskolci, V., Condeelis, J., & Hodgson, L. (2014). A Trio-Rac1-Pak1 signalling axis drives invadopodia disassembly. Nature Cell Biology, 16(6), 571–583. https://doi.org/10.1038/NCB2972
87. Müller, P. M., Rademacher, J., Bagshaw, R. D., Wortmann, C., Barth, C., van Unen, J., Alp, K. M., Giudice, G., Eccles, R. L., Heinrich, L. E., Pascual-Vargas, P., Sanchez-Castro, M., Brandenburg, L., Mbamalu, G., Tucholska, M., Spatt, L., Czajkowski, M. T., Welke, R. W., Zhang, S., … Rocks, O. (2020). Systems analysis of RhoGEF and RhoGAP regulatory proteins reveals spatially organized RAC1 signalling from integrin adhesions. Nature Cell Biology, 22(4), 498–511. https://doi.org/10.1038/S41556-020-0488-X
88. Munjal, A., Philippe, J. M., Munro, E., & Lecuit, T. (2015). A self-organized biomechanical network drives shape changes during tissue morphogenesis. Nature 2015 524:7565, 524(7565), 351–355. https://doi.org/10.1038/nature14603
89. Nalbant, P., & Dehmelt, L. (2018). Exploratory cell dynamics: A sense of touch for cells? Biological Chemistry, 399(8), 809–819. https://doi.org/10.1515/HSZ-2017-0341
90. O'Shaughnessy, E. C., Yi, J. J., & Hahn, K. M. (2016). Biosensors of small GTPase proteins for use in living cells and animals. Optical Probes in Biology, 137–166. https://doi.org/10.1201/B18007-12/
91. Ohba, Y., Kurokawa, K., & Matsuda, M. (2003). Mechanism of the spatio-temporal regulation of Ras and Rap1. The EMBO Journal, 22(4), 859. https://doi.org/10.1093/EMBOJ/CDG087
92. Oliveira, A. F., & Yasuda, R. (2013). An Improved Ras Sensor for Highly Sensitive and Quantitative FRET-FLIM Imaging. PLOS ONE, 8(1), e52874. https://doi.org/10.1371/JOURNAL.PONE.0052874
93. Palm, D. C., Rohwer, J. M., & Hofmeyr, J. H. S. (2013). Regulation of glycogen synthase from mammalian skeletal muscle – a unifying view of allosteric and covalent regulation. The FEBS Journal, 280(1), 2–27. https://doi.org/10.1111/FEBS.12059
94. Pankov, R., Endo, Y., Even-Ram, S., Araki, M., Clark, K., Cukierman, E., Matsumoto, K., & Yamada, K. M. (2005). A Rac switch regulates random versus directionally

persistent cell migration. Journal of Cell Biology, 170(5), 793–802. https://doi.org/10.1083/JCB.200503152/VIDEO-7

95. Patel, M., Kawano, T., Suzuki, N., Hamakubo, T., Karginov, A. v., & Kozasa, T. (2014). Gα13/PDZ-RhoGEF/RhoA Signaling Is Essential for Gastrin-Releasing Peptide Receptor–Mediated Colon Cancer Cell Migration. Molecular Pharmacology, 86(3), 252–262. https://doi.org/10.1124/MOL.114.093914
96. Pertz, O., Hodgson, L., Klemke, R. L., & Hahn, K. M. (2006). Spatiotemporal dynamics of RhoA activity in migrating cells. Nature 2006 440:7087, 440(7087), 1069–1072. https://doi.org/10.1038/nature04665
97. Raaijmakers, J. H., & Bos, J. L. (2009). Specificity in Ras and Rap signaling. The Journal of Biological Chemistry, 284(17), 10995–10999. https://doi.org/10.1074/JBC.R800061200
98. Ran, F. A., Hsu, P. D., Wright, J., Agarwala, V., Scott, D. A., & Zhang, F. (2013). Genome engineering using the CRISPR-Cas9 system. Nature Protocols 2013 8:11, 8(11), 2281–2308. https://doi.org/10.1038/nprot.2013.143
99. Reig, G., Pulgar, E., & Concha, M. L. (2014). Cell migration: from tissue culture to embryos. Development, 141(10), 1999–2013. https://doi.org/10.1242/DEV.101451
100. Ridley, A. J., Paterson, H. F., Johnston, C. L., Diekmann, D., & Hall, A. (1992). The Small GTP-Binding Protein rat Regulates Growth Factor-Induced Membrane Ruffling. Cell, 70, 401–410.
101. Roebroek, T., Vandenberg, W., Sipieter, F., Hugelier, S., Stove, C., Zhang, J., & Dedecker, P. (2021). Simultaneous readout of multiple FRET pairs using photochromism. Nature Communications 2021 12:1, 12(1), 1–12. https://doi.org/10.1038/s41467-021-22043-0
102. Roquemore, L. (2020). Explore Innovative Techniques to Separate Fluorophores with Overlapping Spectra.
103. Rottner, K., & Schaks, M. (2019). Assembling actin filaments for protrusion. Current Opinion in Cell Biology, 56, 53–63. https://doi.org/10.1016/J.CEB.2018.09.004
104. Sarkar, A., Levine, D. N., Kuzmina, N., Zhao, Y., & Wang, X. (2020). Cell migration driven by self-generated integrin ligand gradient on ligand-labile surfaces. Curr Biol, 30, 4022–4032. https://doi.org/10.1016/j.cub.2020.08.020

105. Seetharaman, S., & Etienne-Manneville, S. (2020). Cytoskeletal Crosstalk in Cell Migration. Trends in Cell Biology, 30(9), 720–735. https://doi.org/10.1016/J.TCB.2020.06.004

106. SenGupta, S., Parent, C. A., & Bear, J. E. (2021). The principles of directed cell migration. Nature Reviews. Molecular Cell Biology, 22(8), 529–547. https://doi.org/10.1038/S41580-021-00366-6

107. Shaner, N. C., Patterson, G. H., & Davidson, M. W. (2007). Advances in fluorescent protein technology. Journal of Cell Science, 120(24), 4247–4260. https://doi.org/10.1242/JCS.005801

108. Shcherbakova, D. M., Cox Cammer, N., Huisman, T. M., Verkhusha, V. v., & Hodgson, L. (2018). Direct multiplex imaging and optogenetics of Rho GTPases enabled by near-infrared FRET. Nature Chemical Biology 2018 14:6, 14(6), 591–600. https://doi.org/10.1038/s41589-018-0044-1

109. Sheetz, M. P., Felsenfeld, D., Galbraith, C. G., & Choquet, D. (1999). Cell migration as a five-step cycle. Biochemical Society Symposium, 65, 233–243. https://europepmc.org/article/med/10320942

110. Smith, F. D., Langeberg, L. K., Cellurale, C., Pawson, T., Morrison, D. K., Davis, R. J., & Scott, J. D. (2010). AKAP-Lbc enhances cyclic AMP control of the ERK1/2 cascade. Nature Cell Biology, 12(12), 1242. https://doi.org/10.1038/NCB2130

111. Spassov, D. S., & Jurecic, R. (2003). The PUF Family of RNA-binding Proteins: Does Evolutionarily Conserved Structure Equal Conserved Function? IUBMB Life, 55(7), 359–366. https://doi.org/10.1080/15216540310001603093

112. Stevens, E. v., & Der, C. J. (2010). Overview of Rho GTPase history. The Rho GTPases in Cancer, 3–27. https://doi.org/10.1007/978-1-4419-1111-7_1/COVER

113. Stock, J., & Pauli, A. (2021). Self-organized cell migration across scales – from single cell movement to tissue formation. Development (Cambridge), 148(7). https://doi.org/10.1242/DEV.191767/238076

114. Subach, F. v., Malashkevich, V. N., Zencheck, W. D., Xiao, H., Filonov, G. S., Almo, S. C., & Verkhusha, V. v. (2009). Photoactivation mechanism of PAmCherry based on crystal structures of the protein in the dark and fluorescent states. Proceedings of the National Academy of Sciences of the United States of America, 106(50), 21097–21102. https://doi.org/10.1073/PNAS.0909204106/SUPPL_FILE/0909204106SI.PDF

115. Suzuki, N., Nakamura, S., Mano, H., & Kozasa, T. (2003). Galpha 12 activates Rho GTPase through tyrosine-phosphorylated leukemia-associated RhoGEF. Proceedings of the National Academy of Sciences of the United States of America, 100(2), 733–738. https://doi.org/10.1073/PNAS.0234057100

116. Svitkina, T. (2018). The Actin Cytoskeleton and Actin-Based Motility. Cold Spring Harbor Perspectives in Biology, 10(1). https://doi.org/10.1101/CSHPERSPECT.A018267

117. Szent-Györgyi, A. (1950). Actomyosin and muscular contraction. Biochimica et Biophysica Acta, 4(1–3), 38–41. https://doi.org/10.1016/0006-3002(50)90006-0

118. Tkachenko, E., Sabouri-Ghomi, M., Pertz, O., Kim, C., Gutierrez, E., MacHacek, M., Groisman, A., Danuser, G., & Ginsberg, M. H. (2011). Protein kinase A governs a RhoA–RhoGDI protrusion–retraction pacemaker in migrating cells. Nature Cell Biology 2011 13:6, 13(6), 660–667. https://doi.org/10.1038/ncb2231

119. Tocci, P., Cianfrocca, R., Semprucci, E., Castro, V. di, Bagnato, A., & Rosanò, L. (2014). Abstract 3144: PDZ-RhoGEF/β-arrestin-1 interaction mediates endothelin A receptor-induced RhoA activation and cell motility in ovarian tumor cells. Cancer Research, 74(19_Supplement), 3144–3144. https://doi.org/10.1158/1538-7445.AM2014-3144

120. Torres-Quesada, O., Mayrhofer, J. E., & Stefan, E. (2017). The many faces of compartmentalized PKA signalosomes. Cellular Signalling, 37, 1–11. https://doi.org/10.1016/J.CELLSIG.2017.05.012

121. Turing, A. M. (1952). The chemical basis of morphogenesis. Philosophical Transactions of the Royal Society of London. Series B, Biological Sciences, 237(641), 37–72. https://doi.org/10.1098/RSTB.1952.0012

122. Turnham, R. E., & Scott, J. D. (2016). Protein kinase A catalytic subunit isoform PRKACA; history, function and physiology. Gene, 577(2), 101. https://doi.org/10.1016/J.GENE.2015.11.052

123. Tutucci, E., Vera, M., Biswas, J., Garcia, J., Parker, R., & Singer, R. H. (2017). An improved MS2 system for accurate reporting of the mRNA life cycle. Nature Methods 2017 15:1, 15(1), 81–89. https://doi.org/10.1038/nmeth.4502

124. Vaidžiulyte, K., Coppey, M., & Schauer, K. (2019). Intracellular organization in cell polarity – placing organelles into the polarity loop. Journal of Cell Science, 132(24). https://doi.org/10.1242/JCS.230995/223940

125. Wang, Q., Liu, M., Kozasa, T., Rothstein, J. D., Sternweis, P. C., & Neubig, R. R. (2004). Thrombin and lysophosphatidic acid receptors utilize distinct rhoGEFs in prostate cancer cells. Journal of Biological Chemistry, 279(28), 28831–28834. https://doi.org/10.1074/jbc.C400105200

126. Watanabe, N., & Mitchison, T. J. (2002). Single-molecule speckle analysis of actin filament turnover in lamellipodia. Science (New York, N.Y.), 295(5557), 1083–1086. https://doi.org/10.1126/SCIENCE.1067470

127. Weiner, O. D., Marganski, W. A., Wu, L. F., Altschuler, S. J., & Kirschner, M. W. (2007). An Actin-Based Wave Generator Organizes Cell Motility. PLOS Biology, 5(9), e221. https://doi.org/10.1371/JOURNAL.PBIO.0050221

128. Weng, G., Bhalla, U. S., & Iyengar, R. (1999). Complexity in Biological Signaling Systems. Science, 284(5411), 92–96. https://doi.org/10.1126/SCIENCE.284.5411.92

129. Wildenberg, G. A., Dohn, M. R., Carnahan, R. H., Davis, M. A., Lobdell, N. A., Settleman, J., & Reynolds, A. B. (2006). p120-catenin and p190RhoGAP regulate cell-cell adhesion by coordinating antagonism between Rac and Rho. Cell, 127(5), 1027–1039. https://doi.org/10.1016/J.CELL.2006.09.046

130. Winkler, A., Barends, T. R. M., Udvarhelyi, A., Lenherr-Frey, D., Lomb, L., Menzel, A., & Schlichting, I. (2015). Structural details of light activation of the LOV2-based photoswitch PA-Rac1. ACS Chemical Biology, 10(2), 502–509. https://doi.org/10.1021/CB500744M

131. Wittmann, T., Dema, A., & van Haren, J. (2020). Lights, cytoskeleton, action: Optogenetic control of cell dynamics. Current Opinion in Cell Biology, 66, 1–10. https://doi.org/10.1016/J.CEB.2020.03.003

132. Wong, K., Pertz, O., Hahn, K., & Bourne, H. (2006). Neutrophil polarization: Spatiotemporal dynamics of RhoA activity support a self-organizing mechanism. Proceedings of the National Academy of Sciences of the United States of America, 103(10), 3639–3644. https://doi.org/10.1073/PNAS.0600092103/SUPPL_FILE/00092FIG7.PDF

133. Worthylake, R. A., Lemoine, S., Watson, J. M., & Burridge, K. (2001). RhoA is required for monocyte tail retraction during transendothelial migration. The Journal of Cell Biology, 154(1), 147–160. https://doi.org/10.1083/JCB.200103048

134. Wu, J., Zaccara, S., Khuperkar, D., Kim, H., Tanenbaum, M. E., & Jaffrey, S. R. (2019). Live imaging of mRNA using RNA-stabilized fluorogenic proteins. Nature Methods 2019 16:9, 16(9), 862–865. https://doi.org/10.1038/s41592-019-0531-7

135. Wu, Y. I., Frey, D., Lungu, O. I., Jaehrig, A., Schlichting, I., Kuhlman, B., & Hahn, K. M. (2009). A genetically encoded photoactivatable Rac controls the motility of living cells. Nature, 461(7260), 104–108. https://doi.org/10.1038/NATURE08241

136. Ydenberg, C. A., Smith, B. A., Breitsprecher, D., Gelles, J., & Goode, B. L. (2011). Cease-fire at the leading edge: New perspectives on actin filament branching, debranching, and cross-linking. Cytoskeleton, 68(11), 596–602. https://doi.org/10.1002/CM.20543

137. Young, K. H. (1998). Yeast Two-hybrid: So Many Interactions, (in) So Little Time…. Biology of Reproduction, 58(2), 302–311. https://doi.org/10.1095/BIOLREPROD58.2.302

138. Zhan, H., Bhattacharya, S., Cai, H., Iglesias, P. A., Huang, C. H., & Devreotes, P. N. (2020). An Excitable Ras/PI3K/ERK Signaling Network Controls Migration and Oncogenic Transformation in Epithelial Cells. Developmental Cell, 54(5), 608-623.e5. https://doi.org/10.1016/J.DEVCEL.2020.08.001

139. Zhang, F., Wang, S., Yin, L., Yang, Y., Guan, Y., Wang, W., Xu, H., & Tao, N. (2015). Quantification of Epidermal Growth Factor Receptor Expression Level and Binding Kinetics on Cell Surfaces by Surface Plasmon Resonance Imaging. Analytical Chemistry, 87(19), 9960–9965. https://doi.org/10.1021/ACS.ANALCHEM.5B02572

140. Zhang, P., Smith-Nguyen, E. v., Keshwani, M. M., Deal, M. S., Kornev, A. P., & Taylor, S. S. (2012). Structure and Allostery of the PKA RIIβ Tetrameric Holoenzyme. Science (New York, N.Y.), 335(6069), 712. https://doi.org/10.1126/SCIENCE.1213979

141. Zhong, H., SuYang, H., Erdjument-Bromage, H., Tempst, P., & Ghosh, S. (1997). The Transcriptional Activity of NF-κB Is Regulated by the IκB-Associated PKAc Subunit through a Cyclic AMP–Independent Mechanism. Cell, 89(3), 413–424. https://doi.org/10.1016/S0092-8674(00)80222-6

Acknowledgements

To start with, I would like to thank Prof. Dr. med. Jan G. Hengstler for agreeing to be my second examiner.

I would like to thank Leif for his supervision and mentorship during my PhD and for the exciting work that I got to do in the lab. Throughout my time in his lab, Leif allowed me to have my own space for me to grow and recognize my own strengths and weaknesses, for which I am very grateful. PhD is full of highs and low and I appreciate the support I received from Leif especially during the lows. Success of a PhD has less to do with the experiments and the project, and a lot more to do with a healthy motivational work environment. Leif has always tried his best to maintain a positive work environment in the lab, especially during stressful times, and I truly appreciate and respect him for that.

I would like to thank people of the Dehmelt Lab for the time I spent with them. I would like to thank Dominic Kamps for helping me start with my work in the lab and my life in Dortmund. I would like to thank Olga Jost, Stefanie Gossen, Eva-Maria Thüring, and Jessica Spindler for their contribution to the RNA scaffold project through their MSc theses.

I would like to especially thank Ricarda Lütig and Lukas Grebe, my two MSc students. They are both very kind and very hardworking people. It was a pleasure spending time with them in the lab. I would like to thank Alicia Hoffman Benito, another amazingly kind and hardworking person. Alicia's positivity created a very warm work environment in the lab and office, and some days my motivation to come to the lab would be to just have a nice chat with her.
I would like to thank Daria Kutcher, a very sharp BSc student I got to work with in the lab. Daria would pick up concepts and directions so quickly and so easily, it was almost effortless supervising her in the lab, especially when the supervision happened during the COVID period.

I would like to thank Caro and Arya, for the short time I spent with them in the lab, and I wish them both very good luck with their PhDs.

I would like to thank Dr. Perihan Nalbant and lab, for the scientific collaboration and discussions. In particular, I would like to thank Rutuja Patwardhan for helping me start with RNAi experiments in our lab.

I would like to thank Dr. Sven Müller for his continuous support with the microscopes. I would also like to thank Henrike Schütz for helping me start with western blotting and for the time I spent during that with Henrike and other people in the lab, Kitso, Manuel, and Hans.
I would also like to mention and acknowledge the scientific support and discussions with the neighboring lab of Daniel Summerer. In particular, I would like to thank Shubhendu, Tzu and Anne for tremendous amount of support and collaboration with daily work life in the lab.
I would like to thank Christa and Lucia for their support through the IMPRS program. I would like to individually mention and thank Christa for the support I received from her through several of our close door discussions.

In the end, I would like to thank my father for financially supporting me with my education which led me to pursue my PhD. I would like to thank my aunt Geeta who's always been a robust driver for me and my siblings for us to get the best possible education that we can.
Finally, I would like to thank Sushil Joseph, a friend, a mentor, my family, for the tremendous amount of support I received from him. It would have been impossible for me to finish my PhD without Sushil in my life.